Understanding how mutations shape the evolution of seasonal influenza virus hemagglutinin

Juhye M. Lee

A dissertation
submitted in partial fulfillment of the
requirements for the degree of

Doctor of Philosophy

University of Washington

2019

Reading Committee:

Jesse D. Bloom, Chair

Trevor Bedford

Adam Geballe

Program Authorized to Offer Degree:
Genome Sciences

University of Washington

Abstract

Understanding how mutations shape the evolution of seasonal influenza virus hemagglutinin

Juhye M. Lee

Chair of the Supervisory Committee:
Associate Member Jesse D. Bloom
Fred Hutchinson Cancer Research Center

Influenza virus hemagglutinin (HA) is under strong selective pressure. These selective forces constrain and drive the evolution of HA in nature. As it evolves, HA rapidly accumulates mutations that can affect its function and antigenicity; the effects of these mutations are a key determinant of the evolutionary success of viral lineages. However, we have a very limited understanding of how mutations to HA affect viral fitness and thereby shape viral evolution in nature. Here I describe my work in which I completely examined the effects of mutations to HA by leveraging the high-throughput techniques of deep mutational scanning and mutational antigenic profiling. Briefly, these techniques enabled me to introduce all of the approximately 10,000 single amino-acid mutations to HA and experimentally test the variants under functional or immune selective pressure. First, I measure the effects of mutations to a recent seasonal H3N2 HA on viral growth in cell culture and relate these measurements to the evolutionary success of mutations in nature. I find that mutations that reach high frequencies in nature tend to be measurably favorable for viral growth, whereas mutations measured as highly deleterious in our experiments rarely reach high frequencies in nature. Previously generated measurements from a diverged H1 HA do not show a strong relationship with success of viral lineages. These findings suggest that experimental measurements of the functional effects of mutations to an H3

HA can help distinguish successful H3N2 viral lineages from those that quickly die out. Next, I apply mutational antigenic profiling to evaluate the ease of viral escape from several strain-specific and broadly-neutralizing antibodies against an H1 HA. Although the virus can readily escape the narrow antibodies and the broad receptor-binding site targeting antibody via mutations with large effect sizes, it is quantifiably harder to escape the stalk-targeting antibodies that we tested. Antibody breadth therefore does not reflect the ease of viral escape by single mutations. Finally, I extend antibody mapping approaches to profile immune selection on H3 HA by polyclonal serum. I observe direct evidence of individuals with highly immunodominant serum responses against HA such that there is selection for single amino-acid mutations with relatively strong effects on neutralization resistance. Mutations in nature have recently emerged at several sites of escape in the experiments, indicating that individuals with immunodominant targeting drive antigenic drift of HA. Overall, this work demonstrates the utility of experimentally mapping mutational effects for improving our understanding of the dynamics of influenza virus evolution in nature.

TABLE OF CONTENTS

LIST OF FIGURES

LIST OF TABLES

ACKNOWLEDGMENTS

According to the ever so wise Jane Austen, "...if a book is well written, I always find it too short," and much the same can be said about graduate school. I was incredibly fortunate to have been surrounded by colleagues and mentors, friends and family who provided me with endless support, pushed me to become a better scientist, and in many ways made my graduate school experience "too short."

I'm extremely grateful to my advisor, Jesse Bloom. My work in graduate school would not have been possible without the guidance and mentorship offered by Jesse. Whenever I encountered obstacles or my projects weren't working well, Jesse was ready to troubleshoot and brainstorm with me and provide words of encouragement. His enthusiasm, which was oftentimes quite *viral*, kept me motivated as I pushed through scientific hurdles. Jesse is also an incredibly generous advisor, quick to extend support and recognition. No matter how busy he was with writing grants or mentoring his many students, Jesse was always willing to provide his time and energy, whether he was reading over my planned experiments or writing a whole new software package to streamline data analysis and visualization (in Comic Sans, no less). What has impressed me the most about Jesse is his willingness to listen to feedback from his trainees, a rare and special quality in a scientific mentor. Jesse has played a key role in my scientific and professional development, and for that, I feel very lucky to have had Jesse as an advisor.

Of course, these acknowledgments would certainly not be complete without thanking Shirleen Soh, Katherine Xue, and Danny Lawrence, my three musketeers and champions. Through all the long and dreary lows and short and sweet highs of graduate school, Shirleen, Katherine, and Danny have proven to be unwavering sources of moral support,

wisdom, and importantly, laughter. Shirleen has been the most thoughtful, insightful, and considerate friend anyone could ask for, and I must thank her for putting up with my moaning during those aforementioned lows of grad school. I am also indebted to Katherine, from whom I learned a great deal about kindness, integrity, and bravery. Thank you to Danny for keeping it real dude, even as he spilled his library on his shirt. I am filled with sadness over the thought of leaving our PB2-H3-within-host-RecA (Zika?) corner, and I will reminisce about our days together, including when Danny texted `rhino` and Shirleen & Danny raced to finish library prep.

Many millions of thanks must also be granted to Rachel Eguia, our fantastic technician, and without whom the completion of my dissertation would not have been possible. Working with Rachel has been such a privilege, from late-night parties in the tissue-culture room to early morning True Crime transfections. I was especially delighted to discover that Rachel and I shared a mutual paranoia about virus supernatant bubbles and drippy Wescodyne. Rachel's cheerfulness alone was enough to brighten the lab, not to mention her delicious baked treats. My fellow lab mates deserve special thanks for creating a respectful and supportive working environment. I especially would like to thank Mike Doud and Heather Machkovech for so remarkably and fearlessly blazing the MSTP trail in Jesse's lab. Thank you to Lauren Gentles for being my high-altitude buddy at Keystone, Sarah Hilton for always being so willing to help me with my silly computational questions, Alistair Russell for his general advice and feedback, Adam Dingens for being my MAPping buddy, and Allie Greaney for listening to me spout a lot of nonsensical theories.

I would like to extend my sincere gratitude to John Huddleston and Trevor Bedford. Both John and Trevor were instrumental in relating my work to natural evolution, which unequivocally strengthened my projects. John was incredibly patient as he helped me learn how to traverse through phylogenetic trees and call the trunk. Trevor's calm presence and perceptiveness always prompted me to take a step back from the minutiae of my

experiments and to reflect upon the deeper impact of my graduate work (and to choose more pleasing color palettes). I also very much appreciate the thought-provoking questions and advice I received from my committee members Adam Geballe, Julie Overbaugh, Stan Fields, and Trevor. To Adam Geballe, thank you for imparting your wisdom, particularly about life as a physician-scientist. The Hutch and UW have created an excellent scientific community in which to train, for which I am particularly grateful. I must also thank the weekly Virus Group meetings for always providing me with such practical and thoughtful feedback, and especially Michael Emerman for organizing the meetings.

I would like to acknowledge my MSTP E-13 colleagues for displaying utmost "whimsy and generosity of spirit" throughout these years we've been together. From Olympic peninsula adventures to Halloween parodies to spontaneous lunch dates, we have grown to become a family, and I feel so pleased that we've shared this journey together.

I'm deeply indebted to my undergraduate research mentor, Joff Silberg. Despite the fact that I had never held a pipette before, Joff had utter faith in me and gave me the chance to work in his lab since my freshman year of college. Joff had a remarkable ability to give me the independence to set up and run my own experiments while providing guidance when necessary, equipping me with skills that I continued to rely on in graduate school.

Finally, I am overcome with gratitude for my parents. They have instilled in me the values of determination and diligence. I cannot imagine how difficult it must have been for them to leave everything behind and make a new life for themselves in the US. Yet they have wholeheartedly done everything in their power and made many sacrifices to ensure that I would have every opportunity available to me. For their love and support, I cannot thank them enough.

Chapter 1
INTRODUCTION

Influenza virus evolves rapidly. Influenza virus circulates worldwide and imposes a significant public health burden [222]. A key feature of influenza virus that has contributed to its persistence in the human population is its ability to evolve rapidly, readily accumulating mutations introduced by its error-prone RNA-dependent RNA polymerase [168, 169]. In particular, the seasonal H3N2 influenza virus hemagglutinin (HA) surface protein fixes approximately three to four amino-acid mutations per year [191, 13]. This rapid evolution enables the virus to evade host immunity, causing annual epidemics and necessitating frequent vaccine updates. For instance, the WHO updates their recommendation for the H3N2 component of the vaccine nearly every one to two years [223].

Furthermore, the evolution of influenza virus is characterized by frequent population turnover [10, 12, 202]. Groups of phylogenetically related strains called clades, each sharing different combinations of mutations, emerge and circulate globally. These clades compete with each other for susceptible hosts until eventually one clade overtakes the virus population and the other clades die out [10, 12, 202, 159, 114]. This population turnover occurs approximately every three to five years for seasonal influenza virus [12]. Previous work has indicated that evolutionarily successful clades tend to have higher fitness than clades that remain at low frequency [10, 202, 159, 138]. An examination of the fundamental features that underlie viral fitness can therefore enable identification of strains likely to persist in nature.

Various forces shape the evolution of influenza virus hemagglutinin.

HA must maintain its function to enable viral growth.

HA is the most abundant surface protein of influenza virus, forming a metastable homotrimer anchored to the viral membrane [189]. HA is responsible for mediating viral entry into host cells by binding to a sialic acid receptor. Upon receptor binding and subsequent endocytosis of the virus, HA undergoes a large conformational change triggered by the low pH environment of the endosome. This conformational change enables fusion of the viral and host membranes [189].

Each HA monomer consists of two subunits, termed HA1 and HA2, which are formed upon proteolytic cleavage and subsequent activation of the HA0 precursor [81, 37]. HA can also be structurally divided into two subdomains: the surface-exposed globular head domain which contains the receptor-binding pocket, and the membrane-proximal stalk domain which bears the components for fusion [189]. This HA structure is quite well-conserved across multiple subtypes in spite of relatively low sequence identity among the subtypes [85, 181].

As HA accumulates mutations during the course of its evolution, it will invariably acquire mutations that may impact its ability to properly fold or function. Because the virus is evolutionarily constrained to maintain efficient viral growth and replication, mutations that disrupt any component of HA's important functions have implications for host infection, transmission, and ultimately viral fitness. In particular, the receptor-binding pocket and the stalk domain are relatively conserved both within and across HA subtypes, presumably due to their crucial roles in receptor binding and fusion, respectively [162, 219]. Substitutions in or proximal to the receptor-binding pocket have been shown to reduce or abolish binding to sialic acid [142, 153].

In addition, influenza virus carries a segmented genome, yet does not appreciably undergo intrasegment recombination [21]. As a result, the virus cannot place multiple beneficial mutations onto the same background, and beneficial mutations become linked to deleterious mutations. Clades with low deleterious mutation load consequently have

higher fitness than clades with high mutation load [202, 114, 138]. Experimental and modeling work have suggested that mutations deleterious to viral fitness can limit the rate of antigenic evolution and are an important determinant of clade success [202, 114, 138, 146]. A major goal in the study of influenza virus evolution is to thereby identify mutations that are detrimental to viral fitness, which may help inform predictions of clades likely to succeed in nature.

HA must continuously evade host adaptive immunity.

Strong selective pressure to evade host adaptive immunity is a major force driving HA evolution. Adaptive immunity against influenza virus is predominantly mediated by antibodies against the HA and NA surface proteins [41]. Despite the ability of this antibody response to provide protection against viral infection, the effectiveness of this immunity is transient, protecting from re-infection for approximately five years [41, 118]. The short duration of protective immunity can be attributed to *antigenic drift*, or the rapid accumulation of mutations at sites targeted by immunity [189, 191].

Most neutralizing antibodies elicited against HA target the globular head domain [212]. These antibodies generally neutralize virus by physically blocking HA from binding to its receptor [16]. Interestingly, the immunodominance of the head domain has been shown to be fairly widespread among diverse animal models and viral subtypes [2]. As a consequence of this immense immune pressure, the head domain of human influenza virus HA accumulates mutations at a faster rate than does the stalk domain [111].

Neutralizing antibodies targeting the stalk domain, on the other hand, are not as prevalent as head-targeting antibodies, largely owing to the steric inaccessibility of the stalk [148, 151]. This may explain why the prevalence of stalk-reactive antibodies tends to increase with age, as repeated exposures boost these antibodies [151, 152, 110]. Importantly, stalk-binding antibodies can broadly neutralize multiple subtypes due to the conservation of the stalk domain [165]. A number of passive immunization experiments in

animal models have exhibited the protective effects afforded by these antibodies against diverse viral subtypes [39, 108, 64, 154]. Stalk-binding antibodies are therefore of great interest for their potential use as universal vaccines.

We have a limited understanding of how mutations shape HA evolution.

It is challenging to predict the functional effects of mutations to HA.

Despite its rapid and continuous evolution, HA has sampled only a limited number of the many possible amino-acid mutations. Hence, it is a daunting task to predict the functional effects of any one of these mutations. In principle, substitutions at sites that are tolerant of mutations have only minor effects on viral fitness, whereas substitutions at constrained sites adversely affect fitness.

Although we can attempt to quantify the "evolvability" of a given site by examining that site's variability among naturally occurring variants, this variation is confounded by external selective forces which shape evolution. For instance, immune selection exerts diversifying pressure at sites targeted by antibodies [28, 226]. Thus, the degree of selection influences the tendency of a site to mutate in nature. This is also illustrated by the finding that glycosylation motifs evolved rapidly in human H1 HA but not in swine H1 lineages from 1918 to 2008 [215]. Conservation in nature is accordingly not a strict reflection of mutational tolerance.

An alternative approach is to simply consider sites likely to be under strong immune selection separately from those sites that are not. A landmark study in which the authors sought to predict fitness effects of mutations employed such an approach [138]. In this model, residues were classified as either "epitope" or "non-epitope" largely based on sets of pre-defined sites deemed to be under antibody selection from classical studies. All mutations at non-epitope sites are then treated as detrimental to viral fitness while those at epitope sites are beneficial to fitness, but this assumption certainly does not fully cap-

ture the spectrum of mutational effects. Mutations at so-called non-epitope sites may not necessarily reduce viral fitness. Indeed, mutations at non-epitope sites do occur and occasionally fix in nature [226]. Conversely, mutations at epitope sites may not strictly affect antigenicity and immune evasion [158, 230]. Nevertheless, the assumptions of this model are merely a reflection of the fact that it is difficult to know *a priori* the effect of any given mutation, but perhaps experimentally we can perform such quantifications.

Current approaches for monitoring antigenic evolution have several drawbacks.

Routine surveillance of circulating strains currently rely heavily on characterizing the antigenic properties of these strains using the hemagglutination inhibition (HAI) assay. This assay, originally developed in 1943, tests the ability of antisera raised in once-infected ferrets to block binding of viral isolates to red blood cells [95]. A new vaccine strain is recommended if circulating strains are determined to be antigenically evolved relative to the existing vaccine strain. However, this assay suffers several limitations.

The HAI assays are inherently low-throughput and labor-intensive as they require testing individual antisera against large panels of viruses. In addition, recent H3N2 strains agglutinate red blood cells poorly, making antigenic characterization of these strains quite arduous [66, 190]. Notably, epitopes targeted by immune sera from singly infected ferrets do not necessarily recapitulate the epitopes targeted by human sera [134]. In stark contrast to once-infected ferrets, humans have complex influenza virus infection and/or vaccination histories that influence their serum responses against HA [134, 135, 36]. Ferret sera are thus an imperfect surrogate of anti-influenza immunity in humans.

To overcome some of the experimental limitations of the HAI assays, recent studies have developed models to predict antigenic phenotypes, incorporating sequence or phylogenetic data [204, 90, 158]. Nonetheless, these models still ultimately rely on HAI data generated using ferret immune sera for the predictions. Measurements of the effect of mutations on escape from human immunity should therefore be more relevant to estimations

of antigenic characteristics.

It is unclear how mutations contribute to antigenic evolution.

Numerous studies have recapitulated in the lab HA's propensity for rapid antigenic evolution, isolating mutants resistant to neutralization by single monoclonal antibodies, even after a single passage [236, 214, 80, 29]. Although several seminal studies have designated five distinct non-overlapping antigenic regions (denoted regions A through E) in H3 HA, these regions were defined decades ago using a limited set of monoclonal antibodies and have not been validated in more recent strains [122, 224, 211]. A number of the antibodies used to define these regions were isolated from primary influenza infections in animal models. Importantly, we still have a very limited understanding of the relative contribution of mutations at any one of these sites to antigenic evolution.

Substitutions at only one of seven key residues in two antigenic regions were previously shown to be sufficient to engender large effects on antigenic drift [113]. Yet, substitutions in other antigenic regions routinely occur during natural evolution, and even clades with mutations at one or more of these seven defined residues may die out soon after emergence [158]. These observations indicate that mutations outside of these seven positions can have large effects on antigenic drift and even mutations at classically defined antigenic sites may not always alter antigenicity. A deeper understanding of how mutations affect antigenicity of HA is essential for identifying viral strains that can escape host immunity.

Furthermore, while it is fairly easy to select *de novo* escape variants from most strain-specific antibodies, it has been largely unexplored if the virus can as easily escape from broadly-neutralizing antibodies targeting more conserved epitopes in HA. In particular, it is unclear if strong immune selection exerted by broadly-neutralizing antibodies can drive antigenic drift in these conserved epitopes. Several studies have shown that it is possible to isolate escape mutants with broadly-neutralizing antibodies [4, 31, 77, 208],

but from these studies we are still not able to directly compare the ease of viral escape across different antibodies. This is especially crucial to study as major efforts toward the development of broadly-neutralizing antibodies for use as vaccines or therapeutics continue to expand.

It is perplexing how HA evolves to evade humoral immunity.

It has been well-established that HA can readily escape adaptive immunity [41, 118]. However, a long-standing and critical question in the study of antigenic drift is how HA escapes from polyclonal immunity. In principle, multiple antibodies with distinct epitope specificities are present in a complex polyclonal mixture, but a given mutation in HA will only escape a small fraction of these antibodies. Yet, antigenic drift in nature occurs at a rate that is much more appreciable than the expected frequency of isolating a variant completely resistant to the combined specificities of antibodies in polyclonal immunity [236, 122]. Why do we observe this discrepancy?

One possible mechanism of escape from polyclonal immunity, particularly at sub-neutralizing levels, is to augment HA receptor avidity by adsorptive mutations [235, 93]. Another plausible explanation for antigenic drift in the face of polyclonal immunity is that in some individuals, immune targeting of HA is dominated by a small set of antibodies [236, 155]. This would allow single amino-acid mutations to confer resistance to neutralization by sera.

Several observations suggest that some individuals do indeed possess immunodominant serum responses against HA. Classical selection experiments in which virus is passaged in the presence of serum can isolate single amino-acid variants that are resistant to serum neutralization [51, 49]. In recent studies, the majority of antibodies reactive to HA were found to be populated by relatively few but persistent clonotypes in numerous individuals [126, 127]. Nonetheless, these findings provide only indirect evidence of immunodominant antibody targeting. Classic selections are additionally biased by the

composition of mutations present in the initial viral stock and do not necessarily select the mutations with the strongest effect sizes on escape. Mapping the selective immune specificities in polyclonal serum in a systematic manner consequently requires alternative techniques from classical approaches.

We can leverage high-throughput approaches to experimentally assay many HA variants. To methodically and unbiasedly quantify the effects of mutations to HA, we can introduce and independently generate viruses expressing every possible amino-acid mutation at each site in the protein. This would be incredibly labor-intensive as it would require the generation of 19 amino acids $\times$ 567 sites, or at least 10,000 variants. However, new high-throughput technologies, namely *deep mutational scanning*, have now made it possible to assay in parallel many variants of a given protein [74, 75]. This massively parallel approach is a powerful method for investigating sequence-function relationships for a given protein.

Deep mutational scanning facilitates an examination of mutational effects on viral growth in cell culture

The technique of deep mutational scanning involves creating a diverse HA mutant DNA library, then generating virus libraries harboring each HA variant. To measure the effects of each amino acid on viral growth, which we quantify as a site-specific amino-acid preference, we passage the mutant viruses in cell culture to select for functional HA variants and deep sequence the libraries before and after selection [209, 59]. These measurements also provide an estimation of the inherent mutational tolerance because we now have a greater degree of control over the selective pressures acting on HA in our experiments (i.e., functional selection in the absence of immune selection).

While laboratory conditions can never fully represent the selective pressures that act on HA in nature, we can benchmark our measurements by applying the site-specific pref-

erences to inform phylogenetic models [17, 94]. The performance of this model can then be compared to more traditional codon substitution models. In doing so, we are able to evaluate how well our experimental measurements capture the constraints on the protein's evolution in nature.

Even so, these preferences may shift as the protein evolves away from its initial sequence or as protein homologs diverge [83, 89, 156, 171, 186, 198, 199]. Previous work from our lab has examined the shift in mutational effects in viral protein homologs, specifically influenza virus NP [58] and HIV Env [87]. These studies found mostly small to modest shifts, with large shifts only at a handful of sites. It is important to note, however, that the proteins in these studies are relatively conserved at 94% identity between the two NP variants and at 86% identity between the Env variants. It is uncertain if the mutational shifts would be more dramatic for homologs that are more diverged such as HA, which share $\sim$40% identity between the H1 and H3 subtypes. It is important to elucidate the extent of these shifts in amino-acid preference if we want to extrapolate our measurements of mutational effects to diverse strains.

Mutational antigenic profiling allows us to completely map viral escape from immunity

In an extension of deep mutational scanning, our lab has pioneered an approach, referred to as *mutational antigenic profiling*, to examine how mutations affect escape from immunity [60, 56]. This method involves subjecting virus libraries bearing every possible single-variant HA compatible with viral growth to immune selection with an antibody. Variants able to escape antibody neutralization will be enriched in the immune-selected condition relative to the mock-selected control, enabling comprehensive mapping of viral escape.

Work published from our lab applied mutational antigenic profiling to map escape in HA from single monoclonal antibodies [60]. The results of this study reveal prominent discrepancies in the escape profiles down to the mutation level among the antibodies

tested. However, the antibodies in this study were rather strain-specific, and the potential for escape from more broadly-neutralizing antibodies remains an open question. Notably, mutational antigenic profiling may improve our understanding of escape from polyclonal serum, which is more physiologically relevant and reflective of immune selection on HA in nature.

Layout of dissertation. In the following chapters, I describe my work elucidating the effects of mutations to HA on viral growth and escape from immunity by leveraging high-throughput approaches. Our lab has previously employed deep mutational scanning to reproducibly estimate the preferences of the highly lab-adapted WSN/1933 H1N1 HA [209, 59]. However, prior to my work, no such measurements existed for a more recent human seasonal H3N2 HA, which would be of direct relevance for estimating mutational effects for more contemporaneous strains.

In **Chapter 2**, I measure the effects on viral growth in cell culture of all possible single amino-acid mutations to a seasonal H3 HA. In collaboration with John Huddleston, a graduate student in Trevor Bedford's lab, we related the evolutionary outcome of mutations in nature to their experimentally measured effects on viral growth. We find a modest but significant correlation between mutational effect and the evolutionary success of mutations in nature, indicating that our experimental measurements may be of utility for distinguishing successful and unsuccessful clades.

In **Chapter 3**, I describe work with fellow graduate student Mike Doud, in which we develop a framework for comparing the ease of viral escape from different antibodies utilizing mutational antigenic profiling. We employ this approach to completely map escape from several strain-specific and broadly-neutralizing antibodies in an H1 HA. The results of this study reveal widely varying effect sizes on escape across the antibodies. Interestingly, the virus escapes a broad antibody targeting the receptor-binding pocket as easily as it escapes strain-specific antibodies. In contrast, mutations selected by broadly-neutralizing stalk antibodies have small effect sizes on escape. We therefore show that the virus's

capacity to escape by single amino-acid mutations varies across antibodies.

Because immunity against HA is polyclonal rather than monoclonal, in **Chapter 4** I systematically map immune selection on HA by polyclonal serum. Astonishingly, I find evidence of individuals with highly immunodominant antibody targeting of HA, such that single amino-acid mutations can confer resistance to serum neutralization. The selected escape mutations exhibit variation in their effect sizes across individual serum samples. Many of the strongest sites of escape selected in our experiments have mutated recently in natural H3N2 strains. Together these findings provide insight into how immunodominant serum responses may drive antigenic drift of influenza virus HA in nature.

Chapter 2

DEEP MUTATIONAL SCANNING OF HEMAGGLUTININ HELPS PREDICT EVOLUTIONARY FATES OF HUMAN H3N2 INFLUENZA VARIANTS

A version of this chapter has been previously published as:

Juhye M. Lee, **John Huddleston**, Michael B. Doud, Kathryn A. Hooper, Nicholas C. Wu, Trevor Bedford, and Jesse D. Bloom. Deep mutational scanning of hemagglutinin helps predict evolutionary fates of human H3N2 influenza variants. *Proceedings of the National Academy of Sciences*, 115(35):E8276-E8285, 2018.

Bold face indicates equal contribution.

2.1 Abstract

Human influenza virus rapidly accumulates mutations in its major surface protein hemagglutinin (HA). The evolutionary success of influenza virus lineages depends on how these mutations affect HA's functionality and antigenicity. Here we experimentally measure the effects on viral growth in cell culture of all single amino-acid mutations to the HA from a recent human H3N2 influenza virus strain. We show that mutations that are measured to be more favorable for viral growth are enriched in evolutionarily successful H3N2 viral lineages relative to mutations that are measured to be less favorable for viral growth. Therefore, despite the well-known caveats about cell-culture measurements of viral fitness, such measurements can still be informative for understanding evolution in nature. We also compare our measurements for H3 HA to similar data previously generated for a distantly related H1 HA, and find substantial differences in which amino acids are preferred at many sites. For instance, the H3 HA has less disparity in mutational tolerance between the head and stalk domains than the H1 HA. Overall, our work suggests that experimental measurements of mutational effects can be leveraged to help understand the evolutionary fates of viral lineages in nature — but only when the measurements are made on a viral strain similar to the ones being studied in nature.

2.2 Introduction

Seasonal H3N2 influenza virus evolves rapidly, fixing 3 to 4 amino-acid mutations per year in its hemagglutinin (HA) surface protein [72, 14]. Many of these mutations contribute to the rapid antigenic drift that necessitates frequent updates to the annual influenza vaccine [191]. This evolution is further characterized by competition and turnover among groups of strains called clades bearing different complements of mutations [10, 202, 159, 114, 12]. Clades vary widely in their evolutionary success, with some dying out soon after emergence and others going on to take over the virus population. Several lines of evidence indicate that successful clades have higher fitness than clades

that remain at low frequency [10, 202, 159, 138]. A key goal in the study of H3N2 evolution is to identify the features that enable certain clades to succeed as others die out.

Two main characteristics distinguish evolutionarily successful clades from their competitors: greater antigenic change, and efficient viral growth and transmission. In principle, experiments could be informative for identifying how mutations affect these features. Most work on influenza evolution to date has utilized experimental data to assess the antigenicity of circulating strains [204, 90, 158, 113, 32, 133]. However, the non-antigenic effects of mutations also play an important role [174, 202, 138, 114]. Specifically, due to influenza virus's high mutation rate [99, 201, 120] and lack of intra-segment recombination [21], deleterious mutations become linked to beneficial ones. The resulting accumulation of deleterious mutations can affect non-antigenic properties central to viral fitness [138]. However, there are no large-scale quantitative characterizations of how mutations to H3N2 HA affect viral growth.

It is now possible to use deep mutational scanning [75] to measure the functional effects of all single amino-acid mutations to viral proteins [209, 231, 59, 86, 175, 87]. However, the only HA for which such large-scale measurements have previously been made is from the highly lab-adapted A/WSN/1933 (H1N1) strain [209, 231, 59]. Here, we measure the effects on viral growth in cell culture of all mutations to the HA of a recent human H3N2 strain. We show that these experimental measurements can help discriminate evolutionarily successful mutations from those found in strains that quickly die out. However, the utility of the experiments for understanding natural evolution depends on the similarity between the experimental and natural strains: measurements made on an H1 HA are less informative for understanding the evolutionary fate of H3 viral strains.

2.3 Results

2.3.1 Deep mutational scanning of HA from a recent strain of human H3N2 influenza virus

We performed a deep mutational scan to measure the effects of all amino-acid mutations to HA from the A/Perth/16/2009 (H3N2) strain on viral growth in cell culture. This strain was the H3N2 component of the influenza vaccine from 2010-2012 [220, 221]. Relative to the consensus sequence for this HA in Genbank, we used a variant with two mutations that enhanced viral growth in cell culture, G78D and T212I (Figure A.1 and File S1). The G78D mutation occurs at low frequency in natural H3N2 sequences, and T212 is a site where a mutation to Ala rose to fixation in human influenza in $\sim$2011.

We mutagenized the entire HA coding sequence at the codon level to create mutant plasmid libraries harboring an average of $\sim$1.4 codon mutations per clone (Figure A.2). We then generated mutant virus libraries from the mutant plasmids using a helper-virus system that enables efficient generation of complex influenza virus libraries [59] (Figure 2.1A). These mutant viruses derived all their non-HA genes from the lab-adapted A/WSN/1933 strain. Using WSN/1933 for the non-HA genes reduces biosafety concerns, and also helped increase viral titers. To further increase viral titers, we used MDCK-SIAT1 cells (Madin-Darby canine kidney cells overexpressing 2,6-sialyltransferase) [143] that we engineered to constitutively express TMPRSS2 (Transmembrane Protease, Serine 2), which cleaves the HA precursor to activate it for membrane fusion [22, 23].

After generating the mutant virus libraries, we passaged them at low multiplicity of infection (MOI) in cell culture to create a genotype-phenotype link and select for functional HA variants (Figure 2.1A). All experiments were completed in full biological triplicate (Figure 2.1B). We also passaged and deep sequenced library 3 in duplicate (library 3-1 and 3-2) to gauge experimental noise *within* a single biological replicate. As a control to measure sequencing and mutational errors, we used the unmutated HA gene to generate and passage viruses carrying wildtype HA.

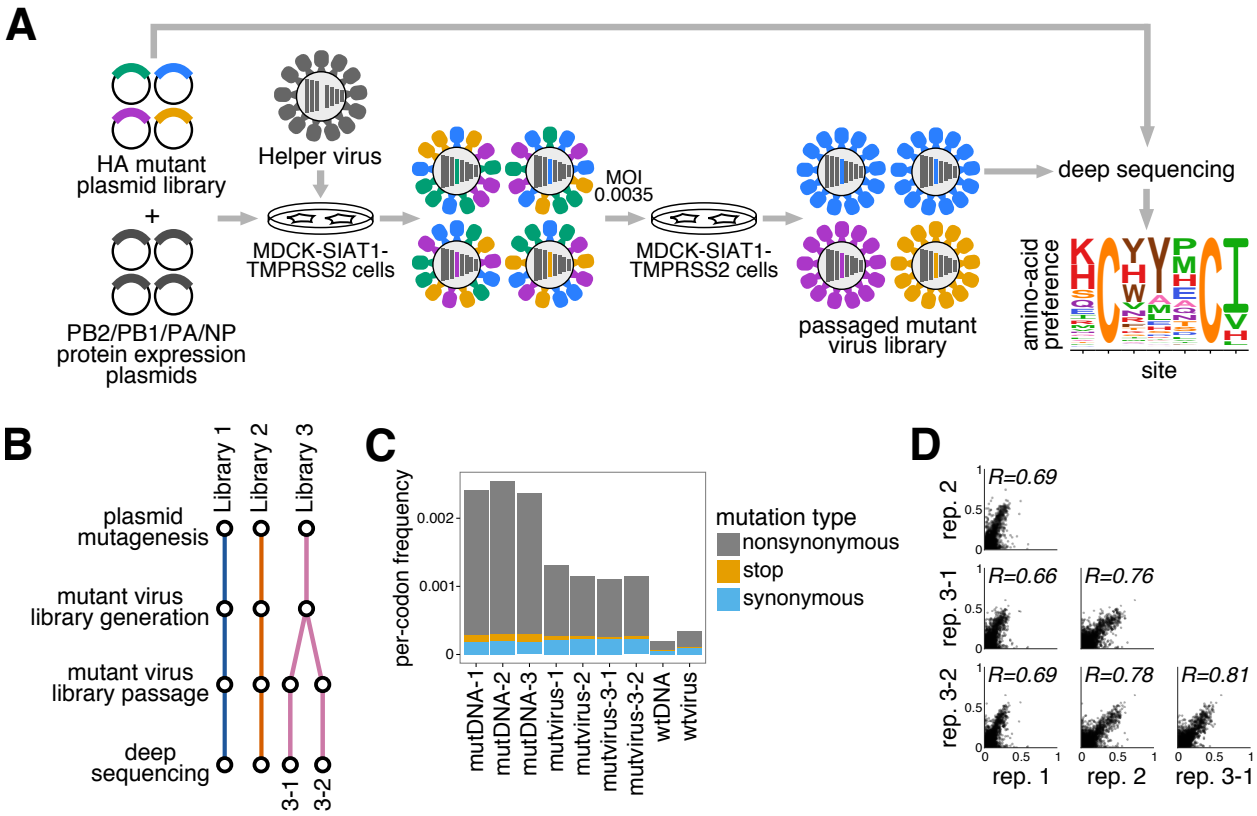

Figure 2.1: **Deep mutational scanning of the Perth/2009 H3 HA. (A)** We generated mutant virus libraries using a helper-virus approach [59], and passaged the libraries at low MOI to establish a genotype-phenotype linkage and to select for functional HA variants. Deep sequencing of the variants before and after selection allowed us to estimate each site's amino-acid preferences. **(B)** The experiments were performed in full biological triplicate. We also passaged and deep sequenced library 3 in duplicate. **(C)** Frequencies of nonsynonymous, stop, and synonymous mutations in the mutant plasmid DNA, the passaged mutant viruses, and wildtype DNA and virus controls. **(D)** The Pearson correlations among the amino-acid preferences estimated in each replicate.

Deep sequencing of the initial plasmid mutant libraries and the passaged mutant viruses revealed selection for functional HA mutants. Specifically, stop codons were purged to 20-45% of their initial frequencies after correcting for error rates estimated by sequencing the wildtype controls (Figure 2.1C). The incomplete purging of stop codons is likely because genetic complementation due to co-infection [141, 26] enabled the persistence of some virions with nonfunctional HAs. We also observed selection against many nonsynonymous mutations (Figure 2.1C), with their frequencies falling to 30-40% of their

initial values after error correction.

We next quantified the reproducibility of our deep mutational scanning across biological and technical replicates. We first used the deep sequencing data for each replicate to estimate the preference of each site in HA for all 20 amino acids as described in [18]. Because there are 566 residues in HA, there are $566 \times 19 = 10,754$ distinct measurements (the 20 preferences at each site sum to one [18]). The correlations of the amino-acid preferences between pairs of replicates are shown in Figure 2.1D. The biological replicates were well-correlated, with Pearson's R ranging from 0.69 to 0.78. Replicate 1 exhibited the weakest correlation with other replicates; this replicate also showed the weakest selection against stop and nonsynonymous mutations (Figure 2.1C), perhaps indicating more experimental noise. The two technical replicates 3-1 and 3-2 were only slightly more correlated than pairs of biological replicates, suggesting that bottlenecking of library diversity during viral passage contributes most of the experimental noise.

2.3.2 Our measurements are consistent with existing knowledge about HA's evolution and function

How do the HA amino-acid preferences measured in our experiments relate to the evolution of H3N2 influenza virus in nature? This question can be addressed by evaluating how well an experimentally informed codon substitution model (ExpCM) using our measurements describes H3N2 evolution compared to standard substitution models [19, 94]. Table 2.1 shows that an ExpCM using the across-replicate average of our measurements greatly outperforms conventional substitution models. This result indicates that our experiments authentically capture some of the constraints on HA evolution. A substitution model in which the amino-acid preferences were averaged across all sites (ExpCM, site avg.) performs no better than conventional substitution models, demonstrating that the reason that our measurements are informative is because they capture site-specific constraints. The relative rate of nonsynonymous to synonymous substitutions (dN/dS or ω) is

Model	$\triangle$AIC	Log Likelihood	Stringency	ω
ExpCM	0.0	-8441	2.47	0.91
GY94 M5	2094	-9482	–	0.36 (0.30, 0.84)
ExpCM, site average	2501	-9692	0.67	0.32
GY94 M0	2536	-9704	–	0.31

Table 2.1: **Substitution models informed by the experiments describe HA's evolution better than traditional models.** Shown are the maximum likelihood phylogenetic fit to an alignment of human H3N2 HAs using ExpCM [94], ExpCM in which the experimental measurements are averaged across sites (site avg.), and M0 and M5 versions of the Goldman-Yang (GY94) model [234]. Models are compared by Akaike information criterion (AIC) [173] computed from the log likelihood (LnL) and number of model parameters. The ω parameter is dN/dS for the Goldman-Yang models, and the relative dN/dS after accounting for the measurements for the ExpCM. For the M5 model, we give the mean followed by the shape and rate parameters of the gamma distribution over ω.

$\ll$1 for conventional substitution models (Table 2.1). However, the relative rate of nonsynonymous to synonymous substitutions after accounting for the amino-acid preferences measured in our experiments (ω for the ExpCM) is close to one (Table 2.1), indicating that most purifying selection against nonsynonymous substitutions is accounted for in the deep mutational scanning. The ExpCM stringency parameter [94] is 2.47 (Table 2.1), indicating that natural selection favors the same amino acids as the experiments but with greater stringency. Throughout the rest of this paper, we use the amino-acid preferences re-scaled [19, 94] by this stringency parameter. These re-scaled preferences are shown in Figure 2.2.

Examination of Figure 2.2 reveals that the experimentally measured amino-acid preferences generally agree with existing knowledge about HA's structure and function. For instance, sites that form structurally important disulfide bridges (sites 52 & 277, 64 & 76, 97 & 139, 281 & 305, 14 & 137-HA2, 144-HA2 & 148-HA2) [213] strongly prefer cysteine. At residues involved in receptor binding, there are strong preferences for the amino acids that are known to be involved in binding sialic acid, such as Y98, D190, W153, and S228 [216, 142, 163, 233]. A positively charged amino acid at site 329 is important for cleavage of the HA0 precursor into the mature form [200], and this site strongly prefers arginine.

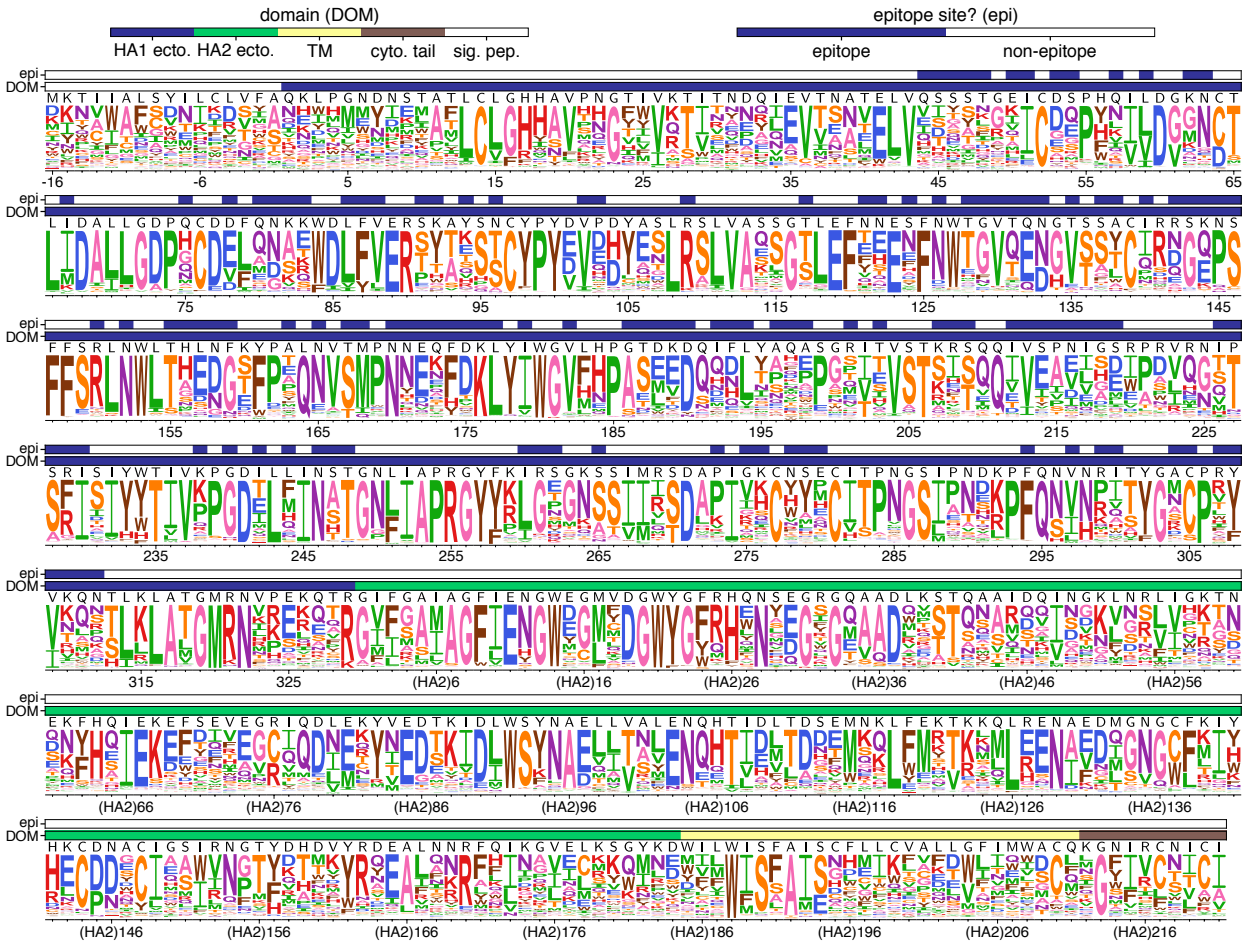

Figure 2.2: **The site-specific amino-acid preferences of the Perth/2009 HA measured in our experiments.** The height of each letter is the preference for that amino acid, after taking the average over experimental replicates and re-scaling [94] by the stringency parameter in Table 2.1. The sites are in H3 numbering. The top overlay bar indicates whether or not a site is in the set of epitope residues delineated in [226]. The bottom overlay bar indicates the HA domain (sig. pep. = signal peptide, HA1 ecto. = HA1 ectodomain, HA2 ecto. = HA2 ectodomain, TM = transmembrane domain, cyto. tail. = cytoplasmic tail). The letters directly above each logo stack indicate the wildtype amino acid at that site.

However, there are also some differences between the amino-acid preferences measured in our experiments and amino-acid frequencies in natural H3 HA sequences (Figure A.3). Most surprisingly, the start codon does not show a particularly strong preference for methionine (Figure 2.2). We validated that a virus carrying a mutation at this site from methionine to lysine does in fact reach appreciable titers (Figure A.4), perhaps because

of alternative translation-initiation at a downstream or upstream start site as has been described for other HAs [82]. Our measurements also suggest mutational tolerance at some other sites that are relatively conserved among natural HAs, such as the N-linked glycosylation motifs near the beginning of HA1 and the transmembrane domain (Figure 2.2). We validated that viruses with mutations to the glycosylation motifs at sites 22 or 38, or a site in the transmembrane domain, do in fact grow to high titers (Figures A.5 and A.6, respectively). The disparity between the relative conservation of these sites in nature and their mutational tolerance in our study could be because cell culture does not fully capture the constraints on HA function in nature, or could be because these sites are not under strong immune pressure and so mutations at them are not positively selected in nature.

2.3.3 There is less difference in mutational tolerance between the HA head and stalk domains for H3 than for H1

Our experiments measure which amino acids are tolerated at each HA site under selection for viral growth. We can therefore use our experimentally measured amino-acid preferences to calculate the inherent mutational tolerance of each site, which we quantify as the Shannon entropy of the re-scaled preferences. In prior mutational studies of H1 HAs, the stalk domain was found to be substantially less mutationally tolerant than the globular head [209, 231, 59, 91].

We performed a similar analysis using our new data for the Perth/2009 H3 HA. Surprisingly, the head domain of the H3 HA is *not* more mutationally tolerant than the stalk domain (Figure 2.3). Specifically, whereas solvent-exposed residues in the head domain are substantially more mutationally tolerant than those in the stalk domain for the WSN/1933 H1 HA, the trend is actually reversed for the Perth/2009 H3 HA (Figure 2.3B). This difference between the relative mutational tolerances of the H1 and H3 HAs is robust to the cutoff used to define surface residues (Figure A.7). For instance, for the H3 HA, the short helix A in the stalk domain is as mutationally tolerant as many surface-exposed residues

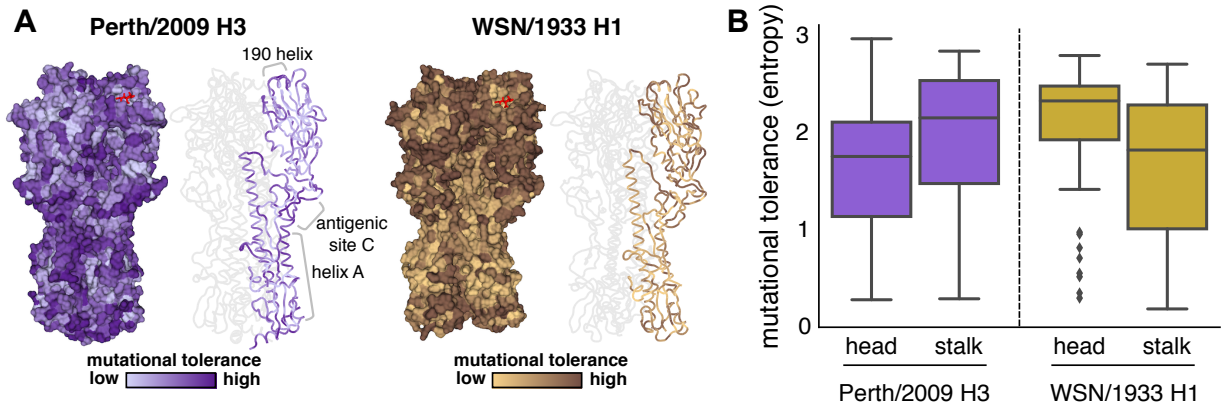

Figure 2.3: **Mutational tolerance of each site in H3 and H1 HAs. (A)** Mutational tolerance as measured in the current study is mapped onto the structure of the H3 trimer (PDB 4O5N; [129]). Mutational tolerance of the WSN/1933 H1 HA as measured in [59] is mapped onto the structure of the H1 trimer (PDB 1RVX; [79]). Different color scales are used because measurements are comparable among sites within the same HA, but not necessarily across HAs. Both trimers are shown in the same orientation. For each HA, the structure at left shows a surface representation of the full trimer, while the structure at right shows a ribbon representation of just one monomer. The sialic acid receptor is shown in red sticks. **(B)** The mutational tolerance of solvent-exposed residues in the head and stalk domains of the Perth/2009 H3 HA (purple) and WSN/1933 H1 HA (gold). Residues falling in between the two cysteines at sites 52 and 277 were defined as belonging to the head domain, while all other residues were defined as the stalk domain. A residue was classified as solvent exposed if its relative solvent accessibility was ≥ 0.2; Figure A.7 shows that the results are robust to the choice of solvent accessibility cutoff. Note that the mutational tolerance values are not comparable between the two HAs, but are comparable between domains of the same HA.

in the head domain—something that is not the case for the H1 HA. Helix A forms part of the epitope of many broadly neutralizing anti-stalk antibodies [140, 121, 31].

We also see high mutational tolerance in many of the known antigenic regions of H3 HA [224]. For instance, antigenic region B is an immunodominant area, and many recent major antigenic drift mutations have occurred in this region [32, 113, 172]. We find that the most distal portion of the globular head near the 190-helix, which is part of antigenic region B, is highly tolerant of mutations (Figure 2.3A). Antigenic region C is also notably mutationally tolerant.

Many residues inside HA's receptor binding pocket are known to be highly functionally

constrained [225, 142], and our data indicates that these sites are relatively mutationally intolerant in both H3 and H1 HAs (Figure 2.3A). In contrast, the residues surrounding the receptor binding pocket are fairly mutationally tolerant, which may contribute to the rapidity of influenza's antigenic evolution, since mutations at these sites can have large effects on antigenicity [224, 113].

2.3.4 Our measurements can help distinguish between mutations that reach low and high frequencies in nature

Mutations occurring in the H3N2 virus population experience widely varying evolutionary fates (Figure 2.4). Some mutations appear, spread and fix in the population, while others briefly circulate before disappearing. We take the maximum frequency reached by a mutation as a coarse indicator of its effect on fitness, since favorable mutations generally reach higher frequencies than unfavorable ones [71]. Here, we follow the population genetic definition of *mutation* and track the outcome of each individual mutation event; for example, although R142G occurs multiple times on the phylogeny we track each of these mutations occurring on different backgrounds separately. As such, each mutation is shown as a separate circle on a separate branch in Figure 2.4. However, because multiple mutations on the same phylogeny branch cannot be disentangled, when multiple mutations occurred on a single branch, we assigned a single mutational effect based on the sum of effects of each mutation.

After annotating mutations and their frequencies on the phylogeny in this way (Figure 2.4), it is visually obvious that there are relatively few circulating mutations that we measure to be strongly deleterious—and that such deleterious mutations rarely reach high frequency when they do occur.

We next sought to quantify the correlation between a mutation's experimentally measured effect and the maximum frequency it attained during natural evolution. To calculate a given mutation's effect, we simply took the logarithm of the ratio of the preferences for

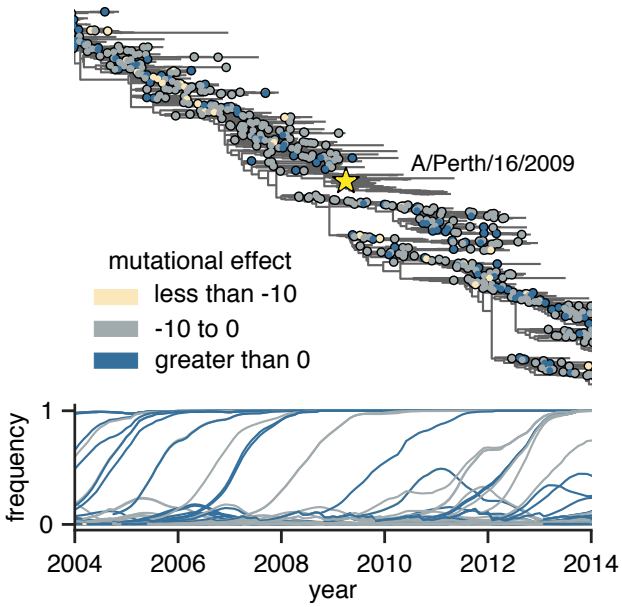

Figure 2.4: **Frequency trajectories of individual mutations and their relation to the experimentally measured effects of these mutations.** The top panel shows the subset of the full H3N2 HA tree in Figure A.8 from 2004 to 2014. Circles indicate individual amino-acid mutations, and are colored according to the mutational effect measured in our deep mutational scanning (negative values indicate mutations measured to be deleterious to viral growth). The Perth/2009 strain is labeled with a star, and nodes in the clade containing the Perth/2009 strain were excluded from our analyses. The bottom panel shows the frequency trajectory of each mutation, with trajectories colored according to the mutational effects as in the top panel. It is clear that most mutations that reach high frequency are measured to be relatively favorable in our experiments. Figure A.11 shows a similar layout but colors mutations by whether they are in HA's head or stalk domain.

the mutant and wildtype amino acids at that site. To minimize effects related to the genetic background of the strain used in the experiment, we excluded mutations closely related to the experimental strain itself and partitioned the remaining mutations into 1,022 mutations pre-dating and 299 mutations post-dating the Perth/2009 strain (Figure A.8). We additionally excluded mutations from the post-Perth partition that were sampled in 2014 or after, since these mutations have not had enough time for their evolutionary fates to be fully resolved. We used these pre-Perth and post-Perth partitions to test the utility of our measurements for both post-hoc and prospective analyses, respectively. We quantified the relationship between mutational effects and maximum mutation frequencies in

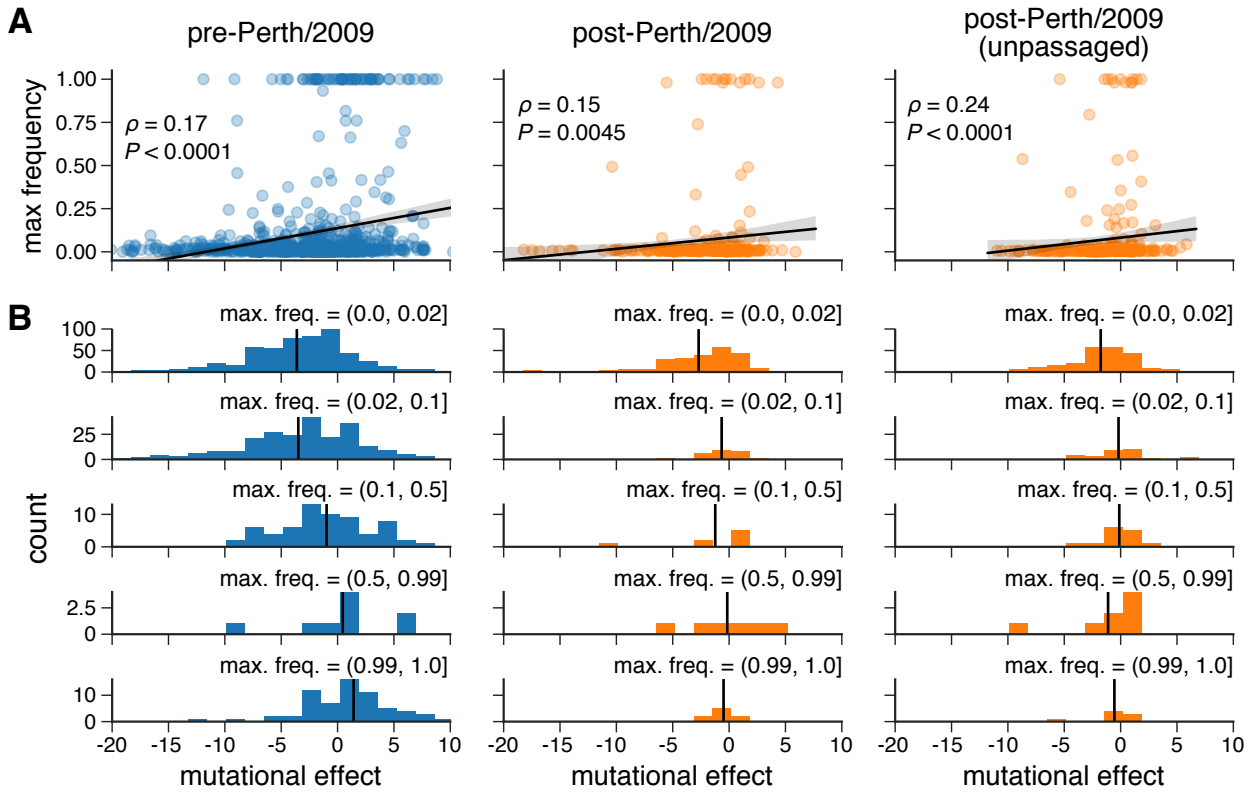

Figure 2.5: **Experimental measurements are informative about the evolutionary fate of viral mutations. (A)** Correlation between the effects of mutations as measured in our deep mutational scanning of the Perth/2009 HA and the maximum frequency reached by these mutations in nature. The plots show Spearman ρ and an empirical P-value representing the proportion of 10,000 permutations of the experimental measurements for which the permuted ρ was greater than or equal to the observed ρ. **(B)** The distribution of mutational effects partitioned by maximum mutation frequency. The vertical black line shows the mean mutation effect for each category. The analysis is performed separately for pre-Perth/2009, post-Perth/2009, and unpassaged isolates from the post-Perth/2009 partitions of the tree (see Figure A.8).

the H3N2 phylogeny via Spearman rank correlation (Figure 2.5A). In both pre-Perth and post-Perth time periods, we found a modest, but statistically significant relationship between mutational effect and maximum mutation frequency (pre-Perth $\rho = 0.17$, post-Perth $\rho = 0.15$). The similar effect sizes for both the pre- and post-Perth partitions shows that our experimental measurements can help explain the evolutionary fates of mutations in strains that post-date the experimentally studied strain, as well as to retrospectively analyze mutations that precede the experimental strain.

Many of the HAs in sequence databases are from viral isolates that were passaged in cell-culture or eggs, which can cause lab-adaptation mutations that confound evolutionary analyses [145]. To check that our results were robust to such lab-adaptation mutations, we repeated our analysis using only HA sequences derived from viruses that had not been passaged in the lab. Because sequencing of unpassaged primary isolates has only recently become commonplace, we could only perform this analysis for the post-Perth partition of the phylogenetic tree. Figure 2.5A shows that the correlation between our measured mutational effects and the maximum frequency was even stronger for mutations from unpassaged viral isolates ($\rho = 0.24$).

The trends in Figure 2.5A are most strongly driven by the behavior of substantially deleterious mutations. We investigated this further by partitioning mutations into those that reach low, medium and high frequencies, and those that fix in the population (Figure 2.5B). The mutations that reach higher frequencies have a more favorable mean effect. Mutations measured to be substantially deleterious almost never reach high frequency. Overall, these results demonstrate that measurements of how mutations affect viral growth in cell culture are informative for understanding the fates of these mutations in nature: in particular, if a mutation is measurably deleterious to viral growth, that mutation is unlikely to prosper in nature.

2.3.5 Measurements made on an H1 HA are less informative for understanding the evolution of H3 influenza

To determine how broadly experimental measurements can be generalized across HAs, we repeated the foregoing analysis of H3N2 mutation frequencies, but using mutational effects measured in our prior deep mutational scanning of the WSN/1933 H1 HA [59] (Figure A.9), which is highly diverged from the Perth/2009 H3 HA (the two HAs only have 42% protein sequence identity). Figure 2.6 shows that the correlations between the H1 experimental measurements and the maximum frequency that mutations reach during

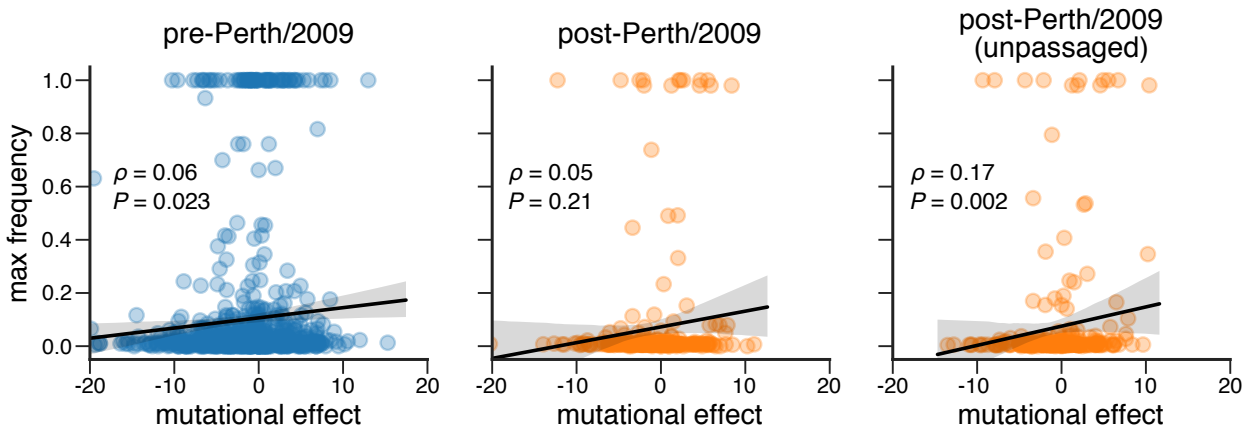

Figure 2.6: **Experimental measurements on an H1 HA are less informative about the evolutionary fate of H3N2 mutations.** This figure repeats the analysis of the H3N2 mutation frequencies in Figure 2.5A, but uses the deep mutational scanning data for an H1 HA as measured in [59]. Figure A.10 shows the histograms comparable to those in Figure 2.5B. The empirical P-value represents the result of 1,000 permutations.

H3N2 viral evolution are consistently weaker than those using H3 experimental measurements (compare Figure 2.6 to Figure 2.5A). Therefore, the utility of an experiment for understanding natural evolution degrades as the experimental sequence becomes more diverged from the natural sequences that are being studied.

2.3.6 There are large differences between H3 and H1 HAs in the amino-acid preferences of many sites

An obvious hypothesis for why the H1 deep mutational scanning is less useful for understanding the evolution of H3N2 influenza viruses is that the effect of the same mutation is often different between these two HA subtypes. To determine if this is the case, we examined how much the amino-acid preferences of homologous sites have shifted between H3 and H1 HAs. Prior experiments have found only modest shifts in amino-acid preferences between two variants of influenza nucleoprotein with 94% amino-acid identity [58] and variants of HIV envelope (Env) with 86% amino-acid identity [87]. However, the H1 and H3 HAs are far more diverged, with only 42% amino-acid identity (Figure 2.7A).

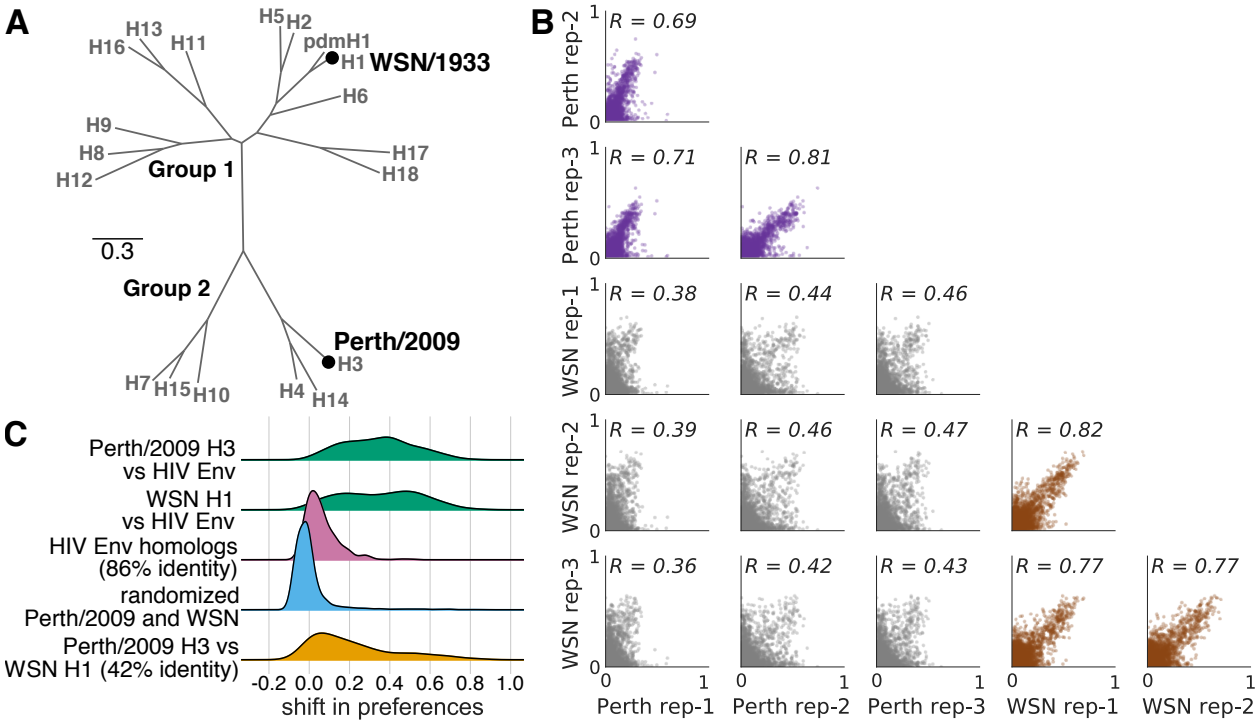

Figure 2.7: **There are large shifts in the effects of mutations between H1 and H3 HAs.** **(A)** Phylogenetic tree of HA subtypes, with the WSN/1933 H1 and Perth/2009 H3 HAs labeled. **(B)** All pairwise correlations of the amino-acid preferences measured in the three individual deep mutational scanning replicates in the current study and the three replicates in prior deep mutational scanning of the H1 HA [59]. Comparisons between H3 replicates are in purple, those between H1 replicates are in brown, and those across H1 and H3 replicates are in gray. R indicates the Pearson correlation coefficient. **(C)** We calculated the shift in amino-acid preferences at each site between H3 and H1 HAs using the method in [87], and plotted the distribution of shifts for all sites. The shifts between H3 and H1 (yellow) are much larger than the null distribution (blue) expected if all differences are due to experimental noise. The shifts are also much larger than those previously observed between two variants of HIV Env that share 86% amino-acid identity (pink). However, the shifts between H3 and H1 are less than the differences between HA and HIV Env (green).

One simple way to investigate the extent of shifts in amino-acid preferences is to correlate measurements from independent deep mutational scanning replicates on H1 and H3 HAs. Figure 2.7B shows that replicate measurements on the same HA variant are more correlated than those on different HA variants.

To more rigorously quantify shifts in amino-acid preferences after correcting for experimental noise, we used the statistical approach in [58, 87]. Figure 2.7C shows the

distribution of shifts in amino-acid preferences between H3 and H1 HAs after correcting for experimental noise. Although some sites have small shifts near zero, many sites have large shifts. These shifts between H3 and H1 are much larger than expected from the null distribution that would be observed purely from experimental noise. They are also much larger than the shifts previously observed between two HIV Envs with 86% amino-acid identity [87]. However, the typical shift between H3 and H1 is still smaller than that observed when comparing HA to the non-homologous HIV Env protein. Therefore, there are very substantial shifts in mutational effects between highly diverged HA homologs, although the effects of mutations remain more similar than for non-homologous proteins.

2.3.7 Properties associated with the shifts in amino-acid preferences between H3 and H1 HAs

What features distinguish the sites with shifted amino-acid preferences between H3 and H1 HAs? The sites of large shifts do not obviously localize to one specific region of HA's structure (Figure 2.8A). However, at the domain level, sites in HA's stalk tend to have smaller shifts than sites in HA's globular head (Figure 2.8B). The HA stalk domain is also more conserved in sequence [162], suggesting that conservation of amino-acid sequence is correlated with conservation of amino-acid preferences. Consistent with this idea, sites that are absolutely conserved across all 18 HA subtypes are significantly less shifted than sites that are variable across HA subtypes (Figure 2.8B). Presumably these sites are under consistent functional constraint across all HAs.

Despite their high sequence divergence, H1 and H3 adopt very similar protein folds [85, 181]. However, there are differences in the rotation and upward translation of the globular head subdomains relative to the central stalk domain among different HA subtypes [85, 181]. Previous work has defined clades of structurally related HA subtypes [85, 181]. One such clade includes H1, H2, H5, and H6, whereas another clade includes H3, H4, and H14 HAs (Figure 2.7A). Sites that are conserved at different amino-

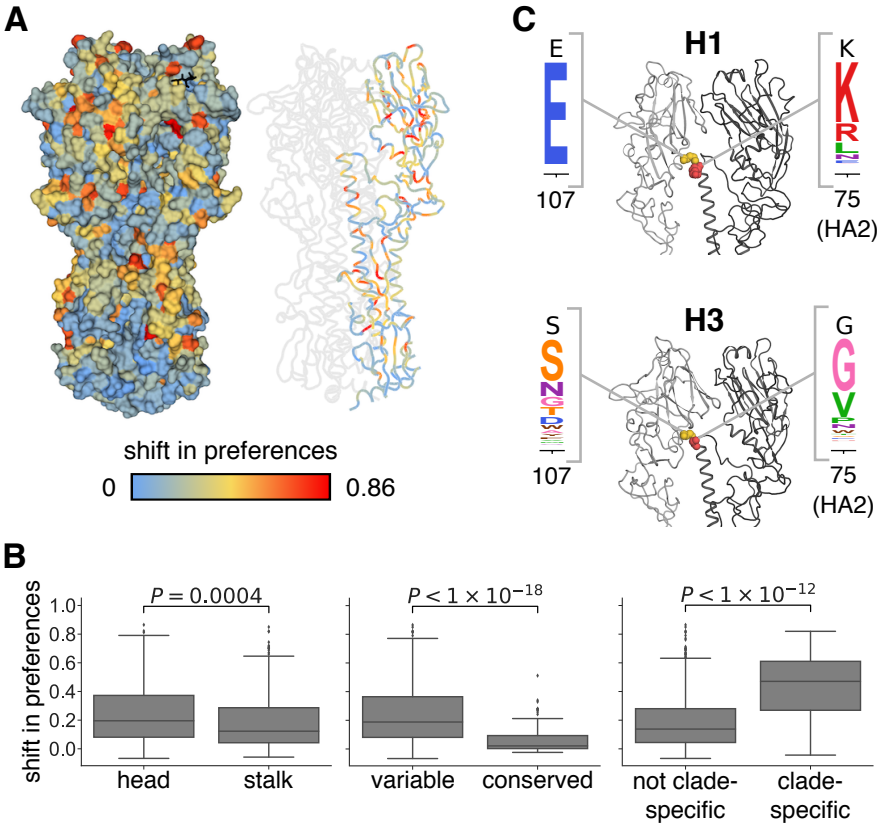

Figure 2.8: **Sites with strongly shifted amino-acid preferences between H3 and H1 HAs. (A)** The shift in amino-acid preferences between the H3 and H1 HA at each site as calculated in Figure 2.7C is mapped onto the structure of the H3 HA. **(B)** Amino-acid preferences of sites in the stalk domain are less shifted than those in the head domain. Sites absolutely conserved in all 18 HA subtypes are less shifted than other sites. Sites with one amino-acid identity in the clade containing H1, H2, H5, and H6 and another identity in the clade containing H3, H4, and H14 are more shifted than other sites. **(C)** Sites 107 and 75(HA2) help determine the different orientation of the globular head domain in H1 versus H3 HAs. These sites are shown in spheres on the structure of H1 and H3 and colored as in panel (A), and the experimentally measured amino-acid preferences in the H1 and H3 HAs are shown. One monomer is in dark gray, while the HA1 domain of the neighboring monomer is in lighter gray.

acid identities in these two clades tend to have exceptionally large shifts in amino acid preferences (Figure 2.8B). The clade containing H1 has an upward translation of the globular head relative to the clade containing H3. This structural shift has been attributed largely to the interaction between sites 107 and 75(HA2) [85, 181]. Specifically, the clade containing H1 has a taller turn in the interhelical loop connecting helix A and helix B in

the stalk domain, and this tall turn is stabilized by a hydrogen bond between Glu-107 and Lys-75(HA2) (Figure 2.8C). In deep mutational scanning of the H1 HA, site 107 has a high preference for Glu and 75(HA2) strongly prefers positively charged Lys and Arg. In contrast, the interhelical loop in H3 HA makes a sharper and shorter turn which is facilitated by a Gly at 75(HA2). In the deep mutational scanning of the Perth/2009 H3 HA, site 75(HA2) prefers Gly and to a lesser extent Val, while site 107 is fairly tolerant of mutations. Therefore, some of the shifts in HA amino-acid preferences can be rationalized in terms of changes in HA structure.

2.4 Discussion

We have measured the effects of all possible single amino-acid mutations to the Perth/2009 H3 HA on viral growth in cell culture and demonstrated that these measurements have some value for understanding the evolutionary fate of these mutations in nature. Specifically, mutations measured to be more beneficial for viral growth tend to reach higher frequencies in nature than mutations measured to be more deleterious for viral growth. The fact that our experiments can help identify evolutionary successful mutations suggests that they might inform evolutionary forecasting. In their landmark paper introducing predictive viral fitness models that accounted for both antigenic and non-antigenic mutations, Łuksza and Lässig [138] noted that the models could in principle be improved by integrating "diverse genotypic and phenotypic data" that more realistically represented the effects of specific mutations. Our work suggests that deep mutational scanning may be able to provide such data.

It is important to emphasize that measurements of viral growth in cell culture do *not* represent true fitness in nature. Indeed, a vast amount of work in virology has chronicled the ways in which experiments can select for lab artifacts or fail to capture important pressures that are relevant in nature [46, 205, 125, 227]. As an example, although we identified G78D as favorable for viral growth in cell culture, this mutation never fixes in

nature. Mutations in viral genes other than HA are also important in determining strain success [146, 176]. Given these caveats, it might seem surprising that measuring viral growth in cell culture can be informative about the success of viral strains in nature. Yet, prior to our work, there were no comprehensive studies of the functional effects of mutations to H3 HA on any property that even resembled viral fitness in nature, and modeling work has either omitted the non-antigenic effects of mutations [204, 90, 158] or assumed that all non-epitope mutations had equivalent deleterious effects [138]. The strength of our measurements are not that they perfectly capture fitness in nature, but that they are systematic and quantitative—and so represent an improvement over no information at all. We suspect that performing similar experiments using more realistic and complex selections (e.g., ferrets or primary human airway cultures) might further improve their utility and possibly their generalizability to more divergent strains.

We measured the effects of all single amino-acid mutations to a specific HA, and then generalized these measurements to other H3N2 HAs from a 50-year timespan. These generalizations will only be valid to the extent that the effects of mutations are conserved during HA's evolution. Extensive prior work has shown that epistasis can shift the effects of mutations as proteins evolve [171, 186, 83, 156, 89, 199, 198]. Our work suggests that measurements on a HA from single human H3N2 viral strain can be usefully generalized to at least some extent across the entire evolutionary history of human H3N2 HA. On the other hand, when we compared our measurements for an H3 HA to prior measurements on H1 HA, we found substantial shifts at many sites—much greater than those observed in prior protein-wide comparisons of more closely related homologs [58, 87]. Further investigation of how mutational effects shift as proteins diverge will be important for determining how broadly any given experiment can be generalized when attempting to make evolutionary forecasts.

Our work did not characterize the antigenic effects of mutations, which also play an important role in determining strain success in nature [113, 158]. However, our basic selection and deep-sequencing approach can be harnessed to completely map how mu-

tations affect antibody recognition [60, 61]. But so far, experiments using this approach have not examined antibodies or sera that are relevant to driving the evolution of H3N2 influenza [60, 61], or have used relevant sera but examined a non-comprehensive set of mutations [133]. Future experiments that completely map how HA mutations affect recognition by human sera seem likely to be especially fruitful for informing viral forecasting.

2.5 Materials and Methods

Data and computer code

Deep sequencing data are available from the Sequence Read Archive under BioSample accessions SAMN08102609 and SAMN08102610. Computer code used to analyze the data and produce the results in the paper are on GitHub at `https://github.com/jbloomlab/Perth2009-DMS-Manuscript`.

HA numbering

Sites are in H3 numbering, with the signal peptide in negative numbers, HA1 in plain numbers, and HA2 denoted with "(HA2)". Sequential 1, 2, ... numbering of the Perth/2009 HA can be converted to H3 numbering by subtracting 16 for the HA1 subunit, and subtracting 345 for the HA2 subunit.

Creation of MDCK-SIAT1-TMPRSS2 cells

When growing influenza virus in cell culture, trypsin is normally added to cleave HA into its mature form. To obviate the need for trypsin, we engineered MDCK-SIAT1 cells and MDCK-SIAT1-CMV-PB1 [20] cells to constitutively express the TMPRSS2 protease, which cleaves and activates HA in the human airways [22, 23]. The human TMPRSS2 cDNA ORF was ordered from OriGene (NM_005656) and cloned into a pHAGE2 lentiviral vector under an EF1α-Int promoter followed by an IRES driving expression of mCherry to cre-

ate plasmid pHAGE2-EF1aInt-TMPRSS2-IRES-mCherry-W. We used the lentiviral vector to transduce MDCK-SIAT1 or MDCK-SIAT1-CMV-PB1 cells, and sorted an intermediate mCherry-positive population by flow cytometry. We refer to the sorted bulk population as MDCK-SIAT1-TMPRSS2 cells or MDCK-SIAT1-CMV-PB1-TMPRSS2 cells. There is no selectable marker for the TMPRSS2; however, we maintain the cells at low passage number, and have seen no indication that they lose their ability to support the growth of viruses with H3 HAs in the absence of exogenous trypsin.

Generation of HA codon mutant plasmid libraries

HA and NA genes for the Perth/2009 viral strain were cloned from recombinant virus obtained from BEI Resources (NR-41803) into the pHW2000 [98] influenza reverse-genetics plasmids to create pHW-Perth09-HA and pHW-Perth09-NA.

We initially created a virus with the HA and NA from Perth/2009 and internal genes from WSN/1933, and passaged it in cell culture to test its genetic stability. To generate this virus, we transfected a co-culture of 293T and MDCK-SIAT1-TMPRSS2 in D10 media (DMEM, or Dulbecco's Modified Eagle Medium, supplemented with 10% heat-inactivated FBS, or Fetal Bovine Serum, 2 mM L-glutamine, 100 U of penicillin/mL, and 100 μg of streptomycin/mL) with equal amounts of pHW-Perth09-HA, pHW-Perth09-NA, the pHW18* series of plasmids [98] for all non-HA/NA viral genes, and pHAGE2-EF1aInt-TMPRSS2-IRES-mCherry-W. The next day we changed the media to influenza growth media (IGM, consisting of Opti-MEM supplemented with 0.01% heat-inactivated FBS, 0.3% BSA, 100 U of penicillin/mL, 100 μg of streptomycin/mL, and 100 μg of calcium chloride/mL (no trypsin was added since there was TMPRSS2), and then collected the viral supernatant at 72 hours post-transfection. This viral supernatant was blind passaged in MDCK-SIAT1-TMPRSS2 a total of six additional times. We isolated viral RNA from these passaged viruses and sequenced the HA gene. The passaged HA had two mutations, G78D and T212I, which enhanced viral growth as shown in Figure A.1. The HA

with these two mutations was cloned into pHW2000 [98] and pICR2 [7] to create pHW-Perth09-HA-G78D-T212I and pICR2-Perth09-HA-G78D-T212I. For all subsequent experiments, we used viruses with the HA containing these two mutations to improve titers and viral genetic stability, and this is the HA that we refer to as Perth/2009 in the manuscript text. We used all non-HA genes (including NA) from WSN/1933 to help increase titers and reduce biosafety concerns.

The codon-mutant libraries were generated in the Perth/2009 HA-G78D-T212I background using the PCR-based approach described in [17] with the primer melting-temperature modifications described in [56], using two rounds of mutagenesis. The script to design the mutagenesis primers is at `https://github.com/jbloomlab/CodonTilingPrimers`. We created three independent libraries, one for each biological replicate. The mutant variants were then cloned at high efficiency into the pICR2 [7] vector using digestion with BsmBI, ligation with T4 DNA ligase, and electroporation into ElectroMAX DH10B competent cells (Invitrogen 18290015). We obtained $>$6 million transformants for each replicate. We scraped the plates, expanded the cultures in liquid LB (Luria-Bertani Broth) + ampicillin at 37°C for 3 h with shaking, and then maxiprepped. We randomly chose 31 clones to Sanger sequence to evaluate the mutation rate (Figure A.2).

Generation and passaging of mutant viruses

The mutant virus libraries were generated using the helper-virus approach described in [59] with several modifications, most notably the cell line used. Briefly, we transfected 5×10^5 MDCK-SIAT1-TMPRSS2 cells in suspension with 937.5 ng each of four protein expression plasmids encoding the ribonucleoprotein complex (HDM-Nan95-PA, HDM-Nan95-PB1, HDM-Nan95-PB2, and HDM-Aichi68-NP) [83], and 1250 ng of one of the three pICR2-mutant-HA libraries (or the wildtype control) using Lipofectamine 3000 (ThermoFisher L3000008). We allowed the transfected cells to adhere in 6-well plates and four hours later changed the media to D10 media. Eighteen hours after transfection,

we infected the cells with the WSN/1933 HA-deficient helper virus [59] by preparing an inoculum of 500 $TCID_{50}$ per μL of helper virus (as computed on HA-expressing cells) in IGM, aspirating the D10 media from the cells, and adding 2 mL of the helper-virus inoculum to each well. After three hours, we changed the media to fresh IGM. At 24 hours after helper-virus infection, we harvested the viral supernatants for each replicate, froze aliquots at -80°C, and titered in MDCK-SIAT1-TMPRSS2 cells. The titers were 92, 536, 536, and 734 $TCID_{50}$ per μL for the three library replicates and the wildtype control, respectively.

We passaged 9×10^5 $TCID_{50}$ of the transfection supernatants at an MOI of 0.0035 $TCID_{50}$ per cell. To do this, we plated 4.6×10^6 MDCK-SIAT1-TMPRSS2 cells per dish in fifteen 15-cm dishes in D10 media, and allowed the cells to grow for 24 hours, at which time they were at $\sim 1.7 \times 10^7$ cells per dish. We replaced the media in each dish with 25 mL of an inoculum of 2.5 $TCID_{50}$ of virus per μL in IGM. Three hours post-infection, we replaced the inoculum with fresh IGM for replicates 1, 2, and 3-2. We did not perform a media change for replicate 3-1. As can be seen in Figure 2.1D, the media change does not appear to have a substantial effect, as replicate 3-1 looks comparable to the other replicates. We collected viral supernatant for sequencing 48 hours post-infection.

Barcoded subamplicon sequencing

To extract viral RNA from the three replicate HA virus libraries and the wildtype HA virus, we clarified the viral supernatant by centrifuging at 2000 x *g* for five minutes, then ultracentrifuged 24 mL of the clarified supernatant at 22,000 rpm for 1.5 h at 4°C in a Beckman Coulter SW28 rotor, and extracted RNA using the Qiagen RNeasy Mini Kit by resuspending the viral pellet in 400 μL of buffer RLT supplemented with β-mercaptoethanol, pipetting 30 times, transferring the liquid to a microcentrifuge tube, adding 600 μL 70% ethanol, and proceeding according to the manufacturer's instructions. The HA gene was reverse-transcribed with AccuScript Reverse Transcriptase (Agilent 200820) using

primers P09-HA-For (5'-AGCAAAAGCAGGGGATAATTCTATTAATC-3') and P09-HA-Rev (5'-AGTAGAAACAAGGGTGTTTTTAATTACTAATACAC-3').

We generated the HA PCR amplicons for the three plasmid libraries, the three virus libraries, the wildtype plasmid control, and the wildtype virus control using KOD Hot Start Master Mix (EMD Millipore 71842) using the PCR reaction mixture and cycling conditions described in [17] and the P09-HA-For and P09-HA-Rev primers. We prepared the sequencing libraries using a barcoded-subamplicon strategy [231] to increase the accuracy from deep sequencing. The exact details of this approach are described in [59] (also see `https://jbloomlab.github.io/dms_tools2/bcsubamp.html`). The primers used to generate the subamplicons are in Dataset S2. We performed deep sequencing on a lane of an Illumina HiSeq 2500 using 2 $\times$ 250 bp paired-end reads in rapid-run mode.

Analysis of deep sequencing data

We used the `dms_tools2` software package [18] (`https://github.com/jbloomlab/dms_tools2`, version `2.2.5`) to analyze the deep sequencing data. The algorithm used to estimate the site-specific amino-acid preferences from the deep sequencing counts is described in [18]. The amino-acid preferences for each replicate and for the re-scaled, across-replicate average are provided in Dataset S3. Computer code that performs the entirety of this analysis and shows many detailed plots about read depth and other quality control metrics is available on GitHub at `https://github.com/jbloomlab/Perth2009-DMS-Manuscript/blob/master/analysis_code/analysis_notebook.ipynb`.

Phylogenetic model comparison and fitting of a stringency parameter

For the analysis in Table 2.1, we downloaded all full-length H3 HA sequences from the Influenza Virus Resource [9], and randomly subsampled two sequences per year. These sequences were aligned using `MAFFT` [109] and used to infer a phylogenetic tree using `RAxML` [196] with a GTRCAT model of nucleotide substitution. We then used `phydms` [94]

(`https://github.com/jbloomlab/phydms`, version `2.2.2`) to fit the substitution models listed in Table 2.1.

The amino-acid preferences were re-scaled by the stringency parameter using the approach described in [94]. Note that the re-scaling simply puts the amino-acid preferences on a useful scale for visualization in logo plots, and has no effect on any of the quantitative conclusions relating the deep mutational scanning to natural evolution. The reason is that all of these conclusions use the effects of mutations as calculated using Equation 2.1, and the re-scaling simply acts as a constant multiplier on all mutational effects (e.g., a scale factor) when re-scaled preferences are converted to mutational effects.

The phylogenetic tree of HA subtypes in Figure 2.7A was generated as described in [61].

Quantification of Shannon entropy and relative solvent accessibility

We calculated Shannon entropy, h_r for site r as $h_r = -\sum_x \pi_{r,x} \log(\pi_{r,x})$, where $\pi_{r,x}$ is the preference for amino acid x at site r.

We quantified the absolute solvent accessibility of each site of the H3 HA (PDB 4O5N; [129]) or the H1 HA (PDB 1RVX; [79]) structure using DSSP [107]. We then normalized to a relative solvent accessibility using the absolute accessibilities in [210].

Quantification of mutational effects

We calculated the effects of mutations from the amino-acid preferences that were estimated from the deep mutational scanning data. The effect of mutating site r from amino acid a_1 to a_2 was calculated as

$$\log_2 \frac{\pi_{r,a_2}}{\pi_{r,a_1}} \tag{2.1}$$

where π_{r,a_1} and π_{r,a_2} are the re-scaled preferences for amino acids a_1 or a_2 at site r as shown in Figure 2.2. The WSN/1933 H1 HA amino-acid preferences

are the replicate-average values reported in [59], re-scaled by a stringency parameter of 2.05 (see `https://github.com/jbloomlab/dms_tools2/blob/master/examples/Doud2016/analysis_notebook.ipynb`).

Inference of human H3N2 phylogenetic tree and calculation of maximum mutation frequencies

To generate the tree shown in Figure A.8, we applied Nextstrain's `augur` pipeline [88] (`https://github.com/nextstrain/augur`; commit `006896d`) to publicly available H3N2 HA sequences from GISAID [188] (see Dataset S4), sampling six viruses per month over the time interval of January 1, 1968 to February 1, 2018. We aligned the resulting 2,189 HA sequences with `MAFFT` v7.310 [109] and constructed a maximum likelihood phylogeny from this alignment with `RAxML` 8.2.10 [196]. Ancestral state reconstruction and branch length timing were performed with TreeTime [182]. The phylogenetic tree is available as a JSON file on GitHub at `https://github.com/jbloomlab/Perth2009-DMS-Manuscript/blob/master/analysis_code/data/flu_h3n2_ha_1968_2018_6v_tree.json.gz`. The tree was visualized using `BALTIC` (`https://github.com/blab/baltic`).

The frequency trajectory of each individual mutation on the phylogeny is estimated following Nextstrain's augur pipeline and as first implemented in Nextflu [157]. Herein, mutation frequency dynamics are modeled according to a Brownian motion diffusion process discretized to one-month intervals. The number of viruses sampled in each interval determines the denominator of the mutation frequency calculations. Relative to a simple Brownian motion, the expectation includes an "inertia" term ϵ that adds velocity to the diffusion and the variance includes a term $x(1-x)$ to scale variance according to frequency following a Wright-Fisher population genetic process. This results in the following diffusion process

$$x(t+\mathrm{d}t) = \mathcal{N}\big(x(t) + \epsilon\,\mathrm{d}x,\ \mathrm{d}t\,\sigma^2\,x(t)\,(1-x(t))\big), \tag{2.2}$$

with 'volatility' parameter σ^2. The term $\mathrm{d}x$ is the increment in the previous timestep, so

that $\mathrm{d}x = x(t) - x(t - \mathrm{d}t)$. We used $\epsilon = 0.7$ and $\sigma^2 = 0.05$ to maximize fit to empirical trajectory behavior.

We also include a Bernoulli observation model for mutation presence / absence among sampled viruses at timestep t. This observation model follows

$$f(x,t) = \prod_{v \in V} x(t) \prod_{v \notin V} (1 - x(t)), \tag{2.3}$$

where $v \in V$ represents the set of viruses that have the mutation and $v \notin V$ represents the set of viruses that do not have the mutation. Each frequency trajectory is estimated by simultaneously maximizing the likelihood of the process model and the likelihood of the observation model via adjusting frequency trajectory $\mathbf{x} = (x_1, \ldots, x_n)$.

We also repeated the above analyses using only viruses that were sequenced directly without passaging. Routine direct sequencing did not begin until the early 2000s [145]. To construct a tree with a similar number of viruses as the original analysis, we sampled 30 viruses per month between January 1, 2000 and April 1, 2018, producing a tree with 2,374 unpassaged viruses with `augur` (commit: `6d9f708`). We included the passaged DMS strain, A/Perth/16/2009, in the resulting tree to enable comparison between pre-Perth and post-Perth clades.

Analysis of mutational shifts

To compare the Perth/2009 H3 and WSN/1933 H1 HA preferences, we first aligned the wildtype HA sequences using `MAFFT` [109]. To quantify the shifts in preference for every alignable site while accounting for experimental noise, we used the approach described in [87] and used the $\text{RMSD}_{\text{corrected}}$ values as our quantification of the extent of each shift.

For the plots shown in Figure 2.8B, any residues falling between Cys-52 and Cys-277 were defined as the head domain, and all other residues were defined as the stalk domain. We used the multiple sequence alignment of the HA subtype sequences from [61]

to identify sites that are absolutely conserved across all subtypes, or in the different clades described in Figure 2.8.

Validation of individual point mutants

To validate the viral growth of Perth/2009 HA point mutants M(-16)K, C52A, C52C, T24F, T40V, S287A, and C199(HA2)K, we used site-directed mutagenesis to introduce the amino-acid mutation into the Perth/2009 HA bidirectional reverse genetics plasmid, and verified the sequence of two clones for each mutant by Sanger sequencing. We generated these individual mutant viruses carrying GFP in the PB1 segment using a protocol described in [20, 100], and the PB2, PA, NP, NA, M, and NS segments of the A/WSN/1933 (H1N1) strain. To rescue each mutant GFP-carrying virus in duplicate, we transfected a co-culture of 4×10^5 293T-CMV-PB1 and 0.5×10^5 MDCK-SIAT1-CMV-PB1-TMPRSS2 cells with the eight reverse genetics plasmids and the pHAGE2-EF1aInt-TMPRSS2-IRES-mCherry-W plasmid. Each well received a transfection mixture of 100 μL DMEM, 3 μL BioT transfection reagent, and 250 ng of each plasmid. We changed the media in each well with 2 mL IGM eight hours post-transfection. At 53 hours post-transfection, transfection supernatants were harvested, clarified by centrifugation at 2000 $\times$ *g* for five minutes, aliquoted, and frozen at -80°C.

To titer the GFP-carrying viruses, we plated 1×10^5 MDCK-SIAT1-CMV-PB1-TMPRSS2 cells per well in 12-well plates in IGM. Four hours after plating, we infected cells with dilutions of viral supernatant. At 16 hours post-infection, we selected wells with 1 to 10% of cells that were GFP-positive and analyzed the fraction of GFP-positive cells by flow cytometry to calculate the titer of infectious particles per μL.

Acknowledgments

We thank Sarah Hilton, Hugh Haddox, and Sidney Bell for helpful discussions about data analysis, and Richard Neher for sharing analysis code and providing helpful comments

on the manuscript. We thank the Fred Hutch Genomics Core for performing the Illumina deep sequencing. This work was supported by grant R01 AI127893 from the NIAID of the NIH to JDB and TB and grant U19 AI117891 to TB. JML was supported in part by the Center for Inference and Dynamics of Infectious Diseases (CIDID), which is funded by grant U54GM111274 from the NIGMS of the NIH. The research of JDB is supported in part by a Faculty Scholar grant from the Howard Hughes Medical Institute and the Simons Foundation, and a Burroughs Wellcome Young Investigator in the Pathogenesis of Infectious Diseases grant. TB is a Pew Biomedical Scholar and is supported by NIH R35 GM119774.

Chapter 3

HOW SINGLE MUTATIONS AFFECT VIRAL ESCAPE FROM BROAD AND NARROW ANTIBODIES TO H1 INFLUENZA HEMAGGLUTININ

A version of this chapter has been previously published as:

Michael B. Doud, **Juhye M. Lee**, and Jesse D. Bloom. How single mutations affect viral escape from broad and narrow antibodies to H1 influenza hemagglutinin. *Nature Communications*, 9(1):1386, 2018.

Bold face indicates equal contribution.

3.1 Abstract

Influenza virus can escape most antibodies with single mutations. However, rare antibodies broadly neutralize many viral strains. It is unclear how easily influenza virus might escape such antibodies if there was strong pressure to do so. Here we map all single amino-acid mutations that increase resistance to broad antibodies to H1 hemagglutinin. Our approach not only identifies antigenic mutations but also quantifies their effect sizes. All antibodies select mutations, but the effect sizes vary widely. The virus can escape a broad antibody to hemagglutinin's receptor-binding site the same way it escapes narrow strain-specific antibodies: via single mutations with huge effects. In contrast, broad antibodies to hemagglutinin's stalk only select mutations with small effects. Therefore, among the antibodies we examine, breadth is an imperfect indicator of the potential for viral escape via single mutations. Antibodies targeting the H1 hemagglutinin stalk are quantifiably harder to escape than the other antibodies tested here.

3.2 Introduction

Nearly all viruses show some antigenic variation. However, the extent of this variation ranges widely. For instance, although both measles virus [15, 206] and polio virus [42, 52, 62] exhibit antigenic variation, the magnitude of this variation is small. Therefore, immunity to these viruses is lifelong [166, 183]. In contrast, human influenza virus exhibits much more antigenic variation. So although infection with an influenza virus strain provides long-term immunity to that exact strain [24, 48, 238], the virus's rapid antigenic evolution erodes the effectiveness of this immunity to that strain's descendants within $\sim$5 years [41, 118].

One possible reason that viruses exhibit different amounts of antigenic variation is that they have disparate evolutionary capacities to escape the immunodominant antibodies generated by natural immune responses [136, 35, 78]. According to this explanation, human influenza virus undergoes rapid antigenic drift because most neutralizing antibodies target epitopes on the viral hemagglutinin (HA) protein that are highly tolerant of

mutational change. This explanation is supported by classic experiments showing that it is easy to select viral mutants that escape most antibodies [236, 214], as well as by the observation that mutations that alter antigenicity arise frequently during influenza's evolution globally [113, 32, 170, 158, 217] and within individual humans with long-term infections [232]. A corollary of this explanation is that influenza virus's capacity for antigenic drift would be reduced if most antibodies instead targeted epitopes that were less mutationally tolerant.

Verifying this corollary has become of practical importance with the discovery of broadly neutralizing antibodies against influenza virus. These antibodies typically target conserved epitopes in HA's stalk [203, 67, 39] or receptor-binding site [130, 69, 185], and neutralize a wide range of viral strains. Broad antibodies are usually less abundant in human serum than antibodies to antigenically variable epitopes on the head of HA [70, 6]. However, major efforts are underway to elicit broad antibodies by vaccination or administer them directly as therapeutics [116, 38].

If these efforts succeed, the epitopes of broad antibodies could come under stronger antigenic selection in human influenza virus. Might such selection then drive antigenic variation in these epitopes? There is precedent for the idea that the immune status of the host population can shape influenza virus evolution: the virus undergoes faster antigenic drift in long-lived humans that accumulate immune memory than in short-lived swine that are mostly naive [187, 139], and poultry vaccination may accelerate antigenic drift of avian influenza [124, 30]. But alternatively, perhaps broad antibodies are broad because the virus has difficulty escaping them regardless of selection from host immunity.

So far, there is limited data to distinguish between these possibilities. Several studies have shown that the head domain of HA is more mutationally tolerant than the stalk domain where many broad antibodies bind [209, 231, 91]. However, these studies did not select for antibody escape, so it is difficult to relate their measurements to the virus's evolutionary capacity under immune selection. Other work has shown that it is possible to select antigenic mutants with broad antibodies [237, 31, 68, 77, 65, 4], demonstrating

that these epitopes are not entirely refractory to change. But given that antibodies can select some antigenic variation even in measles virus [15, 206] and polio virus [42, 52], the existence of selectable mutations does not necessarily imply that influenza virus can escape broad antibodies as easily as it drifts away from narrow strain-specific ones. The fundamental problem is that existing studies have not quantified the ease of viral escape in a way that can be compared across antibodies in an apples-to-apples fashion.

Here we systematically quantify the results of selecting all single amino-acid mutations to an H1 HA with several broad and narrow antibodies. Critically, our approach quantifies the *magnitude* of the antigenic effect of every mutation in a way that can be directly compared across antibodies. We find that even the broadest antibodies select antigenic mutations. However, the magnitudes of the antigenic effects vary greatly across antibodies. Single mutations make the virus completely resistant to both narrow strain-specific antibodies and a broad antibody that targets residues in HA's receptor-binding site. But no single mutation does more than modestly increase the virus's resistance to two broad antibodies against the HA stalk. Therefore, broad anti-stalk antibodies are quantifiably more resistant to viral escape via single amino-acid mutations than the other antibodies tested here.

3.3 Results

3.3.1 Fraction of each viral mutant that escapes neutralization

We can visualize the outcome of antibody selection on viral populations containing antigenic mutations as in Figure 3.1. If a mutation strongly escapes neutralization, then all virions with this mutation survive antibody treatment at a concentration where other virions are mostly neutralized (Figure 3.1A). This escape is manifested by a large shift in the neutralization curve for the mutant (Figure 3.1B). If we draw vertical lines through the overlaid neutralization curves, we can calculate the fraction of virions with each mutation that survive neutralization at each antibody concentration. These fractions can be repre-

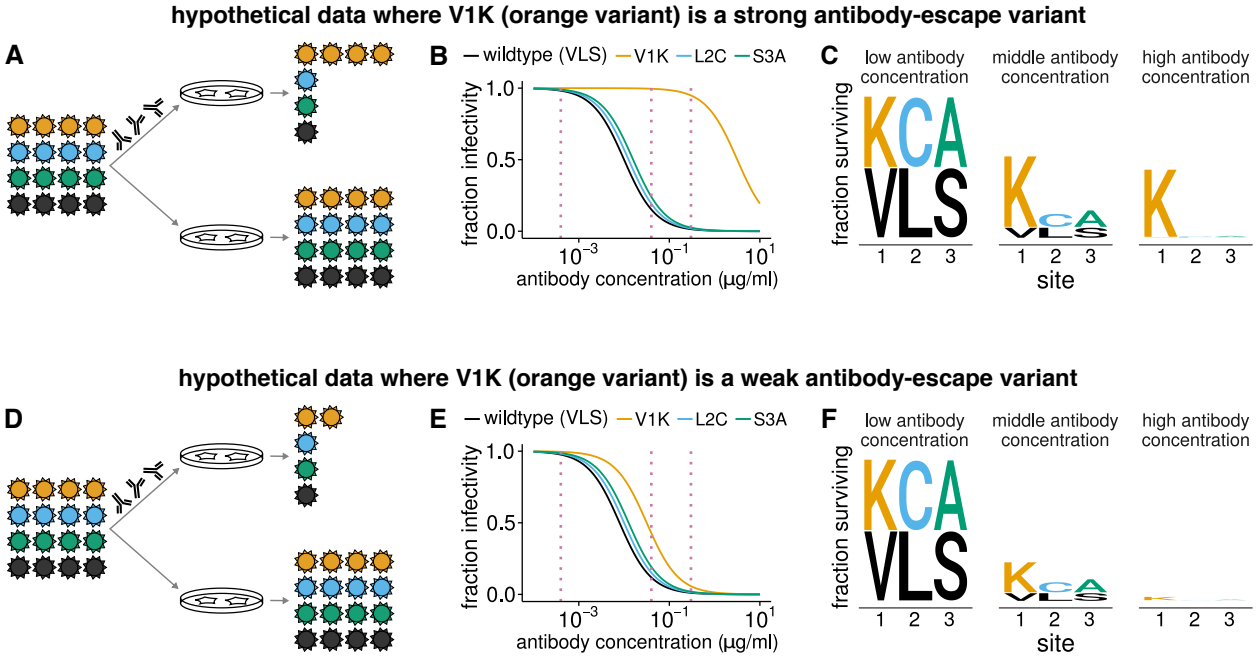

Figure 3.1: **Quantifying the fraction of virions with each mutation that escape antibody neutralization.** This figure shows hypothetical data for four viral variants. **(A)** Virions with the V1K mutation (orange) completely survive an antibody concentration where most other virions are neutralized. **(B)** This resistance is manifested by a large shift in V1K's neutralization curve. **(C)** For each dotted vertical line drawn through the neutralization curves in (B), we calculate the fraction of virions with that mutation that survive the antibody, and indicate this fraction by the height of the letter corresponding to that amino acid at that site. **(D-F)** Similar data to the first three panels, but now V1K has only a small antigenic effect, and so only modestly increases the fraction of virions that survive antibody treatment.

sented using logo plots, where the height of each letter is proportional to the fraction of virions with that amino acid at a site that survive (Figure 3.1C). Large letters correspond to strong escape mutations.

Now consider the case where a mutation has just a small antigenic effect, and so only slightly increases the fraction of virions that survive neutralization (Figure 3.1D). In this scenario, the neutralization curve shifts only slightly (Figure 3.1E). In the logo plot representation, the antigenic mutation is only slightly larger than other amino acids (Figure 3.1F), since possessing the mutation only modestly increases the chance that a virion survives antibody treatment. These logo plots therefore provide a way to both identify

antigenic mutations and quantify the magnitudes of their effects in a way that is directly comparable across antibodies.

Our goal is to determine the fraction of mutant virions that survive antibody neutralization for *all* mutations to HA. One way to do this would be to measure individual neutralization curves for each of the $19 \times 565 = 10,735$ single amino-acid mutants of the 565-residue HA protein. However, individually creating and assaying that many mutants would be exceedingly time-consuming and expensive. Fortunately, we have shown that antibody selection on all viral mutations can be assayed in a single experiment using mutational antigenic profiling [60, 56]. This approach involves generating viral libraries containing all mutations to the protein of interest, selecting these viruses with or without antibody, and using an accurate deep-sequencing method to determine the relative frequencies of each mutation.

These frequencies can be analyzed to calculate the fraction of virions with each mutation that survive antibody treatment. Specifically, the deep sequencing determines the frequencies of virions carrying amino-acid a at site r in the antibody-selected and mock-selected conditions, which we denote as $\rho_{r,a}^{\text{selected}}$ and $\rho_{r,a}^{\text{mock}}$, respectively. We can also measure the total fraction of the viral library that survives the antibody, which we denote as γ. The fraction of variants with amino-acid a at site r that survive antibody selection is then simply

$$F_{r,a} = \gamma \times \frac{\rho_{r,a}^{\text{selected}}}{\rho_{r,a}^{\text{mock}}}. \tag{3.1}$$

For instance, in Figure 3.1A, the frequency of virions with the orange mutation is $\rho_{r,a}^{\text{selected}} = \frac{4}{7}$ in the antibody selection and $\rho_{r,a}^{\text{mock}} = \frac{4}{16}$ in the mock selection. The overall fraction of virions that survive the antibody in Figure 3.1A is $\gamma = \frac{7}{16}$. Therefore, we use Equation 3.1 to calculate that the fraction of variants with the orange mutation that survive is $F_{r,a} = \frac{7}{16} \times \frac{4/7}{4/16} = 1$. Performing the analogous calculation for Figure 3.1D correctly determines that fraction of virions with the orange mutation that survive the antibody is only 0.5 for the scenario in that figure panel. In the analyses of real data below, we will plot the excess

fraction surviving *above* the overall library average, which is

$$F_{r,a}^{\text{excess}} = \max\left(0, F_{r,a} - \gamma\right). \tag{3.2}$$

Importantly, Equations 3.1 and 3.2 correct for effects on viral growth due to normalization by the mock-selected control, and so measure only antigenicity and not viral growth provided that the virus at least grows well enough to be present in the library. Details of how the calculations are extended to account for sequencing errors and sampling statistics are in the Materials and Methods. Open-source software that performs all steps in the analysis beginning with the deep sequencing data is available at `https://jbloomlab.github.io/dms_tools2/`.

3.3.2 Broad and narrow antibodies that neutralize influenza virus

We applied this approach to anti-HA antibodies with a range of breadths and epitopes. The crystal structures or sites of escape mutations selected by these antibodies are shown in Figure 3.2A. We chose two broad antibodies, FI6v3 and C179, that target the stalk of HA [39, 165, 63]. FI6v3 is extremely broad, and neutralizes both group 1 and group 2 HAs (Figure 3.2B). C179 is less broad, and neutralizes only some group 1 HAs (Figure 3.2B). We also chose a broad antibody, S139/1, that crystallographic studies have shown binds to residues in HA's receptor-binding pocket [130], and which can neutralize both group 1 and group 2 HAs [237, 130]. Finally, we re-analyzed deep sequencing data from prior mutational antigenic profiling of three narrow strain-specific antibodies, H17-L19, H17-L10, and H17-L7 [60]. These narrow antibodies bind the Ca2, Ca1, and Cb antigenic regions on HA's globular head [29], and only neutralize a narrow slice of H1 viruses.

We performed our experiments using the lab-adapted A/WSN/1933 (H1N1) strain of influenza. This strain is derived from an early seasonal H1N1 that was extensively passaged in the lab, where it adapted to become neurotropic and trypsin independent [205].

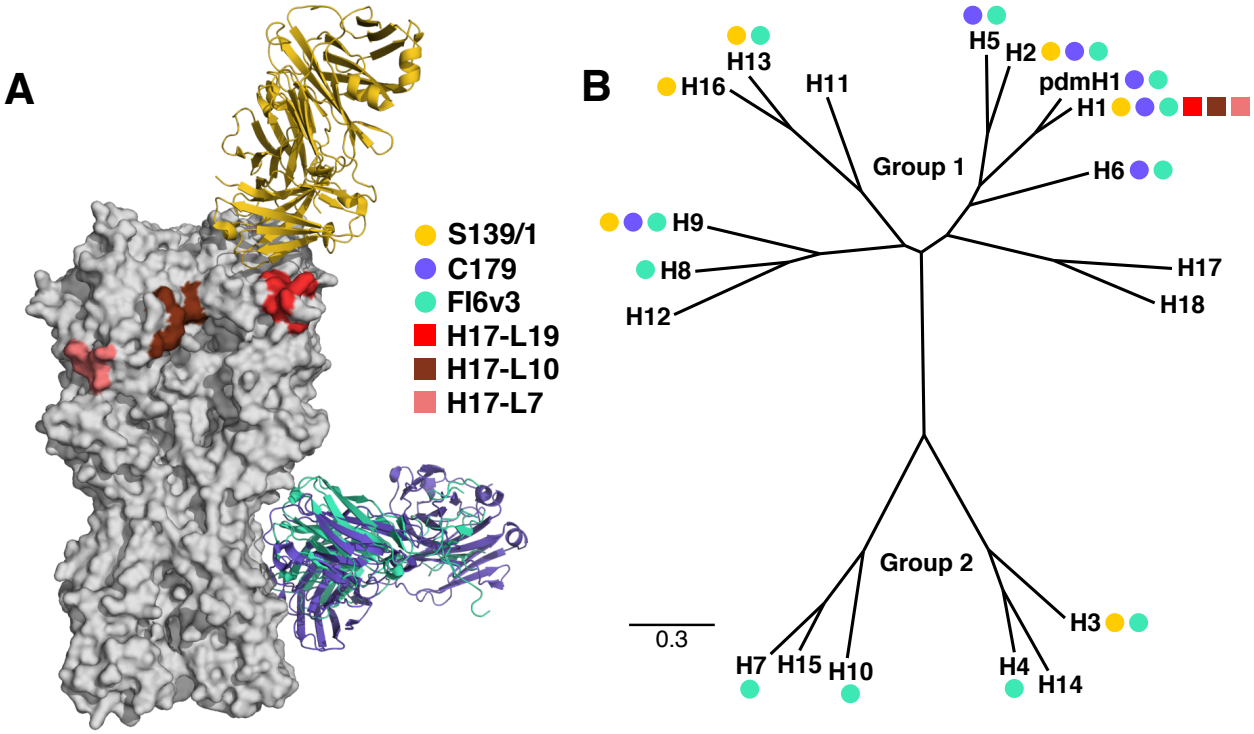

Figure 3.2: **Epitopes and breadth of broad and narrow antibodies targeting HA. (A)** Crystal structures of the broad antibodies and sites of escape mutations selected by the narrow ones superimposed on the structure of the HA trimer (PDB 1RVX [79]). S139/1 (PDB 4GMS [130]) targets residues in the receptor-binding pocket; C179 (PDB 4HLZ [63]) and FI6v3 (PDB 3ZTN [39]) target the stalk. The sites of escape mutations for H17-L19, H17-L10, and H17-L7 are those mapped by Doud et al [60]. **(B)** A phylogenetic tree of HA subtypes. Circles (broad antibodies) and squares (narrow antibodies) denote reported antibody binding or neutralization activity against that subtype. Not all antibodies have been tested against all subtypes.

But despite these unusual properties, the virus is neutralized by most broad antibodies that target other H1 viruses, including those used in this study (Figure 3.3). Our experiments utilize fully infectious influenza virus rather than pseudovirus, which is important since the accessibility of some epitopes can vary with HA density, which differs between fully infectious virus and pseudovirus [39, 106].

The wildtype virus is neutralized by all the antibodies, with IC50s between 0.01 and 1 μg/ml (Figure 3.3). However, our selections are performed on mutant virus libraries, not wildtype virus. Because these libraries have different capacities to escape each antibody,

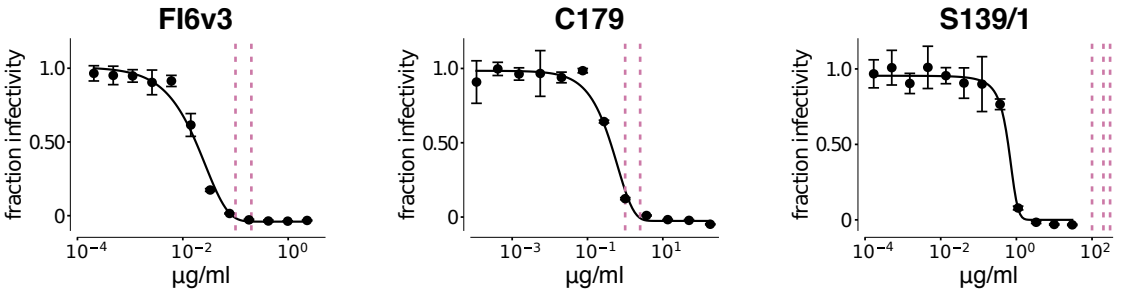

µg/ml	Avg fraction infectivity
0.1	0.016
0.2	0.0031

µg/ml	Avg fraction infectivity
1.0	0.0072
2.5	0.0025

µg/ml	Avg fraction infectivity
100	0.033
200	0.024
300	0.020

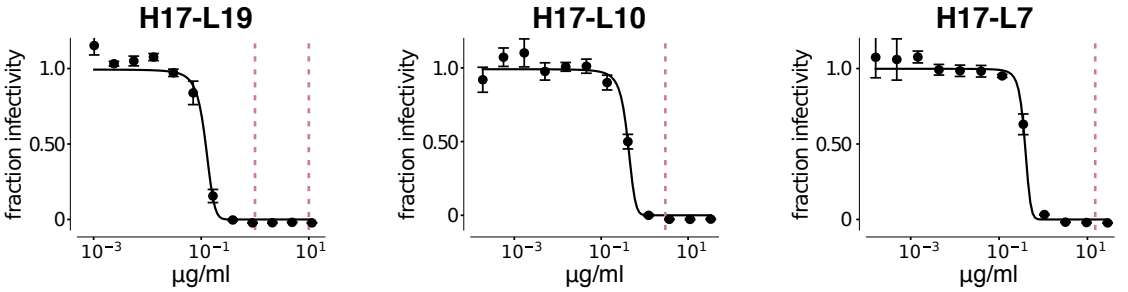

µg/ml	Avg fraction infectivity
1.0	0.013
10.0	0.0035

µg/ml	Avg fraction infectivity
3.0	0.0017

µg/ml	Avg fraction infectivity
15.0	0.0013

Figure 3.3: **Neutralization of wildtype virus by each antibody, and the fraction of mutant library virions surviving at each concentration used in our experiments.** The curves show neutralization of the wildtype A/WSN/1933 virus. Each point represents the mean and standard deviation of three measurements. The vertical dotted lines show the concentrations of antibody that were then used in the mutant virus library selections, and the tables give the overall fraction of the mutant virus libraries that survived at each concentration, determined by qRT-PCR. As described in the text, the antibody concentrations were chosen to give similar fractions of the mutant virus libraries that survive, rather than to fall at uniform positions on the neutralization curves of the wildtype virus.

the fraction of each library that survives high antibody concentrations will vary among antibodies. For instance, at concentrations that neutralize 99% of the wildtype virus, we expect a larger fraction of a library to survive an antibody for which there are many HA escape mutations than an antibody with few HA escape mutations. Therefore, rather than using the same concentration for all antibodies, we selected concentrations for each

antibody where between 2% and 0.1% of the libraries survived in order to strongly select for escape mutations (Figure 3.3). Slight differences among antibodies in the fraction surviving within this range should not strongly affect our results, since Equations 3.1 and 3.2 account for such differences via the γ term. However, to confirm the robustness of our results, we used several concentrations of each broad antibody (Figure 3.3).

3.3.3 The effects of all mutations on antibody neutralization

We performed mutational antigenic profiling using the three broad antibodies at the concentrations indicated in Figure 3.3 (the fraction of each library neutralized at each of these concentrations is listed in Supplementary Table B.1). All experiments were performed in full biological triplicate using three independently generated virus libraries carrying single amino-acid mutations to HA [59]. Importantly, as described previously [59], these virus libraries were generated by mutagenizing HA at the *codon* level rather than at the nucleotide level. Performing codon mutagenesis is important, because single-nucleotide mutations access only about a third of the possible amino-acid mutations from a given codon, whereas codon mutations access all possible amino-acid mutations.

The correlations among replicates of the mutational antigenic profiling, in terms of the measured fraction-surviving above average for each possible amino-acid mutation, are shown in Supplementary Fig. B.1. For the remainder of this paper, we will refer to the median antigenic effect of each mutation across replicates.

It is immediately obvious that the narrow strain-specific antibodies and the antibody targeting residues in HA's receptor-binding pocket (S139/1) select mutations with large antigenic effects. For all four of these antibodies, there are multiple sites in HA where mutations enable a substantial fraction of virions to survive high antibody concentrations (Figure 3.4). Specifically, there are mutations that enable over a third of virions to survive at concentrations where virtually all wildtype virions are neutralized (Supplementary Fig. B.2). Therefore, the virus can escape these four antibodies with the sort of

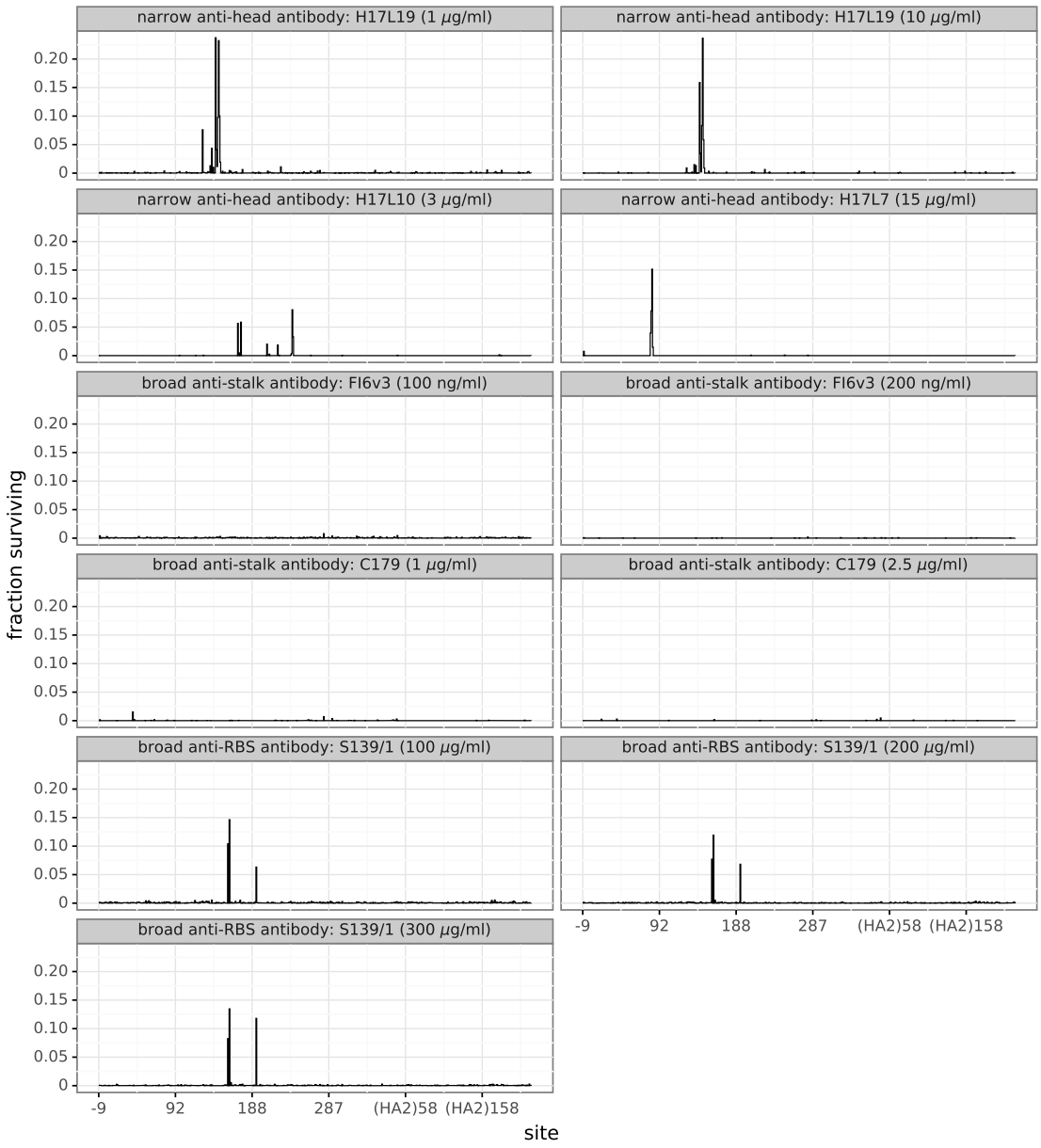

Figure 3.4: **Strain-specific and anti-receptor-binding-site antibodies select mutations with large antigenic effects, but anti-stalk antibodies only select small-effect mutations.** The excess fraction of virions with a mutation at each site that survive the antibody, averaging across all amino-acid mutations at each site (see Equation 3.10). There are multiple sites of large-effect mutations for H17L19, H17L10, H17L7, and S139/1—but none for FI6v3 and C179. Supplementary Fig. B.2 shows the excess fraction surviving for the largest-effect mutation at each site. Supplementary Figs. B.3, B.4, B.5, B.6, B.7, and B.8 show all mutations using logo plots. Sites are labeled in H3 numbering.

large-effect single amino-acid mutations that characterize traditional influenza antigenic drift [236, 214, 113, 32, 170, 158].

In contrast, the stalk-targeting antibodies C179 and FI6v3 select no strong escape mutants. If we look at the results for these antibodies on the same scale as the other antibodies, we see only a few small bumps in the fraction of virions surviving (Figures 3.4 and Supplementary Fig. B.2). Only if we zoom in can we see that there are actually a few sites where mutations slightly increase the fraction of virions surviving C179 and FI6v3 (Supplementary Figs. B.3, B.4, B.5, B.6, B.7, and B.8). But the effect sizes of these antigenic mutations are tiny compared to the other antibodies—especially for FI6v3. Therefore, the HA of A/WSN/1933 influenza virus is far less capable of escaping these anti-stalk antibodies by single mutations than it is of escaping the other four antibodies.

3.3.4 Selected mutations are near antibody binding footprints

Antigenic mutations selected by narrow strain-specific antibodies against HA are thought to occur at residues in or near the physical binding footprint of the antibody [236, 214, 29]. We examined whether this was the case for the broad antibodies used in our experiments. Figure 3.5A shows a zoomed-in view of the sites of mutations selected by each antibody, as well as their locations on HA's structure. It is immediately clear that the selected mutations are nearly all in or close to the antibody-binding footprint.

For the S139/1 antibody that targets residues in the HA receptor-binding pocket, there are strong escape mutations at sites 156, 158, and 193 (Figure 3.5A; sites are in H3 numbering). These three sites fall directly in the physical binding footprint of the antibody [130], and are the same three sites where previous work has selected escape mutants in H1, H2, and H3 HAs [237]. Our data show that numerous different amino-acid mutations at each site confer neutralization resistance. The mutation with the largest effect, G158N, introduces an N-linked glycosylation motif.

Although the anti-stalk antibodies C179 and FI6v3 only select mutations with small

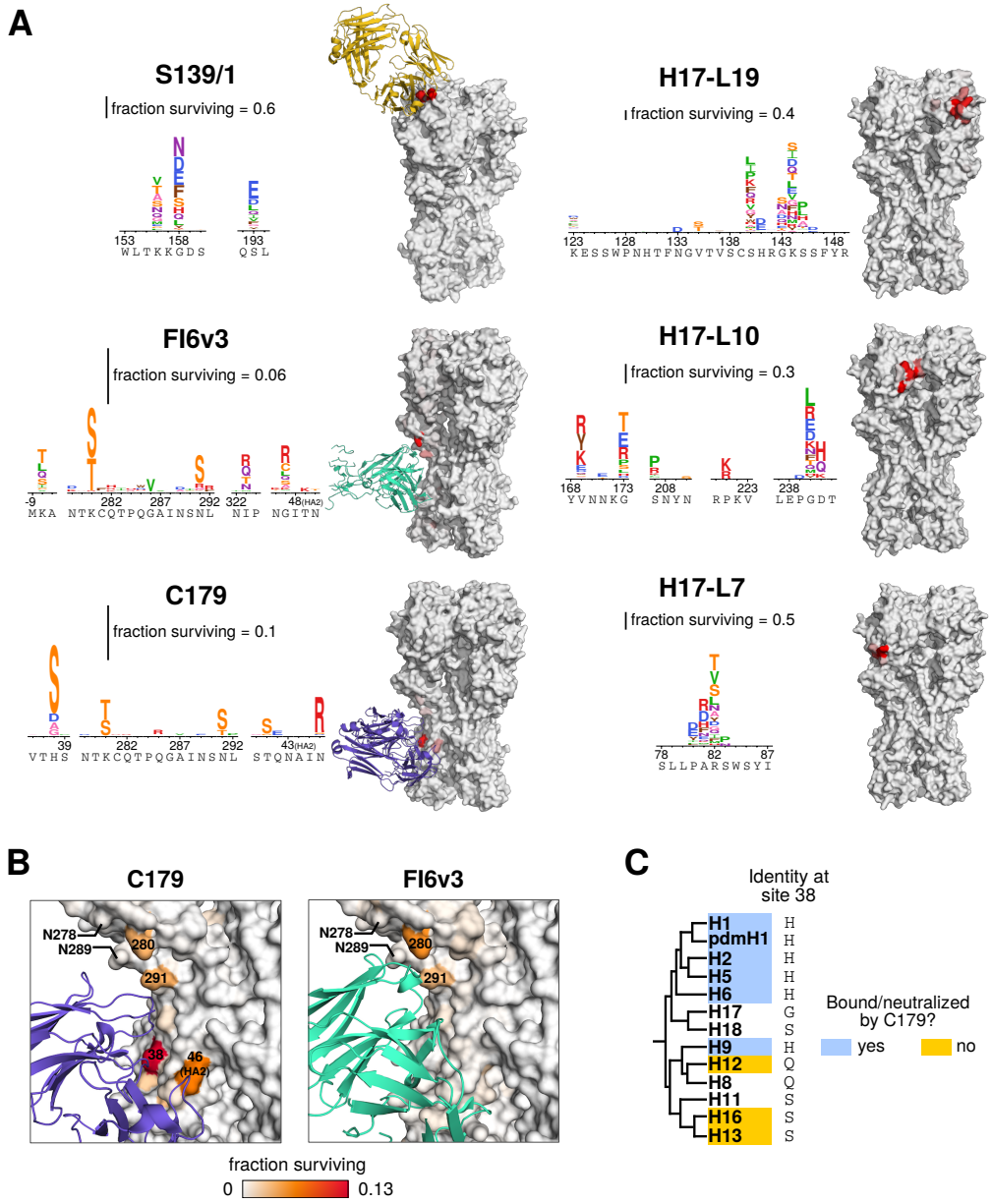

Figure 3.5: **Mutations selected by broad and narrow antibodies.** **(A)** Logo plots show sites where mutations have the largest effect. Letter heights are proportional to the excess fraction of virions with that mutation that survive antibody, as indicated by the scale bars. Structures are colored white to red by the excess fraction surviving for the largest-effect mutation at each site, with each antibody scaled separately. **(B)** Sites of selection from anti-stalk antibodies, with the same coloring scale for both antibodies. Selection for serine or threonine at sites 280 and 291 introduces glycosylation sites at 278 and 289, respectively. **(C)** Cladogram of group 1 HA subtypes. The amino acid at site 38 is indicated. Colors indicate whether a subtype has been reported in the literature to be bound or neutralized by C179.

effects, these mutations almost all fall in or near the physical binding footprints of the antibodies (Figure 3.5A). The two antibodies have similar epitopes and angles of approach [63], and they select identical mutations at several sites (Figure 3.5B). The three largest-effect mutations for FI6v3 (K280S, K280T, and N291S) all introduce glycosylation motifs near the epitope, and all three mutations have similar magnitude antigenic effects in both FI6v3 and C179.

However, C179 selects several mutations that do not have any apparent effect on FI6v3 (Figure 3.5A, Supplementary Fig. B.6). The most notable of these C179-specific mutations are at site 38. The additional breadth of FI6v3 over antibodies such as C179 that neutralize only group 1 HAs is because FI6v3 can accommodate a glycan on the asparagine at site 38 that is present in group 2 HAs [39, 203, 67]. However, the H38S mutation that has the largest effect on C179 resistance in our experiments does not introduce a glycosylation motif, showing that there are also other ways to escape anti-stalk antibodies at this site. Interestingly, group 1 HA subtypes that are susceptible to C179 tend to possess a histidine at site 38, but subtypes that are not bound or neutralized by C179 often possess a serine (Figure 3.5C).

The FI6v3 antibody also weakly selects several mutations at residue -8, which is part of HA's signal peptide (Figure 3.5A). This signal peptide is cleaved from the mature HA protein [45, 27], although mutations at this site can affect HA's expression level [164], which might conceivably affect HA density on virions and subsequently antibody neutralization [39, 106].

3.3.5 Validation by neutralization assays

Do the mutations identified in our mutational antigenic profiling actually have the expected effect on antibody neutralization? We have previously validated many of the large-effect antigenic mutations selected by the narrow antibodies H17-L19, H17-L10, and H17-L7 [60]. However, the mutations selected by the broad anti-stalk antibodies have much

smaller effects in our mutational antigenic profiling—especially for the broadest antibody, FI6v3. We therefore tested some of these FI6v3-selected mutations using neutralization assays on individual viral mutants.

Figure 3.6 shows that the mutational antigenic profiling is highly predictive of the results of the neutralization assays, even for small-effect mutations. As discussed in the previous section, the three mutations most strongly selected by FI6v3 introduce glycosylation motifs at sites 278-280 or 289-291 (Figure 3.5A,B). We created viruses carrying each of these mutations (K280S, K280T, and N291S) and validated that all three modestly but significantly increased resistance to FI6v3 (Figure 3.6A, Supplementary Fig. B.9). As a control, we also validated that a mutation at one of these sites (K280A) that does *not* have an effect in our mutational antigenic profiling does not significantly shift the neutralization curve (Figure 3.6A, Supplementary Fig. B.9).

Our mutational antigenic profiling also identified several non-glycosylation-motif mutations that were selected by FI6v3. We validated that one of these mutations, G47R in the HA2 chain, significantly increased neutralization resistance (Figure 3.6A, Supplementary Fig. B.9)—although as predicted by the mutational antigenic profiling, the magnitude of the effect was small. The most unexpected mutations identified in our mutational antigenic profiling were at site -8 in the signal peptide. We tested one of these mutations, K(-8)T, and it did lead to a very slight increase in neutralization resistance (Figure 3.6A, Supplementary Fig. B.9)—although despite the significance testing in Supplementary Fig. B.9, we remain circumspect about the magnitude of this effect relative to the noise in our neutralization assays. As controls, we also tested three mutations (P80D and V135T, which are escape mutations for H17-L7 and H17-L19, and M17L in HA2) that did *not* have substantial effects in the mutational antigenic profiling, and confirmed that none of them significantly affected neutralization resistance (Figure 3.6A, Supplementary Fig. B.9).

A notable aspect of these validation experiments is the very small effect sizes of the identified mutations on neutralization by FI6v3. Antigenic mutations selected by strain-specific antibodies to HA generally increase the concentration of antibody needed to

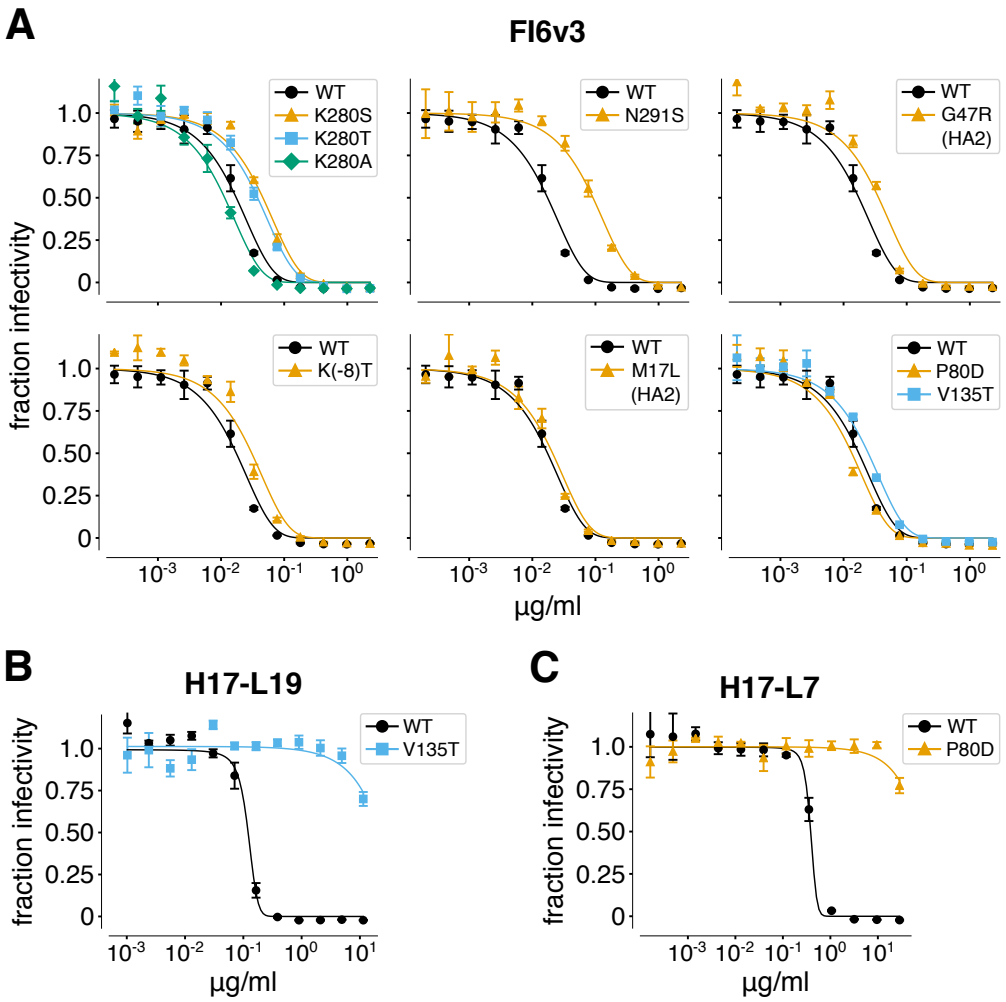

Figure 3.6: **The mutations selected by FI6v3 increase neutralization resistance, but the effects are small. (A)** Neutralization curves of individual viral mutants with FI6v3. The mutations K280S, K280T, N291S, G47R (HA2), and K(-8)T are all expected to increase neutralization resistance based on the mutational antigenic profiling (Figure 3.5A), whereas K280A, M17L (HA2), P80D, and V135T are *not* expected to affect neutralization (Supplementary Fig B.6). All neutralization curves in this panel were performed in triplicate on the same day. This panel shows the average of the replicates; Supplementary Fig. B.9 shows the curves for each replicate individually and performs statistical testing of whether the IC50s for mutants are significantly different than for wildtype. **(B), (C)** In contrast to FI6v3, mutations selected by narrow antibodies have very large effects on neutralization. Shown are neutralization curves for representative escape mutants from H17-L19 and H17-L7 taken from Doud et al [60]. Points indicate mean and standard error of three replicates.

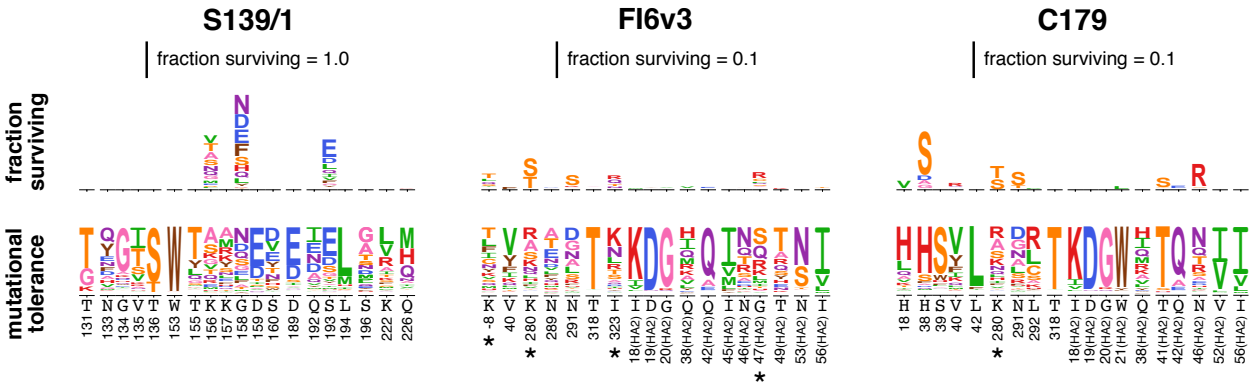

Figure 3.7: **Mutational tolerance of HA sites in the antibody-binding footprints.** These plots show all HA sites within 4 Å of the antibody in the crystal structure, plus any additional sites (marked with a *) where we identified antigenic mutations. The logo plots at bottom show the preference of each HA site for each amino acid under selection for viral replication as measured by Doud and Bloom [59]. For instance, site 153 only tolerates tryptophan, so W occupies the entire height of the preference logo stack. In contrast, site 156 tolerates many amino acids, all of which contribute to the height of the preference logo stack. Above the preference logo stacks are logo plots showing the excess fraction surviving antibody treatment as measured in the current study. Note that scale for these antigenic effects is 10$\times$ smaller for FI6v3 and C179 than for S139/1.

neutralize the virus by orders of magnitude. Neutralization curves for such large-effect escape mutants are in Figure 3.6B,C. Although there are no such large-effect single mutations that escape FI6v3 or C179, the results in Figure 3.6A show that we can still use mutational antigenic profiling to identify mutations that have small but measurable effects on resistance to these antibodies.

3.3.6 HA mutational tolerance and antibody escape

Why are there no large-effect escape mutations from the anti-stalk antibodies? One possibility is that all HA sites in the antibody-binding footprint are intolerant of mutations, meaning that viruses with mutations at these sites cannot replicate and so are not present in our mutant virus libraries. Another possibility is that mutations are tolerated at some HA sites in the antibody footprint, but that the binding energetics are distributed across sites in such a way that none of these tolerated mutations strongly affect neutralization.

We can examine these possibilities using deep mutational scanning data that measures the tolerance of HA for each possible amino-acid mutation. Specifically, we have previously selected our A/WSN/1933 virus HA mutant libraries for variants that can replicate in cell culture, and then used deep sequencing to estimate the preference of each site in HA for each possible amino acid [59]. Figure 3.7 shows these amino-acid preferences for all sites in HA within 4 Å of each broad antibody, with the antigenic effects of the mutations overlaid. Although some HA sites in the antibody footprints strongly prefer a single amino acid, for all antibodies there are also footprint sites that tolerate a fairly wide range of amino acids. In most cases the mutations selected by the antibodies occur at these mutationally tolerant sites. However, there are exceptions—for instance, the H38S mutation selected by C179 is rather disfavored with respect to viral growth, but has a large enough antigenic effect to still be detected in our mutational antigenic profiling.

The data in Figure 3.7 show that the lack of large-effect escape mutants from FI6v3 and C179 is not entirely due to the mutational intolerance of HA sites in the antibody-binding footprints. Some HA sites in each antibody footprint are fairly mutationally tolerant, and contain a range of mutations in the viral libraries used in our antibody selections. However, our mutational antigenic profiling shows that only a fraction of mutations at a fraction of these sites actually affect antibody neutralization. This finding is reminiscent of prior work showing that the binding energetics at protein-protein interfaces can be asymmetrically distributed across sites [104, 43, 44]. The broad anti-stalk antibodies therefore appear to both mostly target mutationally intolerant sites and distribute their binding energetics in such a way that altering the mutationally tolerant HA sites has relatively little effect on neutralization.

3.4 Discussion

We have quantified how all single amino-acid mutations to an H1 influenza virus HA affect neutralization by a collection of broad and narrow antibodies. Our results show that the

virus's inherent evolutionary capacity for escape via point mutations differs across antibodies. Interestingly, antibody breadth is not always an indicator of the difficulty of viral escape. As expected, single amino-acid mutations can make the virus completely resistant to narrow strain-specific antibodies against HA's globular head. However, such mutations can also enable the virus to escape the broad S139/1 antibody targeting residues in HA's receptor-binding pocket, despite the fact that this antibody neutralizes multiple subtypes. But no single mutation has a comparably large effect on neutralization by two broad antibodies targeting HA's stalk, FI6v3 and C179. Therefore, these anti-stalk antibodies are quantifiably more difficult for the virus to escape.

Although there are no large-effect escape mutations from the broad anti-stalk antibodies, there are mutations that more modestly affect neutralization. This finding emphasizes the importance of identifying antigenic mutations in a way that accounts for effect sizes. The classic approach for selecting escape mutations involves treating a virus stock with antibody at a concentration that completely neutralizes wildtype, and looking for viral mutants that survive this treatment [236, 214]. There are no such single mutations for the H1 HA and broad anti-stalk antibodies tested here, since no mutations shift the neutralization curve enough to enable survival at antibody concentrations that fully neutralize wildtype. However, our approach shows that there are mutations that have more modest ($<$10-fold) effects on neutralization by even the broadest antibody. Interestingly, most previous studies [31, 68, 77, 65] that have reported selecting single mutations with large effects ($\gg$10-fold) on neutralization by anti-stalk antibodies have used group 2 (e.g., H3 or H7) HAs rather than group 1 HAs like the one used in our work—although at least one study has selected a large-effect escape mutation to a broad anti-stalk antibody in an H5 group 1 HA [208]. In addition, when interpreting the magnitude of the effects measured in our experiments, it is important to note that we are only assessing how mutations affect neutralization, and not how they affect Fc-mediated functions that are responsible for much of the *in vivo* protection afforded by anti-stalk antibodies [54, 53].

Another important caveat is that our experiments examine *single* amino-acid mutations

to the HA from one influenza virus strain. The protein evolution literature is full of examples of epistatic interactions that enable multiple mutations to access phenotypes not accessible by single mutations [83, 89, 198]. Such epistasis is relevant to HA's evolution. For instance, work by Das et al [47] suggests that the sequential accumulation of mutations can shift the spectrum of available antibody-escape mutations. Wu et al [230] have used deep mutational scanning to directly demonstrate that rampant epistasis enables HA's receptor-binding pocket to accommodate combinations of individually deleterious mutations, some of which affect sensitivity to antibodies. Therefore, our work does not imply any absolute limits on the possibilities for antibody escape when evolution is given sufficient time to explore combinations of mutations. However, single mutations are the most accessible form of genetic variation, and much of influenza virus's natural antigenic drift involves individual mutations that reduce sensitivity to immunodominant antibody specificities [236, 214, 113, 32, 170, 158]. Quantifying the antigenic effects of all such mutations therefore provides a relevant measure of ease of viral antibody escape.

A major rationale for studying broadly neutralizing antibodies is that they are hoped to be more resistant to viral evolutionary escape than the antibodies that dominate natural immune responses to influenza virus [116, 38]. We have used a new approach to quantify the extent to which this is actually true, and shown that neutralization of an H1 virus by broad anti-stalk antibodies is indeed more—although certainly not completely—resistant to erosion by viral point mutations. Going forward, we suggest that completely mapping viral escape mutations will be a useful complement to more traditional techniques that simply characterize the breadth of anti-viral antibodies against circulating strains.

3.5 Materials and Methods

Antibodies

C179 IgG was purchased from Takara Bio Inc (Catalog #M145). FI6v3 was purified from 293F cells (ThermoFisher R79007) transduced with a lentiviral vector encoding a com-

mercially synthesized gene for the IgG form of the antibody, with the heavy and light chains reverse-translated from the protein sequence in the PDB structure 3ZTN [39] as described previously [8]. Genes encoding S139/1 in IgG form were were reverse-translated from the protein sequence in PDB structure 4GMS [130], and used to express and purify protein by the Fred Hutchinson Cancer Research Center protein expression core.

Neutralization assays

We performed neutralization assays using influenza viruses that carried GFP in the PB1 segment. These PB1flank-eGFP were generated in co-cultures of 293T-CMV-PB1 and MDCK-SIAT1-CMV-PB1 cells as described previously [20], using the standard bi-directional pHW181-PB2, pHW182-PB1, pHW183-PA, pHW184-HA, pHW185-NP, pHW186-NA, pHW187-M and pHW188-NS reverse-genetics plasmids [98] for all genes *except* PB1, plus the pHH-PB1flank-eGFP plasmid [20]. Each mutant was generated by repeating this process using a version of the pHW184-HA plasmid that had been engineered by site-directed mutagenesis to carry the indicated mutation. The neutralization assays themselves were performed by using a plate reader to quantify the GFP signal produced by MDCK-SIAT1-CMV-PB1 cells infected by PB1flank-eGFP virus that had been incubated with the indicated antibody concentration as described previously [100]. All neutralization curves in Figure 3.6A represent the mean and standard deviation of three measurements, with the individual replicates shown in Supplementary Fig. B.9. All the neutralization assays for FI6v3 were performed on the same day to eliminate batch effects, with each replicate involving independent serial dilution of the antibody in a separate column of a 96-well plate.

H3 sequence numbering

Unless otherwise indicated, all residues are numbered in the H3 numbering scheme, with the signal peptide in negative numbers, the HA1 subunit as plain numbers, and

the HA2 subunit denoted with "(HA2)". The conversion between sequential numbering of the A/WSN/1933 HA and the H3 numbering scheme was performed using the Python script available at `https://github.com/jbloomlab/HA_numbering`. Supplementary File S5 gives the numbering conversion.

Inference of HA phylogenetic tree

To infer the phylogenetic tree in Figure 3.2, we downloaded one HA sequence per subtype from the Influenza Research Database [239], inferred the phylogenetic tree using `RaxML` [197] with a GTR model, and visualized the tree using FigTree (`http://tree.bio.ed.ac.uk/software/figtree/`). The HA sequences used are in Supplementary File S6. In Figure 3.2, we indicate which HAs each antibody has been reported to bind or neutralize [237, 130, 165, 63, 39]. Among broad antibodies, S139/1 has not been tested against H8 and H11; C179 has not been tested against H8 and H11; and no antibodies have been tested against H17 and H18. The narrow H17-L19, H17-L10, and H17-L7 antibodies have not been tested against any other subtypes—however, since these antibodies have a very limited range even among H1 HAs [29], we assume that they do not bind other subtypes.

For the cladogram in Figure 3.5C, the amino-acid identities at site 38 are from the strains tested against C179 by by Dreyfus et al [63]. For subtypes not tested, the amino-acid identity reported is that in the strain for that subtype in Supplementary File S6.

Mutant virus libraries

The mutant virus libraries are those described in Doud and Bloom [59], and were produced in full biological triplicate. Briefly, these libraries were generated by using codon mutagenesis [17] to introduce random codon mutations into plasmid-encoded HA, and then using a helper-virus strategy that avoids the bottlenecks associated with standard influenza reverse genetics to create the virus libraries. Although a helper virus is used to generate the libraries from plasmids, the viruses in the resulting library carry the full

complement of genes and are fully infectious and replication-competent [59]. This fact is important, since the accessibility of HA epitopes can depend on virion HA density, which is often lower in pseudovirus than in fully infectious virus [39, 106]. Full details of the library generation and sequencing statistics that quantify how completely each of the triplicate libraries covers the possible amino-acid mutations have been described previously [59].

Mutational antigenic profiling

The mutational antigenic profiling was performed as described previously [60]. Briefly, we diluted each of the virus libraries to a concentration of 10^6 $TCID_{50}$ per ml and incubated the virus dilutions with an equal volume of antibody at the intended concentration at 37°C for 1.5 hours. The final antibody concentrations in these mixtures are shown in Figure 3.3. We performed three fully independent replicates of each selection using the three replicate mutant virus libraries. In addition, we performed technical replicates (independent neutralization experiments on the *same* virus library) in some cases as indicated in Supplementary Fig. B.1. The virus-antibody mixtures were used to infect cells, and viral RNA was extracted, reverse-transcribed, and PCR amplified as described previously [60]. In order to obtain high accuracy in the Illumina deep sequencing, we used the barcoded-subamplicon sequencing strategy described by Doud and Bloom [59], which is a slight modification of the strategy of Wu et al [231].

We also estimated the overall fraction of virions surviving each antibody selection. These fractions are denoted by γ in this paper. The average of these fractions across libraries are reported in Figure 3.3, and the values for each individual replicate are in Supplementary Table B.1. The fractions were estimated using qRT-PCR against the viral NP and canine GAPDH as described previously [60]. Briefly, we made duplicate 10-fold serial dilutions of each of the virus libraries to use as a standard curve of infectivity. We also performed qPCR on the cells infected with the virus-antibody mix. To estimate the fractions, we used linear regression to fit a line relating logarithm of the viral infectious

dose in the standard curve to the difference in Ct values between NP and GAPDH, and then interpolated the fraction surviving for each selection from this regression.

Analysis of deep sequencing data

The deep sequencing data were analyzed using version 2.2.1 of the `dms_tools2` software package [18], which is available at `http://jbloomlab.github.io/dms_tools2`. Supplementary File S7 contains a Jupyter notebook that performs all steps of the analysis beginning with downloading the FASTQ files from the Sequence Read Archive. Detailed statistics about the sequencing depth and error rates are shown in this Jupyter notebook and its HTML rendering in Supplementary File S8.

Calculating fraction of mutants that survive neutralization

In prior mutational antigenic profiling work [60, 56], we calculated the differential selection on each mutation as the logarithm of its enrichment relative to wildtype in an antibody-selected sample versus a mock-selected control. These *mutation differential selection* values are useful for the analysis of individual experiments. However, there is no natural way to compare these values across experiments with different antibodies at different concentrations, since the strength of differential selection depends on details of how the pressure is imposed. We therefore developed the new approach in this paper to quantify the antigenic effect of a mutation in units that can be compared across antibodies and concentrations.

The general principle of the calculations is illustrated in Figure 3.1 and discussed in the first section of the Results. Here we provide details on how these calculations are performed. The deep sequencing measures the number of times that codon x is observed at site r in both the antibody-selected and mock-selected conditions. Denote these counts as $n_{r,x}^{\mathrm{selected}}$ and $n_{r,x}^{\mathrm{mock}}$, respectively. We also perform deep sequencing of a control (in this case, plasmid DNA encoding the wildtype HA gene) to estimate the sequencing error

rate. Denote the counts of codon x at site r in this control as $n_{r,x}^{\text{err}}$. Also denote the total reads at each site r in each sample as $N_r^{\text{selected}} = \sum_x n_{r,x}^{\text{selected}}$, $N_r^{\text{mock}} = \sum_x n_{r,x}^{\text{mock}}$, and $N_r^{\text{err}} = \sum_x n_{r,x}^{\text{err}}$.

We first estimate the rate of sequencing errors at site r as

$$\epsilon_{r,x} = \frac{n_{r,x}^{\text{err}}}{N_r^{\text{err}}}. \tag{3.3}$$

For the wildtype identity at site r, which we denote as $\text{wt}(r)$, the value of $\epsilon_{r,\text{wt}(r)}$ is the fraction of times we correctly observe the wildtype identity $\text{wt}(r)$ at site r versus observing some spurious mutation. For all mutant identities $x \neq \text{wt}(r)$ at site r, $\epsilon_{r,x}$ is the fraction of times we observe the mutation x at site r when the identity is really wildtype. We ignore second-order terms where we incorrectly read one mutation as another, as such errors will be very rare as mutations themselves are rare (most codons are wildtype in most sequences).

We next adjust all of the deep sequencing codon counts in the antibody-selected and mock-selected conditions by the error control. Specifically, the error-adjusted counts for the antibody-selected sample are

$$\hat{n}_{r,x}^{\text{selected}} = \begin{cases} \max\left[N_r^{\text{selected}} \times \left(\frac{n_{r,x}^{\text{selected}}}{N_r^{\text{selected}}} - \epsilon_{r,x}\right), 0\right] & \text{if } x \neq \text{wt}(r) \\ n_{r,x}/\epsilon_{r,x} & \text{if } x = \text{wt}(r). \end{cases} \tag{3.4}$$

An equivalent equation is used to calculate $\hat{n}_{r,x}^{\text{mock}}$. We then sum the error-adjusted codon counts for each amino acid a:

$$\hat{n}_{r,a}^{\text{selected}} = \sum_{\{x|\mathcal{A}(x)=a\}} \hat{n}_{r,x}^{\text{selected}}, \tag{3.5}$$

so that $\hat{n}_{r,a}^{\text{selected}}$ are the error-adjusted counts for the antibody-selected condition summed across all codons x where the encoded amino acid $\mathcal{A}(x)$ is a. An equivalent equation is

used to calculate $\hat{n}_{r,a}^{\text{mock}}$.

Finally, we use these error-adjusted amino-acid counts to estimate the mutation frequencies $\rho_{r,a}^{\text{selected}}$ and $\rho_{r,a}^{\text{mock}}$ that are used in Equation 3.1 to calculate the fraction $F_{r,a}$ of virions with amino acid a at site r that survive the selection. When estimating these mutation frequencies, we add a pseudocount of $P = 5$ to the lower-depth sample, and a depth-adjusted pseudocount to the higher depth sample. The rationale for adding a pseudocount is to regularize the estimates in the case of low counts. Specifically, we estimate the mutation frequencies as

$$\rho_{r,x}^{\text{selected}} = \frac{n_{r,x}^{\text{selected}} + f_{r,\text{selected}} \times P}{N_r^{\text{selected}} + f_{r,\text{selected}} \times P \times A} \tag{3.6}$$

$$\rho_{r,x}^{\text{mock}} = \frac{n_{r,x}^{\text{mock}} + f_{r,\text{mock}} \times P}{N_r^{\text{mock}} + f_{r,\text{mock}} \times P \times A} \tag{3.7}$$

where A is the number of characters (e.g., 20 for amino acids), $f_{r,\text{selected}}$ and $f_{r,\text{mock}}$ are the pseudocount adjustment factors defined as:

$$f_{r,\text{selected}} = \max\left(1, \frac{N_r^{\text{selected}}}{N_r^{\text{mock}}}\right) \tag{3.8}$$

$$f_{r,\text{mock}} = \max\left(1, \frac{N_r^{\text{mock}}}{N_r^{\text{selected}}}\right). \tag{3.9}$$

The pseudocount adjustment factors ensure that P is added to the counts for the lower depth sample, and a proportionally scaled-up pseudocount is added to the higher depth sample. The depth scaling is necessary to avoid systematically biasing towards higher mutation frequencies in the lower depth sample. It is these estimated mutation frequencies that are used in conjunction with γ (the qPCR estimated overall of virions that survive selection) to compute the fraction surviving ($F_{r,a}$) and excess fraction surviving above the library average ($F_{r,a}^{\text{excess}}$) via Equations 3.1 and 3.2.

In some cases, we need to summarize the excess fraction of mutations surviving into a single number for each site, such as for plotting as a function of the site number or

displaying on the crystal structure. There are 19 different $F_{r,a}^{\text{excess}}$ values for non-wildtype amino acids for each site. One summary statistic is the fraction surviving above the library average *averaged* over all 19 amino-acid mutations at site r:

$$\mathcal{F}_r^{avg} = \frac{1}{19} \sum_{\{a|a \neq \text{wt}(r)\}} F_{r,a}^{\text{excess}}. \tag{3.10}$$

Another summary statistic is the *maximum* fraction surviving above average among all 19 amino-acid mutations at site r:

$$\mathcal{F}_r^{max} = \frac{1}{19} \max_{\{a|a \neq \text{wt}(r)\}} \left(F_{r,a}^{\text{excess}}\right). \tag{3.11}$$

In this paper, Supplementary Figs. 3.4 and B.2 show the median of excess fraction surviving taken across all biological and technical replicates at a given antibody concentration (Equation 3.2). The subsequent logo plots show the medians of these values taken across all concentrations for each antibody. The numerical values plotted in these logo plots are in Supplementary File S9. The fraction surviving values *not* adjusted to be in excess of the library average (Equation 3.1) are in Supplementary File S10.

Code that performs these fraction surviving analyses has been added to the `dms_tools2` software package [18] which is available at `http://jbloomlab.github.io/dms_tools2`.

Data availability and source code

Deep sequencing data are available from the Sequence Read Archive under BioSample accession SAMN05789126 at `https://www.ncbi.nlm.nih.gov/sra/?term=SAMN05789126`. Computer code that analyzes these data to generate all the results described in this paper is in Supplementary File S7, and an HTML version of the analysis notebook is in Supplementary File S8. In addition, all of this code as well as the manuscript itself and other data are available on GitHub at `https://github.com/`

jbloomlab/HA_antibody_ease_of_escape. Finally, the dms_tools2 software [18] that performs most of the analysis is available at https://jbloomlab.github.io/dms_tools2/.

Acknowledgments

We thank Adam Dingens, Sarah Hilton, Katherine Xue, Lauren Gentles, and Jeremy Roop for helpful comments on the project and manuscript. We thank the Fred Hutchinson Cancer Research Center genomics core for performing the Illumina deep sequencing, and the protein expression core for expressing and purifying the S139/1 antibody. This work was supported by grant R01AI127893 from the NIAID of the NIH. MBD was supported in part by training grant T32AI083203 from the NIAID of the NIH. JML was supported in part by the Center for Inference and Dynamics of Infectious Diseases (CIDID), which is funded by grant U54GM111274 from the NIGMS of the NIH. The research of JDB is supported in part by a Faculty Scholar Grant from the Howard Hughes Medical Institute and the Simons Foundation.

Chapter 4

MAPPING PERSON-TO-PERSON VARIATION IN VIRAL MUTATIONS THAT ESCAPE POLYCLONAL IMMUNITY TO INFLUENZA HEMAGGLUTININ

A version of this chapter has been previously published as:

Juhye M. Lee, Rachel Eguia, Seth J. Zost, Saket Choudhary, Terry Stevens-Ayers, Michael Boeckh, Aeron Hurt, Seema S. Lakdawala, Scott E. Hensley,and Jesse D. Bloom. Mapping person-to-person variation in viral mutations that escape polyclonal immunity to influenza hemagglutinin. *bioRxiv*, 2019.

4.1 Abstract

A longstanding question is how influenza evolves to escape human immunity, which is polyclonal and can target many distinct epitopes on the virus. Here we map how all amino-acid mutations to influenza's major surface protein affect viral neutralization by polyclonal human sera. The serum of some individuals is so focused that it selects single mutations that reduce viral neutralization by over an order of magnitude. However, different viral mutations escape the sera of different individuals. This individual-to-individual variation in viral escape mutations is *not* present for ferrets, which are frequently used as a model in influenza studies. Our results show how different single mutations help influenza escape the immunity of different members of the human population, a phenomenon that could shape viral evolution and disease susceptibility.

4.2 Introduction

Infection of humans with influenza virus elicits potent neutralizing antibodies targeting the viral hemagglutinin (HA) protein. These antibodies provide long-lasting immunity against the exact viral strain that elicited them [40, 48, 41, 238, 115]. Unfortunately, the effectiveness of this immunity against future strains is rapidly degraded by viral antigenic evolution [13, 191], such that the typical human is infected by influenza virus roughly every five years [41, 118, 177].

Classic studies of this evolutionary process demonstrated that it is easy to experimentally select mutant viruses that escape neutralization by individual monoclonal antibodies [236, 123, 214, 80]. But these same studies also found that monoclonal antibodies target a variety of non-overlapping regions on HA, such that no single viral mutation can escape a mix of antibodies targeting distinct regions [236, 123, 214, 29]. This work therefore posed a perplexing question: given that human immunity is polyclonal, how does influenza virus evolve to escape all the myriad antibody specificities in human sera?

Several explanations have been suggested for this conundrum. One explanation pro-

poses that polyclonal immunity does not actually select mutations that abrogate antibody binding, but rather mutations that increase receptor avidity to provide generalized resistance to neutralization [235, 93]. Another explanation proposes that human immunity is sufficiently focused on one epitope in HA that single viral mutations can appreciably reduce binding by the mix of antibodies in polyclonal sera. This latter explanation has been shown to be true for the immunity of certain individuals against H1N1 influenza [135, 101, 49]. Further support for the idea of focused human immunity comes from mass spectrometry studies showing that HA-binding antibodies in serum after influenza vaccination are often dominated by relatively few "clonotypes" [126, 127], and by escape-mutant selections that have isolated viral mutants with enhanced resistance to human sera [49, 51, 133]. However, none of these studies have systematically characterized the selection that neutralizing human immunity imposes on influenza virus.

Here we harness mutational antigenic profiling [60, 61] to map how all amino-acid mutations to HA affect neutralization of H3N2 influenza virus by human serum. We show that human serum can select single mutations that reduce viral neutralization by over an order of magnitude. Although the escape mutations usually occur in a similar region on HA's globular head, there is remarkable person-to-person variation in their antigenic effect: it is common for a mutation that reduces neutralization by $>$10-fold for one individual's serum to have little effect for another individual's serum. Our work suggests that person-to-person variation in the fine specificity of anti-influenza immunity may play a major role in shaping viral evolution and disease susceptibility.

4.3 Results

4.3.1 Mutational antigenic profiling comprehensively maps immune-escape mutations

Prior work studying immune selection from polyclonal sera has used escape-mutant selections, which simply isolate individual mutant viruses with reduced neutralization sensitivity. As a more comprehensive alternative, we recently developed mutational antigenic

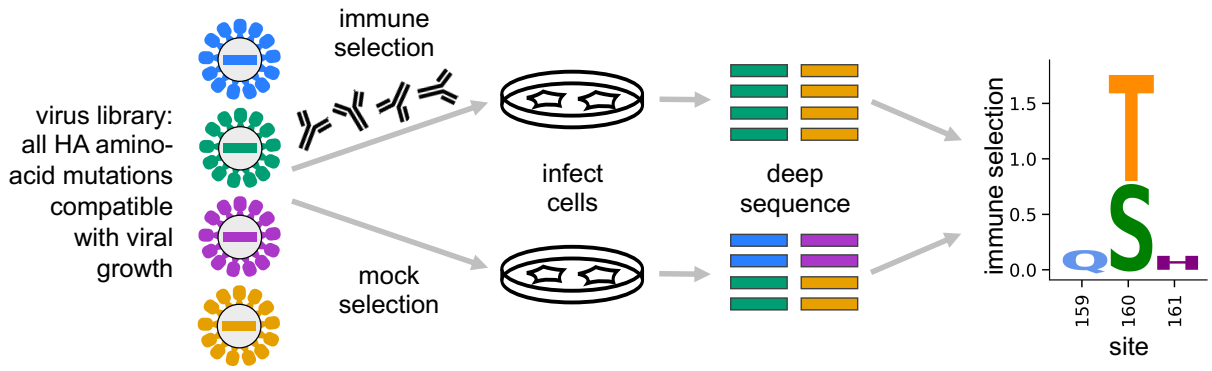

Figure 4.1: **Mutational antigenic profiling of the Perth/2009 H3 HA. (A)** Schematic of mutational antigenic profiling approach. Mutational antigenic profiling quantifies the antigenic effect of all amino-acid mutations to HA. We generate libraries of mutant viruses carrying all mutations to HA compatible with viral growth. We incubate the libraries with antibodies or serum, and infect cells with non-neutralized virus. Viral RNA from infected cells is deep sequenced to measure the frequency of each mutation. We quantify immune selection on each mutation as its log enrichment relative to wildtype in the immune-selected sample versus a mock-selection control. Data are displayed in logo plots, with larger letters indicating stronger immune selection for a mutation.

profiling [60, 61]. As illustrated in Figure 4.1, this approach quantifies how every amino-acid mutation to HA affects viral neutralization. Here we perform mutational antigenic profiling using mutant virus libraries with the HA from A/Perth/16/2009 [128], which was the H3N2 component of the influenza vaccine from 2010 to 2012 [223].

To validate mutational antigenic profiling for these viral libraries, we first performed selections with six monoclonal antibodies isolated from humans who had received the 2010-2011 trivalent influenza vaccine [240, 65]. Based on binding assays to a small HA mutant panel, four antibodies target near the receptor-binding pocket, while two antibodies target lower on HA's head. For each antibody, we performed at least two replicates of mutational antigenic profiling using independently generated virus libraries and an antibody concentration such that $<$10% of the library retained infectivity after neutralization (Figure C.1). Note that the magnitude of the measured immune selection depends on the strength of antibody selection [60], so while heights of letters in our maps of immune selection (i.e., logo plots like the one at right of Figure 4.1) can be compared within a given

map, caution should be used when comparing y-axis scales across maps.

The four antibodies that we expected to target near the receptor binding pocket indeed all selected mutations in this portion of HA (Figure 4.2A,E). Importantly, the selected mutations were consistent across the biological replicates with independently generated mutant virus libraries (Figure C.2), confirming that our approach systematically maps the antigenic effects of all mutations rather than simply selecting one-off viral mutants. The strongly selected mutations occurred at sites that are classically categorized as antigenic region B [224, 229]. However, although the antibodies all targeted the same antigenic region of HA, they selected different escape mutations (Figure 4.2A). These antibody-to-antibody differences in escape mutations validated in traditional neutralization assays (Figure 4.2B). For instance, K160T reduces neutralization by antibody 3C04 by $\sim$100-fold but has no effect on neutralization by antibody 4C01 despite the fact that both antibodies target a similar region of HA (Figure 4.2E).

The two antibodies that we expected to target lower on HA's head indeed selected mutations in this portion of HA, at sites classically categorized as antigenic regions D and E [224, 229]. But again the specific mutations selected by each antibody differed (Figure 4.2C,D,F). Overall, these results validate mutational antigenic profiling for these viral libraries, and underscore the observation that different antibodies targeting an apparently similar epitope often have distinct escape mutations [60, 55].

4.3.2 Contemporary human sera strongly selects specific escape mutations

We next mapped immune selection from polyclonal human sera. We reasoned it that it would be most informative to examine serum collected during the time when the Perth/2009 virus was circulating in the human population. We therefore screened the neutralizing activity of sera collected from 16 healthy adults between 2008 and 2010, and identified four sera that completely neutralized the wild-type Perth/2009 viral strain at a dilution of $\geq$1:40 [which is the HAI titer traditionally assumed to indicate a reduced risk of

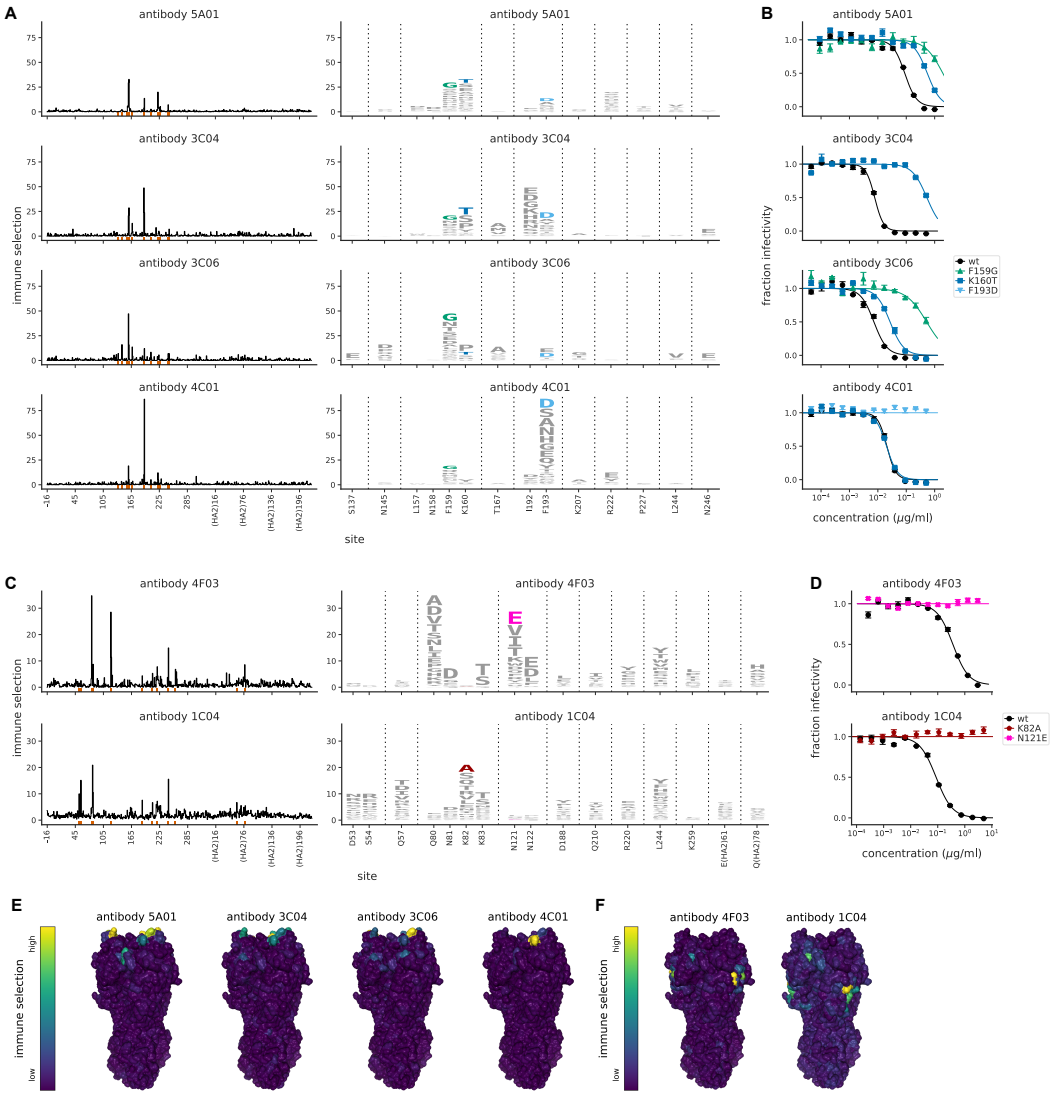

Figure 4.2: **Mutational antigenic profiling of monoclonal antibodies targeting HA. (A)** Maps of immune selection from four antibodies targeting near the receptor binding pocket. Line plots show the total immune selection at each site, and logo plots show mutations at strongly selected sites (indicated by red marks at the bottom of the line plots). **(B)** Neutralization assays validate that mutations mapped to be under strong immune selection indeed have large effects on neutralization. **(C)** Maps of immune selection for two antibodies targeting lower on the HA head and **(D)** corresponding neutralization curves for the most strongly selected escape mutation for each antibody. **(E)** Immune selection mapped onto HA's structure for the antibodies targeting near the receptor binding pocket or **(F)** lower on the HA head. The color scale is calibrated separately for each structure.

infection; 115]. No information on influenza vaccination or infection history was available for these four individuals, who ranged in age from 21 to 65 years old at the time of collection. We performed mutational antigenic profiling using serum dilutions chosen so that $\sim$5% of the mutant virus library survived neutralization, although the exact percentage varied among sera and replicates (Figure C.3).

Despite being polyclonal, each serum strongly selected single escape mutations (Figure 4.3A). The selected mutations occurred at a relatively small number of sites, predominantly in the portion of HA classically categorized as antigenic region B (Figure 4.3A,C). The sites of selection were reproducible across three biological replicates using independently generated mutant virus libraries (Figure C.4).

To validate the mutational antigenic profiling, we performed neutralization assays (Figure 4.3B). In all cases, the most strongly selected mutation in the profiling had a large antigenic effect in a neutralization assay. For three individuals (the 21-year old, 64-year old, and 65-year old), the strongest escape mutation had a $>$10-fold effect on neutralization, and for the remaining individual (the 53-year old) the strongest escape mutation had a $\sim$5-fold effect (Figure 4.3B). So amazingly, the antigenic effect of the strongest escape mutant from three of the polyclonal sera was comparable to that of strongest escape mutant from the monoclonal antibody 5A01 (compare Figure 4.2B to Figure 4.3B). These results show that single mutations can dramatically reduce viral sensitivity to neutralization by polyclonal human sera.

However, the exact mutations that mediate escape differ markedly across sera (Figure 4.3A). For instance, F193D escapes viral neutralization by the serum from the 21-year old individual by $>$10-fold—but has no effect for the serum from the 64-year old (Figure 4.3B). Similarly, F159G escapes neutralization by the 64-year old's serum but has minimal effect on neutralization by the 53-year old (Figure 4.3B). Figure 4.3A,B shows numerous other examples of such person-to-person variation in viral escape mutations. In fact, the only viral mutation that has a consistent antigenic effect across individuals is K160T, which moderately enhances neutralization resistance to all four sera. This serum-

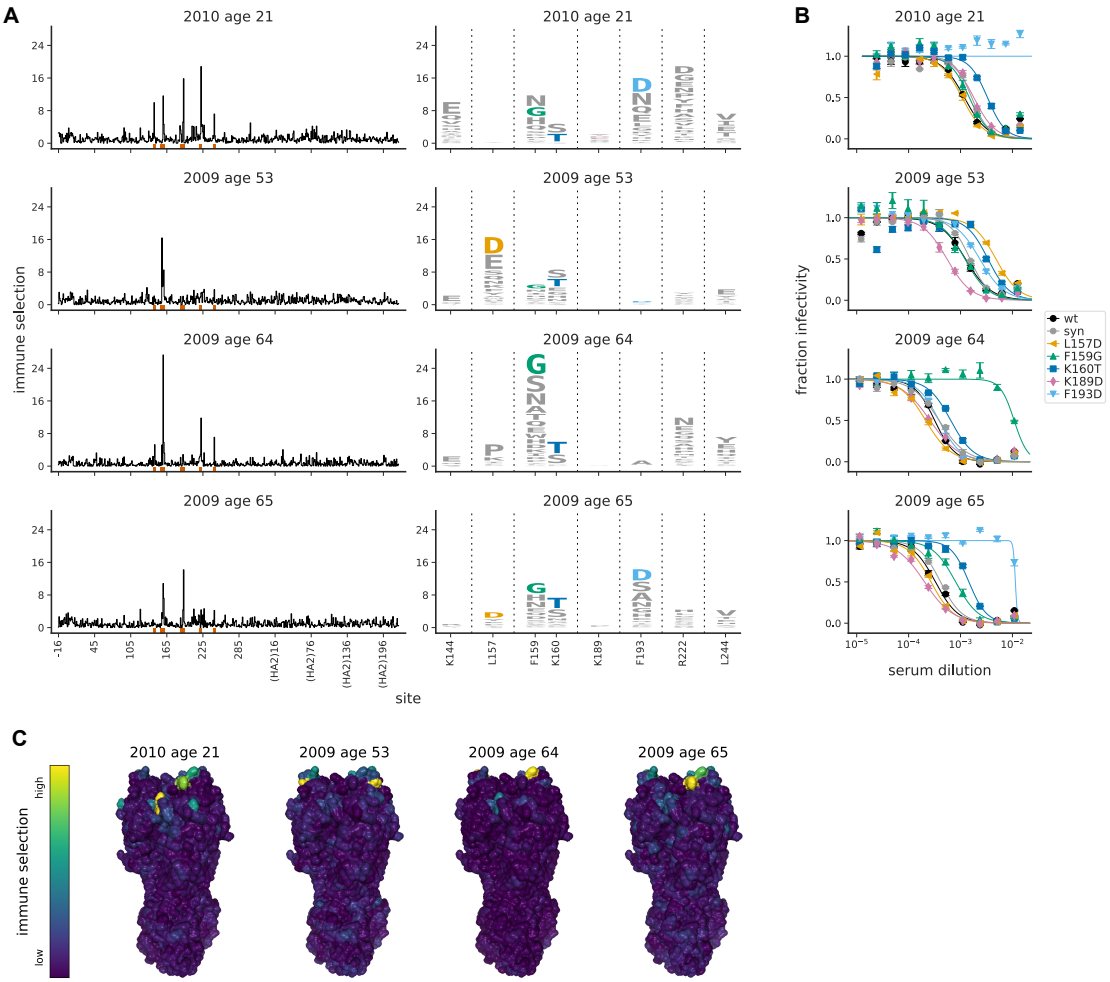

Figure 4.3: **Mutational antigenic profiling of four human serum samples.** Plot titles indicate the year the serum was collected and the age of the individual at that time. **(A)** Line plots show the total immune selection at each site, and logo plots show mutations at strongly selected sites. **(B)** Neutralization assays validate that mutations mapped to be under strong immune selection indeed have large antigenic effects. The "syn" mutant is a control with a synonymous mutation does not change the protein sequence and so should not affect antigenicity. **(C)** Immune selection mapped onto HA's structure for each sera. The color scale is calibrated separately for each structure. Site 189 is shown in the logo plots despite not being a strongly selected site because it is important for ferret sera (see below).

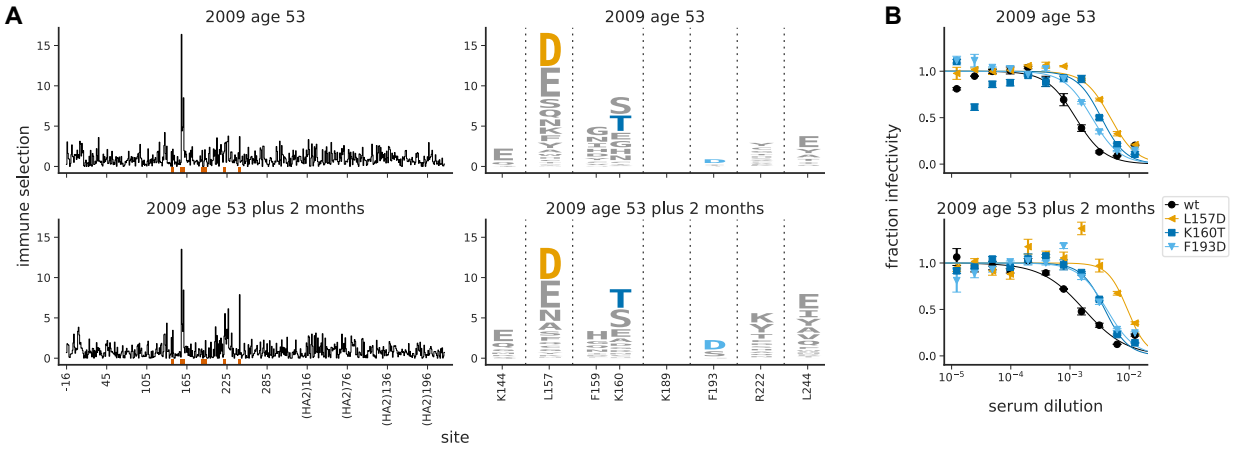

Figure 4.4: **The maps of immune selection are stable over short time periods in the absence of vaccination or infection.** This figure re-displays the **(A)** map of immune selection and **(B)** neutralization curves from Figure 4.3 for the serum from the 53-year old individual alongside comparable data generated using another serum sample from the same individual collected two months later.

to-serum variation shows that we are mapping true antigenic mutants for each serum rather than avidity mutants that generally enhance neutralization resistance [235, 93]. It also demonstrates the limitation simply subdividing HA into broad antigenic regions: although the serum-escape mutations are mostly in classically defined antigenic region B (Figure 4.3C), they have wildly different effects across individuals.

To confirm that our serum-escape maps are replicable over short timeframes during which there are not expected to be large changes in underlying immunity, we examined a second serum sample from the 53-year old individual collected two months after the sample mapped in Figure 4.3. There is no indication that the individual was infected or vaccinated with influenza during these two months. Figure 4.4 shows that the maps are highly similar for the two samples, consistent with the expectation that the serum specificity should remain stable over that time.

4.3.3 Mapping viral escape mutations pre- and post-vaccination

Because vaccination can shape anti-influenza serum responses [73, 240, 132], we next performed mutational antigenic profiling with sera collected from four individuals pre-vaccination and one-month post-vaccination. These individuals, who ranged in age from 25 to 49 years, received the 2015–2016 vaccine, for which the H3N2 component was A/Switzerland/9715293/2013 [223]. Because these sera were collected six years after 2009 from individuals vaccinated with an antigenic successor of Perth/2009, we anticipated that it might be more difficult to select escape mutations, since the sera is likely to have immunity both to Perth/2009-like viruses and their naturally occurring antigenic drift variants.

The serum from one individual (the 25-year old) strongly selected escape mutants even pre-vaccination (Figure 4.5A). This individual's serum also had the most potent pre-vaccination neutralizing activity against Perth/2009, with an inhibitory concentration 50% (IC50) of $\sim$1:800 (Figure 4.5B). The mutation most strongly selected by the pre-vaccination serum (F159G) reduced neutralization by over an order of magnitude (Figure 4.5B). Vaccination of this individual substantially enhanced the serum's potency, dropping the IC50 to $\sim$1:10,000—but F159G continued to have the largest effect on neutralization, still reducing the IC50 by over an order of magnitude (Figure 4.5A,B).

The second most potent pre-vaccination serum (that of the 29-year old, which had an IC50 of $\sim$1:150) also perceptibly selected an antigenic mutation (F159G), but the effect of the mutation was much smaller (Figure 4.5A,B). Vaccination enhanced the serum potency by $\sim$20-fold, and also slightly shifted its specificity (Figure 4.5A,B). Prior to vaccination, F159G but not K144E had a small antigenic effect, whereas the situation was reversed post-vaccination. Notably, both F159 and K144 are mutated in the Switzerland/2013 virus relative to Perth/2009. However, the fact that no mutations greatly alter the IC50 of this individual's serum indicate that it is not narrowly focused on any specific epitope on the Perth/2009 HA.

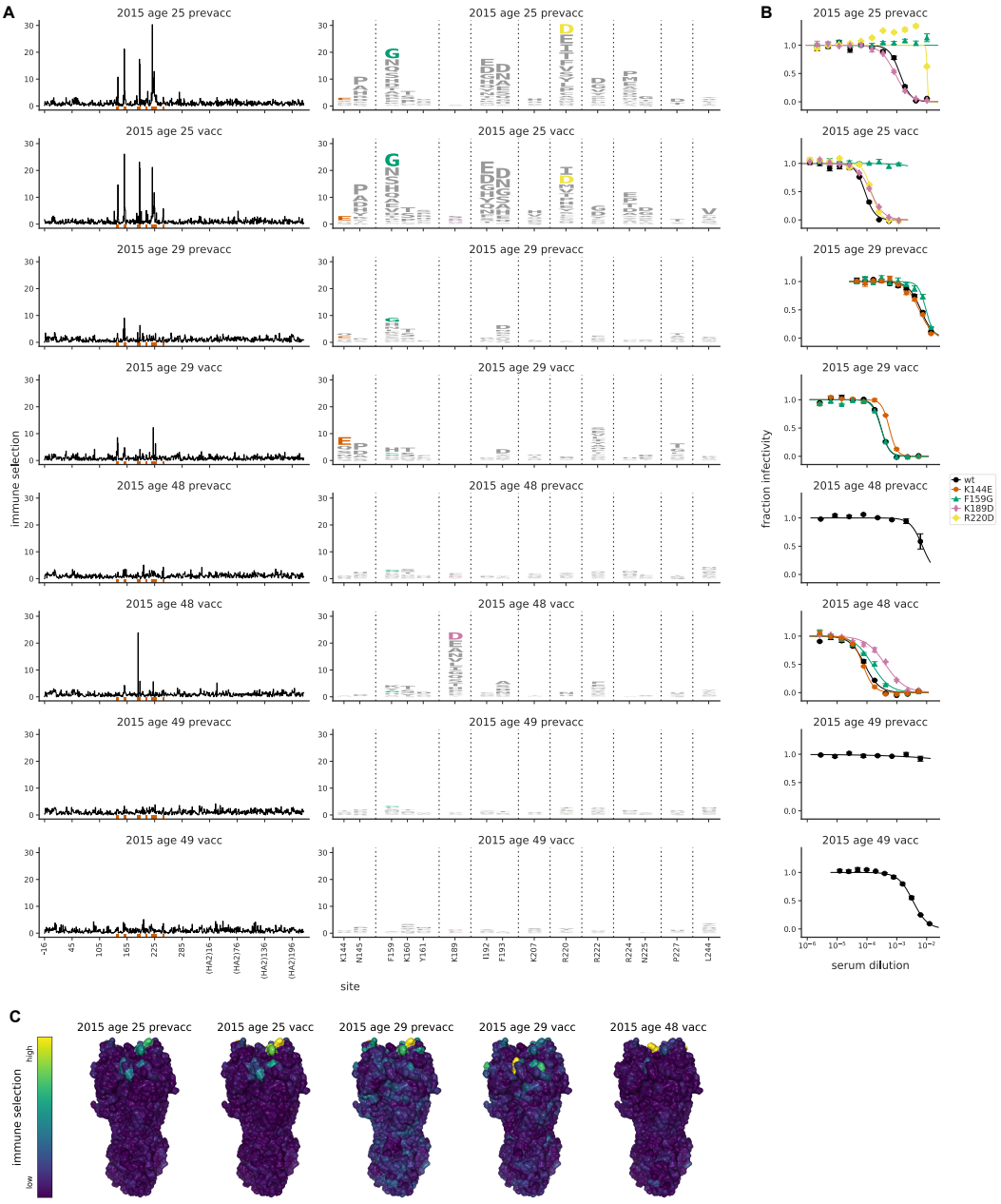

Figure 4.5: **Mutational antigenic profiling of sera from four humans pre- and post-vaccination.** Plot titles indicate the year the serum was collected, the age of the individual at that time, and the vaccination status. **(A)** Line plots show total immune selection at each site, and logo plots show mutations at strongly selected sites. **(B)** Neutralization assays validate that mutations mapped to be under strong immune selection indeed have large antigenic effects. **(C)** Immune selection mapped onto HA's structure for sera that selected escape mutants. The color scale is calibrated separately for each structure.

The remaining two individuals (the 48- and 49-year old) had low serum potency before vaccination (Figure 4.5B), such that we were unable to exert sufficient immune selection to map escape mutations from their pre-vaccination sera (Figure 4.5A and Figure C.7). Vaccination enhanced the serum potency of both individuals (Figure 4.5B). For the 48-year old, this enhanced neutralizing activity was strongly focused, with the K189D mutation decreasing the IC50 of the post-vaccination serum by an order of magnitude (Figure 4.5A,B). But for the 49-year old, the enhanced neutralizing activity was not dominated by any specificity, as the post-vaccination serum did not select any antigenic mutations (Figure 4.5A).

These results show that it is possible to select strong escape mutants even from serum collected well after the Perth/2009 virus circulated from individuals vaccinated with an antigenic successor of this virus. In some cases vaccination shifts the specificity of the serum, whereas in other cases it primarily boosts existing specificities, consistent with prior work using other approaches [73, 126, 127, 92]. As in the previous section, the strong escape mutations are predominantly in antigenic region B of HA (Figure 4.5C)—but again the effects of specific mutations vary markedly among sera.

4.3.4 Immune selection by ferret sera is consistent and different from human sera

The antigenicity of influenza viral strains is currently characterized mostly using sera from ferrets [191]. These ferrets have typically been infected just once with a single viral strain—unlike humans, who have complex exposure histories that may influence their antibody response [134, 135, 6, 84, 36]. To compare selection from human and ferret sera, we performed mutational antigenic profiling using sera from five ferrets. Three ferrets were infected with the Perth/2009 viral strain at the University of Pittsburgh. The other two ferrets were infected at the World Health Organization (WHO) Collaborating Centre in Melbourne, one with Perth/2009 and one with A/Victoria/361/2011 [the immediate antigenic successor of Perth/2009 in the influenza vaccine; 223]. We used ferret sera from different labs and viral strains to sample across factors that might affect serum specificity.

In stark contrast to the person-to-person variation of the human sera, the maps of immune selection were very similar for all post-infection ferret sera (Figure 4.6A). This was true even for the ferret infected with Victoria/2011 rather than Perth/2009 virus—the differences between ferrets infected with these two antigenically distinct H3N2 viruses were smaller than the differences among nearly all the human sera. The strongest selection from the ferret sera focused on sites 189 and 193, with mutations K189D and F193D tending to have a $\sim$5 to 10-fold effect on neutralization (Figure 4.6B). Mutations at a handful of additional sites (such as 142, 144, and 222) were also modestly selected by some ferret sera (Figure 4.6A,B).

Although the ferret sera was similar to the human sera in focusing on antigenic region B of HA (Figure 4.6C), there were notable differences in the specific mutations that were selected. The site where mutations were most strongly selected by all the ferret sera (site 189) had an appreciable antigenic effect for only one of the human sera. The other site where mutations were consistently and strongly selected by the ferret sera (site 193) had an antigenic effect for less than half the human sera. The converse was also true: many sites of mutations strongly selected by human sera (such as 157, 159, and 160) had little antigenic effect for the ferret sera. These findings highlight major differences in the fine specificity of immune focusing between ferrets that have been infected with a single viral strain and humans with complex exposure histories.

4.3.5 The effect of a monoclonal antibody in polyclonal serum

The preceding sections show that polyclonal sera often select single antigenic mutations—a phenomenon more typically associated with monoclonal antibodies. To test how much of a serum's potency must derive from a single antibody before it dominates the selection of escape mutations, we spiked an antibody that targets lower on HA's head into serum that selects mutations at the top of HA's head. We kept the serum at a concentration where $\sim$4% of the viral library survived neutralization by serum alone, and

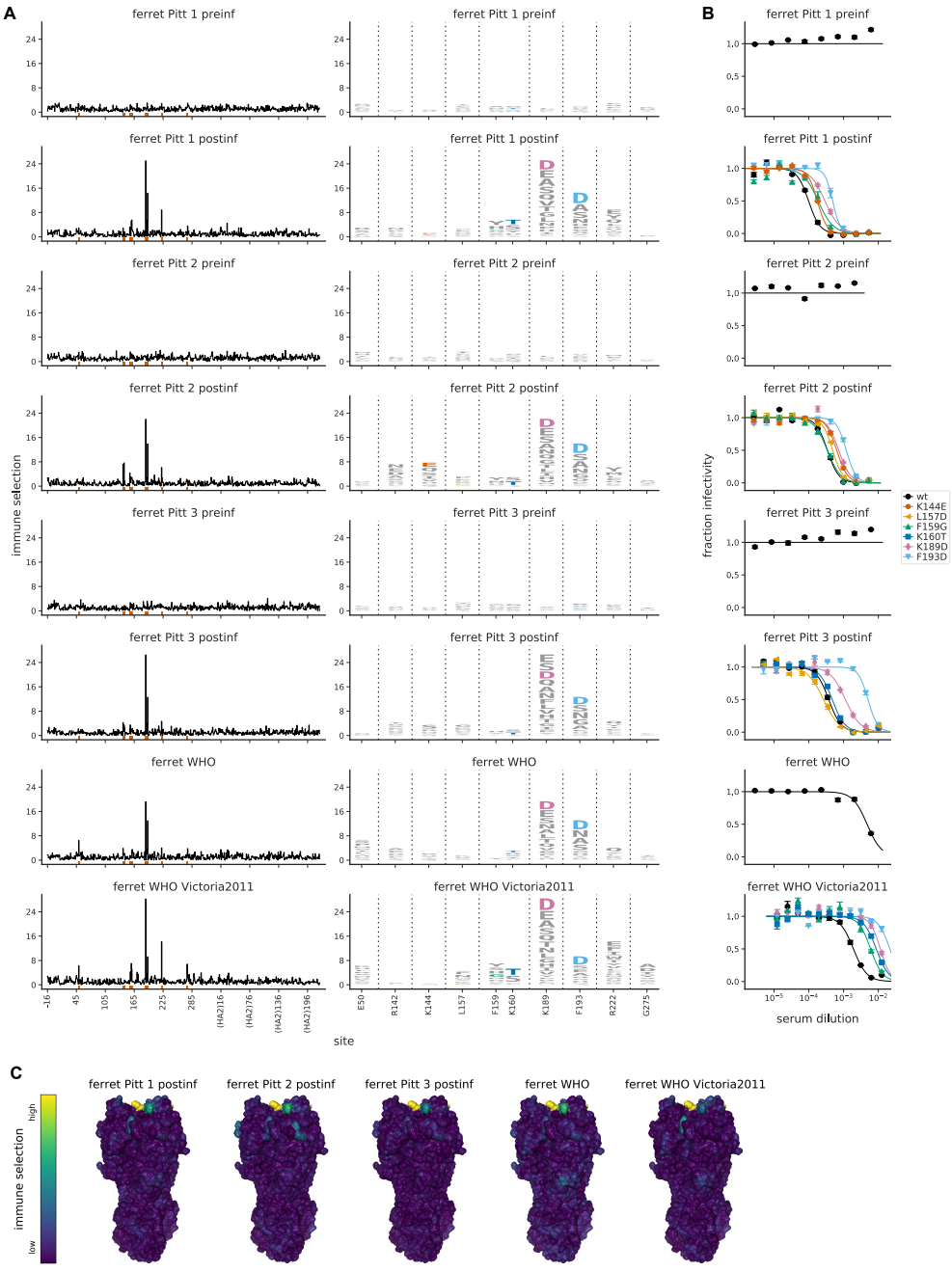

Figure 4.6: **Mutational antigenic profiling of sera from five ferrets.** Plot titles indicate the lab that performed the infection and if the infecting strain was Victoria/2011 rather than Perth/2009. For ferrets from Pittsburgh, both pre- and post-infection sera were analyzed as indicated in the plot titles. **(A)** Line plots show total immune selection at each site, and logo plots show mutations at strongly selected sites. **(B)** Neutralization assays validate that mutations mapped to be under strong immune selection indeed have large antigenic effects. **(C)** Immune selection mapped onto HA's structure for sera that selected escape mutants. The color scale is calibrated separately for each structure.

spiked the antibody at three concentrations. The percents of the viral library that survived neutralization with antibody alone at each of these concentrations were: 25% at the low concentration, 5% at the mid concentration, and 2% at the high concentration (Figure C.11). These concentrations therefore span a range in which the antibody is a modest versus dominant contributor to the overall neutralizing activity of the mix.

Even when the serum was spiked with the lowest concentration of antibody, the mutational antigenic profiling showed signals of selection at sites targeted by the antibody (Figure 4.7A). At the middle antibody concentration, selection from the antibody exceeded that from the serum, although both were still apparent (Figure 4.7A). At the highest antibody concentration, selection at antibody-targeted sites completely overwhelmed selection at serum-targeted sites. Part of the reason the antibody so readily dominated the selection may be that the strongest serum-escape mutations (F159G and F193D) actually sensitize the virus to neutralization by the antibody (Figure 4.7B), a result reminiscent of earlier work showing synergistic effects of mixing antibodies [137, 214]. Overall, these spike-in experiments show that a single antibody can dominate selection if it comprises half or more of a serum's overall potency. Of course, these experiments cannot reveal if the focused selection from human sera is actually driven by a single antibody versus a collection of antibodies targeting a similar epitope.

4.3.6 Many sites strongly selected by human sera change during natural evolution

If our mutational antigenic profiling reflects real antigenic pressure on human influenza virus, then we would expect to observe changes at sites in HA that our experiments mapped as being under selection. To test if this is true, we examined the natural evolution of human H3N2 influenza HA since 2007 at sites with clear signals of antigenic selection from at least one human serum (these are the 16 sites shown in the logo plots of Figure 4.3 and Figure 4.5A).

There has been substantial amino-acid evolution (new variants reaching $\geq$5% fre-

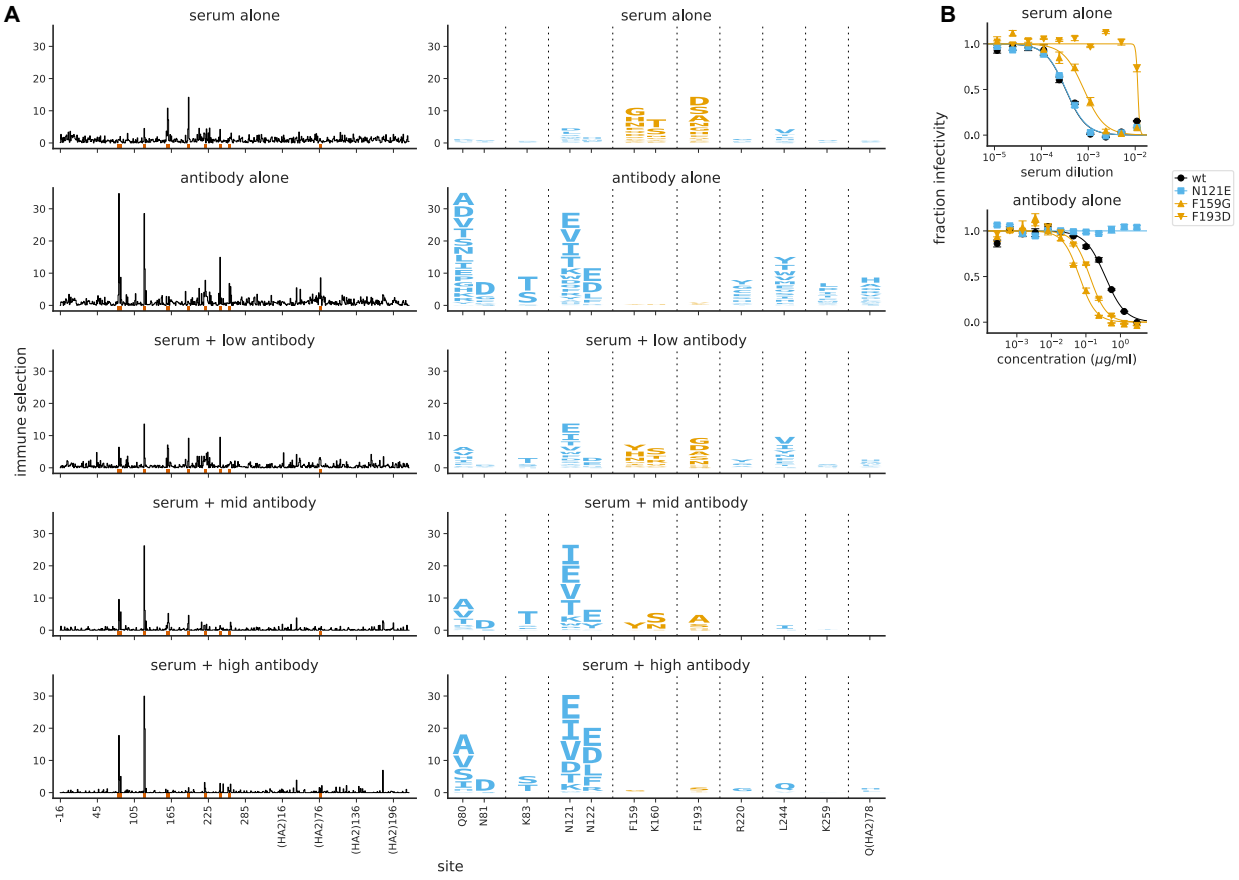

Figure 4.7: **Mutational antigenic profiling of polyclonal human serum spiked with a monoclonal antibody.** The antibody is spiked into the serum at a "low" concentration (antibody alone less potent than serum alone), a "mid" concentration (antibody similarly potent to serum), and a "high" concentration (antibody more potent than serum); see Figure C.11 for details. **(A)** Line plots show the total immune selection at each site, and logo plots show mutations at sites that are strongly selected by the serum (orange) or antibody (blue). **(B)** Neutralization curves for some of the most strongly selected mutations against serum or antibody alone. Note that the antibody is 4F03 from Figure 4.2, the human serum is that from the 65-year old in Figure 4.3, and the antibody-alone and serum-alone panels re-display data from those figures using a different color-scheme and subset of sites in the logo plots.

quency) at nine of the sites strongly selected by the human sera (Figure 4.8). Across all sera that strongly selected mutations, the single largest-effect mutations occurred at five sites: 144, 157, 159, 189, and 193 (Figure 4.3A and Figure 4.5A). During the evolution of human H3N2 influenza, new amino-acid variants have reached $>$10% frequency at all of these sites (Figure 4.8), and differences at three of these sites (144, 159, and 193)

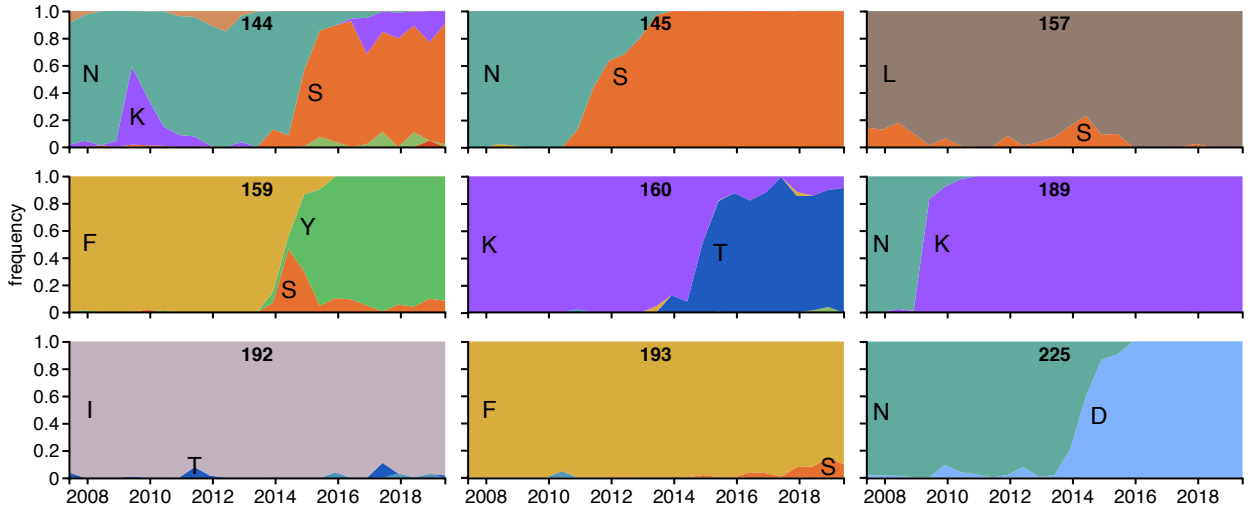

Figure 4.8: **Frequencies of amino acids at key sites in human H3N2 influenza HA between 2007 and 2019.** There are 16 sites under strong immune selection in our mutational antigenic profiling with human sera, and this figure shows the 9 of these sites for which a new amino acid rose to $\geq$5% frequency. The numbers at the top of each plot indicate the site number, and the letters indicate the amino acid identity. The figure panels are taken from the `nextstrain` real-time pathogen evolution website [88, 157].

distinguish the 3C2.A and 3C3.A clades that have recently circulated in humans [11]. Because mutations at these five sites are selected by only some sera, it appears that strong antigenic selection from just a subset of individuals can drive global viral evolution.

The one site where we observed a consistent antigenic effect across almost all human sera was 160, where mutations K160S and K160T caused a moderate increase in neutralization resistance (Figure 4.3A,B and Figure 4.5A). These mutations introduce a N-linked glycosylation motif near the top of HA's head. The K160T mutation appeared among natural human H3N2 viruses in late 2013 and is now present in most circulating viruses (Figure 4.8). Therefore, it also appears that moderate antigenic selection from many individuals can drive global viral evolution.

Notably, the amino-acid that emerges at a site in nature is not always the one that our experiments map as being under the strongest immune selection. There are several possible reasons: First, our experiments probe all amino-acid mutations but natural evolution

is mostly limited to single-nucleotide changes. For instance, L157D is the largest-effect mutation at site 157 (Figure 4.3) but L157S appears in nature (Figure 4.8)—likely because S but not D is accessible from L by a single-nucleotide change. Second, natural evolution selects for viral replication and transmission as well as immune escape. Finally, the context of a mutation may influence its effect: for instance, F159Y has spread in nature but was not selected in our experiments, perhaps because in nature this mutation co-occurred with secondary changes such as N225D [32, 105]. Importantly, it is now feasible to also make high-throughput measurements of how mutations to H3N2 HA affect viral replication [128] and epistatic interactions among sites [228], so it may eventually be possible to build evolutionary models that incorporate all these factors [138, 158].

4.4 Discussion

We have mapped the selection that polyclonal human sera exert on all amino-acid mutations to a H3N2 influenza virus HA. Many sera are highly focused, and select single viral mutations that reduce neutralization by over an order of magnitude. This basic finding that human serum can be focused is consistent with other recent work [135, 101, 49]. But because our experiments mapped selection on all mutations, we were able to systematically quantify the extent of focusing and compare its targets across sera.

A striking result of these comparisons is that the targets of serum selection vary widely from person to person. Viral mutations that greatly reduce neutralization by one individual's serum sometimes have no effect for another individual's serum, which is instead affected by different mutations. These findings starkly contrast with the "avidity" model of influenza immune escape [235, 93], which postulates that the virus evades polyclonal immunity by generically increasing neutralization resistance via mutations that promote receptor binding. Our results suggest a different model: a virus with a single mutation could be strongly favored in pockets of the human population with immunity that is strongly focused on that site. Does such a process actually drive influenza virus evolution? Many

of the mutations mapped in our experiments are at sites that have recently mutated in nature, suggesting that selection from focused human sera may be relevant to viral antigenic drift. However, decisively answering this question will require comparing the serum focusing of individuals with the viral strains that actually infect them.

The sera that we profiled almost always focus on the portion of HA classically categorized as antigenic region B, consistent with other studies reporting that this region is immunodominant in recent H3N2 strains [172, 32, 25]. However, our results highlight the limitations of subdividing HA into broad antigenic regions. These regions were originally defined based on the idea that a mutation in a region abrogated binding of most antibodies targeting that region [214, 224, 29]. Our work shows that this is not true. Even though most of the human sera we map focus on region B, different mutations in this region have very different effects across sera. The specificity of human sera is therefore more fine-grained than the classical categorization of HA into antigenic regions.

Why is the neutralizing activity of human polyclonal sera often so focused? One possibility is that very few distinct antibodies are responsible for the anti-HA activity of any given serum. Indeed, multiple studies have shown that relatively few clonotypes comprise the majority of the anti-HA serum repertoire of a single individual [5, 126, 127]. Our findings further suggest that either most of these clonotypes target the same sites in HA, or that the serum's neutralizing activity is due to very few of the clonotypes. In support of the second idea, recent work has shown that as an individual ages, much of the antibody response is diverted to non-neutralizing epitopes because sites targeted by potently neutralizing antibodies change during viral evolution [92, 177].

Prior work has shown that exposure history is a major determinant of the specificity of human immunity to influenza [134, 6, 84, 36]. However, our work suggests that the relationship between exposure history and serum specificity is complex, as we see strong and variable focusing among individuals ranging from 21 to 65 years. But while our dataset is too small to draw conclusions about the association between age and serum focusing, the importance of history is demonstrated by the lack of variation among ferrets that have

been experimentally infected just once with a defined viral strain. The differences between human and ferret sera also underscore the shortcomings of using ferrets as the primary tool for characterizing viral antigenicity, as has previously been shown for H1N1 [134].

Overall, our work uses a new approach to show that polyclonal human sera can strongly select single antigenic mutations in HA, and that the effects of these mutations vary greatly person to person. Expanding this approach should shed further light on the causes of this variable focusing, and its implications for viral evolution and disease susceptibility.

4.5 Materials and Methods

Data and computer code

Deep sequencing data are on the Sequence Read Archive under BioSample accession numbers SAMN10183083 and SAMN11310465 (viral libraries selected with monoclonal antibodies), SAMN10183146 (monoclonal antibody selection controls), SAMN11310372 (viral libraries selected with human sera), SAMN11310371 (viral libraries selected with ferret sera), SAMN11341221 (viral libraries selected with human sera spiked with monoclonal antibody), and SAMN11310373 (serum selection controls).

The computer code used to analyze the data and generate the paper figures is available on GitHub at `https://github.com/jbloomlab/map_flu_serum_Perth2009_H3_HA`. Key processed data are tracked in this GitHub repository as detailed in the repository's README file, and are also available in the Supplementary files for this manuscript.

HA numbering

All sites are referred to in H3 numbering unless indicated otherwise. The signal peptide is in negative numbers, the HA1 subunit in plain numbers, and the HA2 subunit in numbers denoted with "(HA2)." Sequential 1, 2, ... numbering of the Perth/2009 H3 HA can be converted to H3 numbering simply by subtracting 16 for the H1 subunit, and

subtracting 345 for the HA2 subunit. A file mapping sequential 1, 2, ... numbering to H3 numbering is at https://github.com/jbloomlab/map_flu_serum_Perth2009_H3_HA/blob/master/data/H3renumbering_scheme.csv.

Perth/2009 HA virus used in this study

The "wild-type" Perth/2009 HA used in this study is that from [128]. This HA has two amino-acid mutations (G78D and T212I) relative to the most common Perth/2009 HA sequences in Genbank (there are several variants in Genbank). These two mutations improve viral growth in cell culture [128]. The sequence of HA with these mutations is provided in [128] and at https://github.com/jbloomlab/map_flu_serum_Perth2009_H3_HA/blob/master/data/Perth09_HA_reference.fa. Unless otherwise indicated, when this paper refers to the "Perth/2009 HA" it means this HA. As described below, all other genes in this virus were derived from the lab-adapted A/WSN/1933 (H1N1) strain.

Monoclonal antibodies

The monoclonal antibodies in Figure 4.2 are described in [240] and [65]. These antibodies were isolated from peripheral blood mononuclear cells of human donors seven days post-vaccination with the 2010-2011 influenza vaccine containing the A/Victoria/210/2009 strain as the H3N2 component, using the approach in [192]. The V_H and V_L chains were amplified using single-cell RT-PCR, and cloned into human IgG expression vectors. To produce the monoclonal antibodies, 293T cells were transfected with plasmids encoding the heavy and light chains, and the antibodies were purified using protein A/G affinity purification.

Human sera

The human sera in Figure 4.3 came from a collection of the Vaccine and Infectious Disease Division (VIDD) of the Fred Hutchinson Cancer Research Center. These sera were

collected from prospective bone marrow transplant donors in Seattle, WA. We used neutralization assays to screen sera collected from 16 individuals from 2008 and 2010, and selected the four that neutralized virus with the Perth/2009 HA at $\geq$ 1:40 dilution. No information was available on the influenza vaccination or infection status of these individuals.

The human sera in FIgure 4.5 were collected by the Hensley lab at the University of Pennsylvania, Philadelphia, PA, from four individuals pre-vaccination and four weeks post-vaccination with the 2015-2016 Northern Hemisphere influenza vaccine. The H3N2 component of this vaccine was A/Switzerland/9715293/2013, which is an antigenic successor of Perth/2009 by several vaccine updates: Perth/2009 was the Northern Hemisphere vaccine strain in 2010-2012, A/Victoria/361/2011 was the strain in 2012-2014, A/Texas/50/2012 was the strain in 2014-2015, and Switzerland/2013 was the strain in 2015-2016.

The dates of collection of the human sera are rounded to the nearest year in this paper.

Ferret sera

The serum samples denoted “ferret-Pitt-#” were collected from three ferrets pre-infection and again 23 days post-infection at the University of Pittsburgh. Each ferret was infected with Perth/2009 (H3N2) virus that carries the exact same HA sequence used for the studies in this paper.

The serum samples denoted “ferret-WHO*” were collected from two ferrets post-infection at the World Health Organization Collaborating Centre in Melbourne, Australia. One ferret was infected with the Collaborating Centre’s version of the Perth/2009 H3N2 virus, and the second ferret was infected with the Collaborating Centre’s version of the A/Victoria/361/2011 H3N2 strain. The sera were collected in bleeds performed 14 days after intranasal infection with virus. Experiments were conducted with approval from the University of Melbourne Biochemistry & Molecular Biology, Dental Science, Medicine, Microbiology & Immunology, and Surgery Animal Ethics Committee, in accordance with the

NHMRC Australian code of practice for the care and use of animals for scientific purposes.

Serum preparation

All sera were treated with receptor-destroying enzyme (RDE) and heat-inactivated before use in our experiments, using a protocol adapted from [240]. The RDE treatment was to ensure that the viral libraries would not bind to residual sialic acids present in the serum. One vial of lyophilized RDE II (Seiken, Cat No. 370013) was first resuspended in 20 mL PBS. We then incubated 100 μL of serum with 300 μL of RDE solution at 37°C for 2.5 hours. We next heat-inactivated the serum and RDE by incubating at 55°C for 30 min. Finally, we centrifuged the serum at 20,000 x *g* for 20 min to pellet any precipitated material, collected the supernatant, aliquoted, and stored at -80°C.

Neutralization assays

Neutralization assays were performed using influenza viruses carrying GFP in the PB1 segment. The "wild-type" Perth/2009 viruses were generated using reverse genetics with the following plasmids: pHW-Perth2009-HA-G78D-T212I [128], pHH-PB1flank-eGFP [which encodes GFP on the PB1 segment; 20], and pHW181-PB1, pHW183-PA, pHW185-NP, pHW186-NA, pHW187-M, and pHW188-NS [which encode genes from A/WSN/1933 for the other six segments; 98]. The individual amino-acid mutant viruses tested in the neutralization assays were generated from the same plasmids except the indicated mutation was introduced into the pHW-Perth2009-HA-G78D-T212I plasmid. The "syn" mutant shown in Figure 4.3 has a synonymous F193F mutation.

To generate the viruses, we transfected a co-culture of 4×10^5 293T-CMV-PB1 [20] and 0.5×10^5 MDCK-SIAT1-CMV-PB1-TMPRSS2 [128] cells with the eight reverse genetics plasmids and the pHAGE2-EF1aInt-TMPRSS2-IRES-mCherry-W plasmid [128]. The transfections were performed in D10 media (DMEM, supplemented with 10% heat-inactivated FBS, 2 mM L-glutamine, 100 U of penicillin per milliliter, and and 100 μg of

streptomycin per milliliter). Each well received a transfection mixture of 100 μL DMEM, 3 μL BioT transfection reagent, and 250 ng of each plasmid. We changed the media in each well to 2 mL IGM (Influenza Growth Media, consisting of Opti-MEM supplemented with 0.01% heat-inactivated FBS, 0.3% BSA, 100 U of penicillin per milliliter, 100 μg of stremptomycin per milliliter, and 100 μg of calcium chloride per milliliter) eight hours post-transfection. At approximately 56 hours post-transfection, transfection supernatants were harvested, clarified by centrifugation at 2000 $\times$ *g* for five minutes, aliquoted, and frozen at -80°C. To titer the GFP-carrying viruses, we plated 1×10^5 MDCK-SIAT1-CMV-PB1-TMPRSS2 cells per well in 12-well plates in IGM. We infected cells with dilutions of viral supernatant four hours after plating. At 16 hours post-infection, we chose wells that appeared to show 1 to 10% of cells that were GFP-positive, and determined the exact fraction of GFP-positive cells by flow cytometry to calculate the titer of infectious particles per μL.

The neutralization assays were performed using these GFP-expressing viruses as described previously [100, 61, see also `https://github.com/jbloomlab/flu_PB1flank-GFP_neut_assay`]. All neutralization curves represent the mean and standard error of three replicate curves run on the same 96-well plate. The curve fits are Hill-like curves with the bottom and top constrained to zero and one, and were fit using the `neutcurve` Python package (`https://jbloomlab.github.io/neutcurve/`), version 0.2.4. Detailed information on the curve fitting is available on the project GitHub repository at `https://github.com/jbloomlab/map_flu_serum_Perth2009_H3_HA/blob/master/results/notebooks/analyze_neut.md`. The curve-fit parameters (e.g., IC50s) for all of the neutralization curves shown in this paper are in Dataset S 11.

Mutant virus libraries

For mutational antigenic profiling of some replicates of antibodies 3C06, 3C04, 4C01, and 1C04, we used the exact same mutant virus libraries described in [128]. Specifically, we

used those mutant virus libraries for the replicates labeled as “lib2” for 3C06, 3C04, 4C01; and all replicates of 1C04 in Figure C.2.

However, the titers of the viral libraries from [128] were not sufficient for all the mutational antigenic profiling, so for most of the experiments in the current paper we generated new triplicate stocks of mutant virus libraries using influenza reverse-genetics [98]. This required re-generating the mutant plasmids and mutant virus libraries as described below. These libraries have similar properties to those described in [128], but since they are not exactly the same we re-validated them by deep sequencing the mutant plasmid and mutant virus libraries. The full analysis of this deep sequencing along with plots showing all relevant statistics about the libraries is in Dataset S 14.

To create the new mutant plasmid libraries, we used two rounds of codon mutagenesis [17, 56] to introduce all of the possible codon mutations into the Perth/2009 HA in the pHH21 backbone [160]. The plasmid libraries were generated independently in biological triplicate, starting from independent preps of the wildtype plasmid, using the protocol described in [128]. The mutant amplicons were then cloned at high efficiency into the pHH21 vector using digestion with BsmBI, ligation with T4 DNA ligase, and electroporation into ElectroMAX DH10B competent cells (Invitrogen 18290015). We obtained $>$4 million transformants for each replicate library. We then scraped the plates, expanded the cultures in liquid LB + ampicillin at 37°C for 3 h with shaking, and maxiprepped the cultures. Sanger sequencing of 29 randomly chosen clones showed an average mutation rate of 1.6 codon mutations per clone (Dataset S 14).

To generate the mutant virus libraries by reverse genetics, we transfected 40 wells of six-well plates for each library. Each well contained a co-culture of 5×10^5 293T-CMV-PB1 and 0.5×10^5 MDCK-SIAT1-TMPRSS2 cells in D10 media. We transfected with 250 ng each of pHH-mutant-HA library (or wildtype control), the pHAGE2-EF1aInt-TCmut-P09-HA Perth/2009 HA protein expression plasmid (which expresses the HA protein from wild type Perth/2009 HA), the pHW18* series of plasmids [98] for all non-HA viral genes, and pHAGE2-EF1aInt-TMPRSS2-IRES-mCherry-W. The sequence of the pHAGE2-EF1aInt-

TCmut-P09-HA protein expression plasmid is in Dataset S 15. We changed the media in each well to 2 mL IGM eight hours post-transfection. At 45 hours post-transfection, the transfection supernatants were harvested, clarified by centrifugation at 2,000 $\times$ *g* for five minutes, aliquoted, frozen at -80°C, and titered in MDCK-SIAT1-TMPRSS2 cells. The titers were 2543, 3162, 1000, and 4739 $TCID_{50}$ per microliter for the three library replicates and the wildtype control, respectively.

We passaged 1.125 $\times$ 10^6 $TCID_{50}$ of the transfection supernatants for each library at an MOI of 0.005 $TCID_{50}$ per cell. We did this by plating 3 $\times$ 10^6 MDCK-SIAT1-TMPRSS2 cells per layer of five 5-layered 875 cm^2 flasks (Corning, 353144) in D10 media, and allowed the cells to grow for 24 h, at which time they were at $\sim$9 $\times$ 10^6 cells per layer. We then removed the D10 media from each flask, washed with 50 mL PBS and replaced the media with 130 mL per flask of an inoculum of 1.73 $TCID_{50}$ of virus per microliter in IGM. At three hours post-infection, we replaced the inoculum with fresh IGM for each replicate. We then collected virus supernatant at 42 hours post-infection, clarified the supernatant by centrifuging at 2,000 $\times$ *g* for five minutes, aliquoted, froze at -80°C, and titered in MDCK-SIAT1-TMPRSS2 cells. The titers were 1000, 14677, and 6812 $TCID_{50}$ per microliter for the three library replicates, respectively. The mutant plasmids and mutant viruses were then deep sequenced as in [128] to demonstrate that there was good coverage of mutations in both as described in Dataset S 14. These libraries were used for all the mutational antigenic profiling except for the subset of antibody replicates mentioned at the beginning of this subsection.

Mutational antigenic profiling

We performed the mutational antigenic profiling using the basic process described in [60]. For each serum and for the serum-antibody spike-in experiments, we performed three biological replicates of mutational antigenic profiling each using an independently generated mutant virus library. For each antibody, we performed either two or three biological

replicates each using an independently generated mutant virus library as indicated in Figure C.2. The reason that we only performed two biological replicates for some antibodies is that the noise is less for antibodies than sera.

For the mutational antigenic profiling, we diluted each virus library to 10^6 $TCID_{50}$ per mL, and incubated the virus dilution with an equal volume of antibody and/or serum at the intended dilution at 37°C for 1.5 h. The dilution for all samples are in Dataset S 12, and account for the initial 1:4 dilution of serum during the RDE treatment. These dilutions were generally chosen with the goal of having 1% to 10% of the virus library survive the serum or antibody treatment. We infected between 2×10^5 and 4×10^5 MDCK-SIAT1-TMPRSS2 cells with virus-antibody or virus-serum mix. At 15 hours post-infection, we extracted RNA from the cells, and then reverse-transcribed and PCR amplified full-length HA as in [128]. We then deep sequenced these HAs using a barcoded-subamplicon sequencing strategy to ensure high accuracy. This general sequencing approach was first applied to viral deep mutational scanning by [231]. The exact approach we used is described [59], with the primers for Perth/2009 given in [128]; a more general description of the approach is at `https://jbloomlab.github.io/dms_tools2/bcsubamp.html`. The sequencing was performed using 2×250 nucleotide paired-end reads on Illumina HiSeq 2500's at the Fred Hutchinson Cancer Research Center Genomics Core.

To estimate the overall fraction of virions in the library surviving immune selection, we used qRT-PCR against the viral NP and GAPDH, as described in [60]. Briefly, we made duplicate 10-fold serial dilutions of each virus library to create a standard curve of infectivity. We then performed qPCR for the standard curve of infectivity as well as each library-selected sample. A linear regression line relating the logarithm of the viral infectious dose in the standard curve to the difference in Ct values between NP and GAPDH was used to interpolate the fraction surviving for each selection. The measured percent surviving for each library are in Dataset S 13, and are also plotted in figure supplements for each figure showing mutational antigenic profiling results.

Analysis of deep sequencing data and visualization of results

The deep sequencing data were analyzed using `dms_tools2` [18] version 2.4.12, which is available at `https://jbloomlab.github.io/dms_tools2/`. Briefly, we first determined the counts of each codon at each site in both the immune-selected and mock-selected samples. These counts are at `https://github.com/jbloomlab/map_flu_serum_Perth2009_H3_HA/tree/master/results/renumbered_codoncounts`. These counts were then processed to compute the *differential selection* on each amino-acid mutation at each site, which is our measure of immune selection. The differential selection statistic is described in [60] (see also `https://jbloomlab.github.io/dms_tools2/diffsel.html`), and represents the log enrichment of each mutation relative to wildtype in the immune-selected sample versusa mock-selected control. The differential selection values for each replicate are at `https://github.com/jbloomlab/map_flu_serum_Perth2009_H3_HA/tree/master/results/diffsel`.

To visualize the differential selection, we took the median across replicates of the differential selection for each mutation at each site—these median values are displayed in all logo plots. The numerical values of these across-replicate median differential selection values are in Dataset S 16. The figures in this paper visualize the differential selection in two ways. First, the line plots show the total positive differential selection at each site. Second, the logo plots show the differential selection for each positively selected amino acid at key sites. These line and logo plots were created using the `dmslogo` software package (version 0.2.3), which is available at `https://jbloomlab.github.io/dmslogo/`.

We chose which sites to show in the logo plots in the figures by identifying strong or "significant" sites of immune selection for each serum using the approach described in [55] (excluding the pre-vaccination or pre-infection samples). Each figure panel then shows all sites that were "significant" for any sera or antibody in that panel. This "significance" calculation is heuristic, and involves using robust regression to fit a gamma distribution to all of the positive site differential selection values, equating the P-value to

the fraction of the distribution $\geq$ that site's differential selection, and then calling "significant" sites that have a false discovery rate ≤ 0.05. The code that performs this analysis is at `https://jbloomlab.github.io/dms_tools2/dms_tools2.plot.html#dms_tools2.plot.findSigSel`. In addition, logo plots for all sites for the across-replicate medians for each serum / antibody are in Dataset S 17.

A detailed notebook with the code for all of the foregoing analyses along with explanations and many additional plots is at `https://github.com/jbloomlab/map_flu_serum_Perth2009_H3_HA/blob/master/results/notebooks/analyze_map.md`.

Protein structures

The protein structures are all PDB 4O5N, which is the structure of HA from the A/Victoria/361/2011 (H3N2) strain [129]. The residues are colored by the positive site differential selection values. The visualizations were generated using `nglview` [161] via the Python wrapper package `dms_struct` (`https://jbloomlab.github.io/dms_struct/`). Interactive `mybinder` instances of the notebooks that can be used to rotate and zoom in on the structures are available at the following weblinks:

- Antibodies targeting antigenic region B (Figure 4.2): `https://mybinder.org/v2/gh/jbloomlab/map_flu_serum_Perth2009_H3_HA/master?urlpath=%2Fapps%2Fresults%2Fnotebooks%2Fmap_on_struct_antibody_region_B.ipynb`

- Antibodies target lower on HA's head (Figure 4.2): `https://mybinder.org/v2/gh/jbloomlab/map_flu_serum_Perth2009_H3_HA/master?urlpath=%2Fapps%2Fresults%2Fnotebooks%2Fmap_on_struct_antibody_lower_head.ipynb`

- The "VIDD" human sera (Figure 4.3): `https://mybinder.org/v2/gh/jbloomlab/map_flu_serum_Perth2009_H3_HA/master?urlpath=%2Fapps%2Fresults%2Fnotebooks%2Fmap_on_struct_VIDD_sera.ipynb`

- The “Hensley” human sera (Figure 4.5): https://mybinder.org/v2/gh/jbloomlab/map_flu_serum_Perth2009_H3_HA/master?urlpath=%2Fapps%2Fresults%2Fnotebooks%2Fmap_on_struct_Hensley_sera.ipynb

- The ferret sera (Figure 4.6): https://mybinder.org/v2/gh/jbloomlab/map_flu_serum_Perth2009_H3_HA/master?urlpath=%2Fapps%2Fresults%2Fnotebooks%2Fmap_on_struct_ferret.ipynb

Mutation frequencies in natural sequences

For Figure 4.8, we first identified sites that were under strong or “significant” selection from any of the human serum samples (excluding the pre-vaccination samples in Figure 4.5) using the approach described above. There were 16 such sites; these are the ones shown in the logo plots in Figure 4.3A or Figure 4.5A. For each such site, we then examined the frequency of different amino-acid identities from 2007 to 2019 (see https://github.com/jbloomlab/map_flu_serum_Perth2009_H3_HA/blob/master/results/notebooks/analyze_natseqs.md). This analysis identified nine sites where a new amino-acid identity reached at least 5% frequency. For these nine sites, we then took images of the amino-acid frequencies over time from the nextstrain website [88, 157] and used them to create Figure 4.8.

Acknowledgments

We thank Patrick Wilson for providing the monoclonal antibodies. We thank Hai Nguyen for assistance with using nglview. We thank Trevor Bedford and Kanta Subbarao for helpful advice. We thank the Fred Hutchinson Cancer Research Center Genomics Core for performing the Illumina deep sequencing. This work was supported by grant R01 AI127893 from the NIH / NIAID to JDB. JML was supported by F30 AI136326 from the NIH / NIAID, and the Center for Inference and Dynamics of Infectious Diseases (CIDID),

which is funded by NIH / NIGMS under U54GM111274. JDB is an investigator of the Howard Hughes Medical Institute. The authors declare no competing interests.

Chapter 5
CONCLUSION

During the course of its evolution, influenza virus HA must facilitate efficient viral growth and transmission, and evade host adaptive immunity. As HA evolves, mutations affecting either one or both of these properties determine the evolutionary success of that virus in nature. In this dissertation, I discussed my work to shed light on the complex interplay between the selective forces acting on HA in nature and the effects of mutations under those selective forces. Here I review some of the major findings of my work and potential future avenues of research.

Massively parallel experimental techniques enable us to study the effects of viral mutations in the lab. I harnessed the high-throughput method of *deep mutational scanning* to measure the effects on viral growth in cell culture of all possible single amino-acid mutations to a seasonal H3 HA. In comparing the mutation frequencies before and after selection by deep sequencing, I quantified the *preference* for each amino acid at every site in the protein.

In general, the preferences are consistent with existing knowledge about HA's biochemistry. For example, there is strong preference for the amino acids involved in receptor binding [216, 142, 163, 233], disulfide bridge formation [213], and cleavage [200]. In addition, I applied the amino-acid preferences to inform a site-specific codon-substitution model, which vastly outperforms traditional substitution models. This indicates that our experiments largely capture the constraints on the protein's evolution in nature.

By virtue of our experimental setup, in which we measured the functional effects of mutations in the absence of any immune selection, I was able to estimate the inherent

mutational tolerance at every site. In previous mutational scans of lab-adapted H1 HAs, the stalk domain was found to be quite mutationally intolerant relative to the globular head domain [209, 231, 59, 91]. These observations were used to rationalize (1) the capability for rapid antigenic drift in the head domain under immune pressure, and (2) the relative conservation of the stalk domain. Strikingly, I discovered less disparity in mutational tolerance between the head and stalk domains of the H3 HA than in the H1 HA.

Our work has underscored the power of deep mutational scanning which can lend itself to the study of mutational effects of viral proteins under diverse selection conditions. For instance, passaging the mutant virus libraries in distinct cell types, such as swine or avian-type cells, may uncover pathways to adaptation in diverse hosts. Indeed, a separate study from our lab has mapped the mutations that allow for adaptation of the avian influenza polymerase for viral growth in human hosts [194].

One such application of deep mutational scanning is to study the effects of mutations to H3 HA on viral growth in eggs. This is especially pertinent since the influenza virus vaccine is largely produced in eggs, in which the composition and linkage of sialic acid receptors is dissimilar to the sialic acid receptors found in the human airway [102, 195]. As a result, HA can acquire mutations that not only adapt it to increased receptor-binding and growth in eggs, but may also alter its antigenicity [180, 112, 33, 167, 178]. These types of egg-adaptation mutations have occasionally been responsible for low vaccine effectiveness in certain years [227, 240]. By subjecting the mutant virus libraries to growth in eggs, we may be able to ascertain such egg-adaptive mutations and to pinpoint mutations that allow for growth in eggs but do not change HA's antigenicity.

Another exciting application of deep mutational scanning techniques is to perform functional selections on the HA mutant libraries *in vivo*, such as in ferrets or in mice. The respiratory airway compartments may select for distinct mutations, and transmission studies in ferrets would facilitate an exploration of HA phenotypes that promote transmission [119]. Moving forward, similar extensions of deep mutational scanning approaches may yield

exciting data on mutational effects under various selective pressures.

We can use the measurements of mutational effects to understand viral evolution in nature. HA must maintain its essential functions in order for the virus to remain fit. Although much effort has gone into characterizing viral antigenicity, the non-antigenic effects of mutations are also an important determinant of viral fitness. Yet, no large-scale quantifications of the functional effects of mutations to seasonal H3N2 HA on viral growth existed prior to my work. Generating these quantifications enabled us to examine the relationship between our experimental measurements and the maximum frequency reached by mutations in nature. We found that mutations that we measured to be highly deleterious seldom reach high frequencies in nature. Mutations that reach high frequencies or even reach fixation generally have a more favorable mean effect than those mutations that remain at low frequencies. These results indicated that experimentally defining the effects of mutations on viral growth in cell culture can be of utility for understanding the evolutionary success of viral lineages in nature. Our work also suggests that incorporating these data as well as measurements of the antigenic effects of mutations into fitness models may aid with viral forecasting.

Unsurprisingly, when we applied the effects of mutations measured in a highly diverged H1 HA, there was no correlation between these measurements and H3N2 mutation frequencies. The utility of these experiments thereby degrades as natural strains diverge from the experimental strain. Follow-up work should more precisely determine the extent to which these deep mutational scanning data can be generalized when predicting viral fitness.

The potential for viral escape varies across antibodies. With major efforts toward the use of broadly-neutralizing antibodies as vaccines or therapeutics under way, it has become crucial to characterize the potential for escape from such antibodies. Here I described work in which we formulated a method for calculating the fraction of each viral

mutant that escapes antibody neutralization. This method quantifies the effect sizes of single antigenic mutations and allows us to directly compare these effects across antibodies. Although we find mutations that provide resistance to neutralization from all the antibodies we tested, the effects on escape from the broad stalk-targeting antibodies are much smaller than those from narrow *and* broad antibodies targeting the head domain. A salient implication of these results is that antibody breadth is not a perfect indicator of the ease of viral escape. Our results would seemingly suggest that H1 may be less, but not completely prone to antigenic escape via point mutations from broad anti-stalk antibodies.

Perhaps the H1 we tested exhibits difficulty escaping broad stalk-targeting antibodies because of the low inherent mutational tolerance in its stalk. Despite the fact that mutationally tolerant sites are in close contact (within 4 Å) with the stalk antibodies we tested, the binding energetics of the antibody may be distributed in such a way that neutralization is mediated disproportionately through interactions with mutationally intolerant residues.

Furthermore, a striking finding of my work is the low disparity in mutational tolerance between the head and stalk domains of the H3 HA. In particular, helix A in the stalk domain, which forms the epitope of a number of broad anti-stalk antibodies [140, 121, 31], exhibits relatively high tolerance for mutations. This finding begs the question: Does the ease of viral escape from a given broadly-neutralizing antibody differ across subtypes? Specifically, does the H3 HA also have difficulty escaping stalk-targeting antibodies? Some studies have shown that *de novo* mutations selected for by broad stalk-binding antibodies may have fitness effects on viral growth [31, 65]. Yet, unless we test the antigenic effects of all the possible single mutations to H3 in the context of replication-competent virus, it will be problematic to interrogate the ease of escape from broadly-neutralizing antibodies in this subtype. Further work can evaluate escape from additional broadly-neutralizing antibodies, including ones initially elicited against a group 2 HA subtype. While the two anti-stalk antibodies we tested here, FI6v3 and C179, were initially selected for binding to the group 1 H1 [39, 165], there may be a wide range in the capacity for escape from different classes of broadly-neutralizing antibodies.

Some individuals have very immunodominant serum responses towards HA. Despite strong selection on HA from adaptive immunity, we still have a limited understanding of how polyclonal immunity in serum imposes selection on HA. By leveraging the technique of *mutational antigenic profiling*, I was able to systematically map immune selection on HA by polyclonal serum. My work provided direct evidence that some individuals possess highly immunodominant serum responses against HA, which select for single amino-acid mutations with strong effects on resistance to serum neutralization. In fact, the idea that certain individuals may target HA in an immunodominant fashion was posited in early studies of antigenic variation [236, 155]. Only by systematically testing under immune selection all of the possible single amino-acid replication-competent variants of HA was I able to directly test this hypothesis.

My work demonstrates how immunodominant serum responses can rapidly select for neutralization-resistant mutations with rather large antigenic effect sizes. A number of the sites with the largest effect sizes on escape show variation in natural H3N2 sequences, with some mutations at these sites reaching very high frequencies or even fixation in nature. These findings strongly support the theory that individuals with immunodominant antibody targeting may drive antigenic drift of HA in nature. It would be especially interesting in future experiments to closely examine the within-host variation in influenza-infected individuals with known pre-infection immunodominant serum responses. Although previous studies have found limited within-host variation in acute influenza infections [50, 57, 97, 149, 193], it may be probable that by focusing on those individuals with immunodominant antibody profiles, there exists a greater degree of antigenic variation that parallels antigenic evolution in nature. Indeed, there is evidence of concordance between within-host evolution in long-term H3N2 infections and evolution at the global scale [144, 232].

Moreover, I observed variation in each mutation's effect size on escape across the subjects in our study, indicating that immune selection upon HA varies among individuals. This finding also suggests that antigenic drift mutations may accumulate successively as

the virus is transmitted from one host to another, which is possibly how HA is often able to acquire multiple antigenic site mutations as it evolves.

It is well-established that exposure history to influenza infection and/or vaccination can shape immune targeting of HA [76, 134, 135, 73, 131]. Although all of the individuals I profiled predominantly target a single antigenic region, our mapping approach can feasibly profile many more individuals with diverse exposure histories. Previous studies have implied that younger individuals may narrowly target more variable epitopes in HA while older individuals target more conserved regions [131, 151, 147, 92, 177]. It would therefore be compelling to profile subjects across multiple age groups, including children and the elderly, to directly compare anti-HA targeting in relatively immune-experienced versus immune-naive individuals. Furthermore, recent work has brought attention to the potential implications of immune targeting on disease susceptibility [135, 49]. Therefore it would be interesting to examine if individuals are disproportionately affected by severe influenza virus infection when a drift variant fixes at a site heavily targeted by their sera.

An astonishing finding of my work is the mutational-level consistency in immune targeting in ferret sera. These results have important implications for antigenic characterization and surveillance, which rely heavily on the use of sera from singly infected ferrets. It is therefore vital to characterize the antigenic effects of mutations on escape from human immunity. Sera from ferrets sequentially infected with two diverged viral strains have been shown to mount a response that more closely emulates the epitope targeting in humans with exposure histories to these two strains [134]. In future work, mutational antigenic profiling can assess the degree of similarity between immune targeting in sequentially-infected ferrets and the immune targeting in humans.

In my work, I mapped selection on HA by only neutralizing antibodies in serum. However, there are assuredly additional components of adaptive immunity that exert selection on influenza virus. Still, we have a very limited understanding of how these other constituents of adaptive immunity drive viral evolution. One can leverage mutational antigenic profiling to map escape from mucosal IgA antibodies [179]. It will be important

to study immune selection exerted by non-neutralizing antibodies, which can mediate complement-dependent cellular cytotoxicity and phagocytosis [36, 53, 207, 103]. Future work will need to characterize in great depth anti-NA immunity and its role in driving antigenic drift [150, 184, 218]. All of these directions have the potential to expand our understanding of antigenic evolution in nature.

Appendix A

SUPPLEMENTARY MATERIAL FOR CHAPTER 2

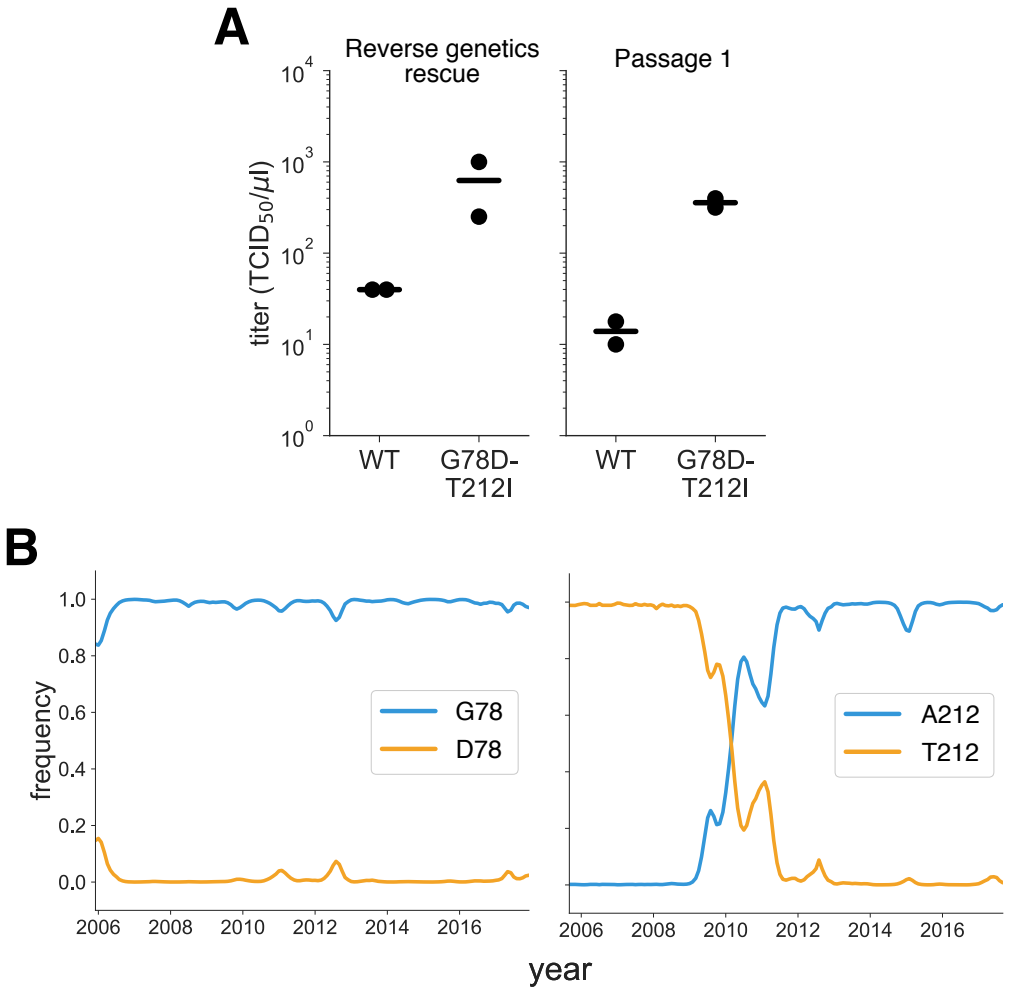

Figure A.1: **Characterization of the G78D-T212I Perth/2009 HA variant. (A)** The G78D-T212I Perth/2009 HA variant supports better viral growth than the wildtype Perth/2009 HA. Viruses were generated in duplicate by reverse genetics with the Perth/2009 NA and WSN internal genes, and passaged once at MOI = 0.01 in MDCK-SIAT1-TMPRSS2 cells. The rescue and passage viral supernatants were collected at 72 hours post-transfection and 44 hours post-infection, respectively, and titered in MDCK-SIAT1-TMPRSS2 cells. The points mark each duplicate and the bar marks the mean. **(B)** The D78 variant remained at a low frequency in natural human H3N2 sequences over the past $\sim$10 years. The A212 variant rose to fixation in $\sim$2011, replacing the T212 variant.

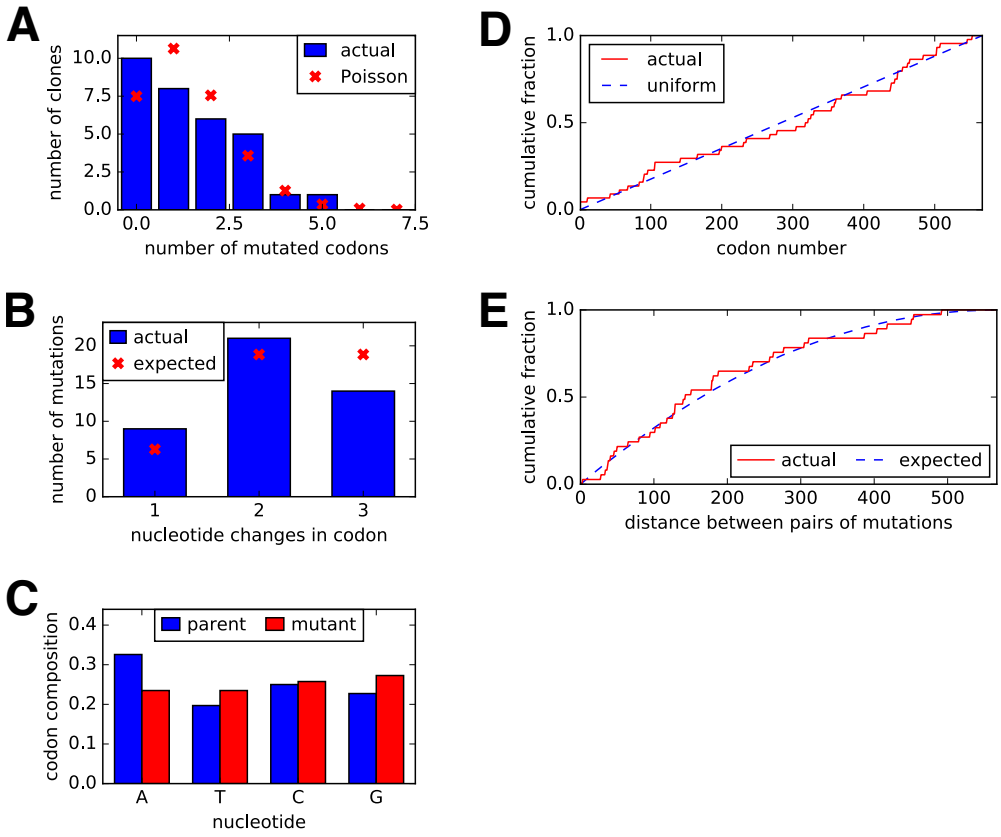

Figure A.2: **Sanger sequencing of 31 randomly chosen clones from the mutant plasmid libraries. (A)** There were an average of ∼1.4 codon mutations per clone across the three plasmid mutant libraries. **(B)** A mixture of one-, two-, and three-nucleotide mutations were present, with slightly fewer triple-nucleotide changes than expected. **(C)** Nucleotide frequencies were uniform in the codon mutations. **(D)** The mutations were distributed relatively evenly across the length of the HA coding sequence. **(E)** We calculated the pairwise distances between mutations for clones carrying more than one mutation. The cumulative distribution of these distances is shown in the red line. The blue line indicates the expected distribution if mutations in multiply mutated genes are randomly dispersed along the sequence.

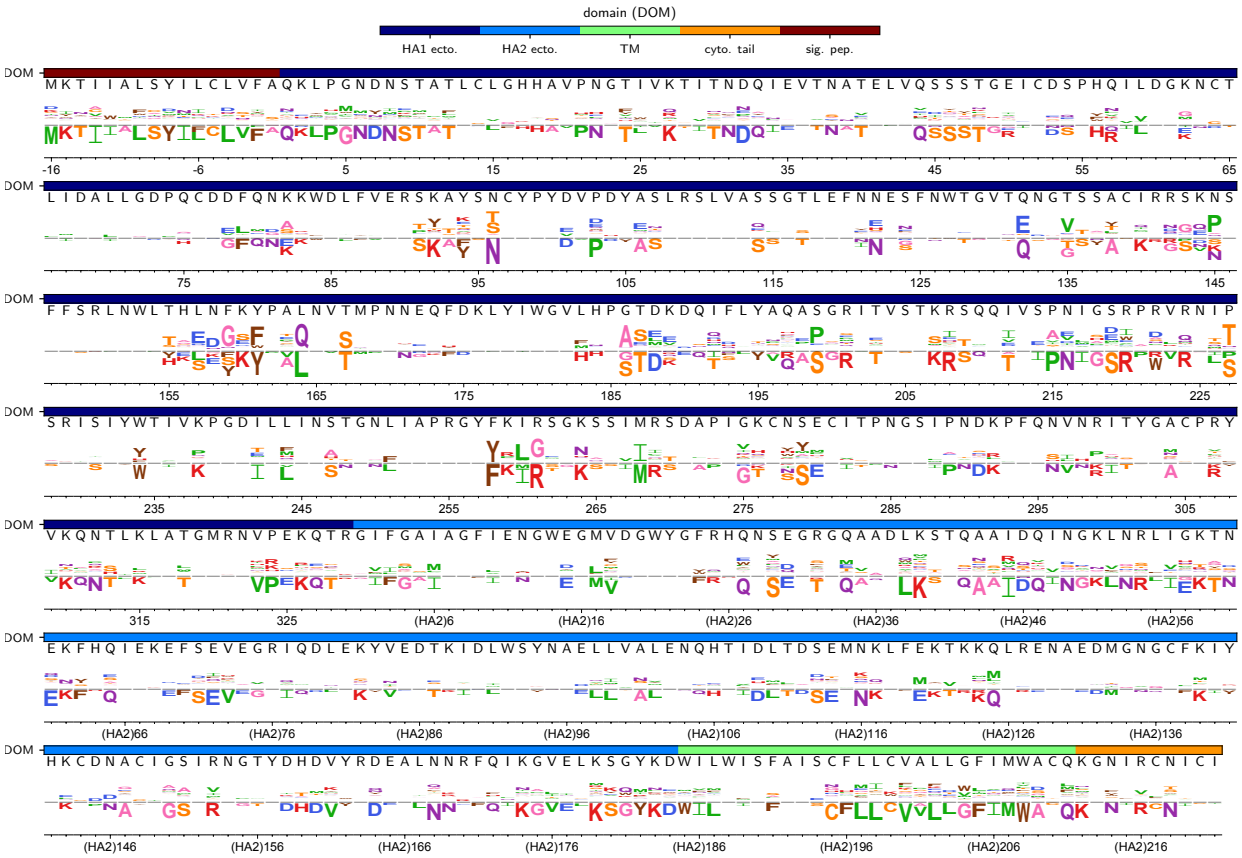

Figure A.3: **Sites where there are strong differences between our experimental measurements and the amino-acid frequencies among natural HA sequences.** We calculated the distance between our H3 measurements and the alignment frequencies using the same approach as in Figure 2.7, but using the alignment frequencies in place of the H1 preferences. For each site, the height of each letter above or below the line indicates how much more or less preferred that amino acid is in our experiments compared to its frequency nature. The overlays show the same information as in Figure 2.2 (domain and wildtype amino acid). The sites are in H3 numbering. The HA alignment used to calculate the natural frequencies is the same one used in Table 2.1.

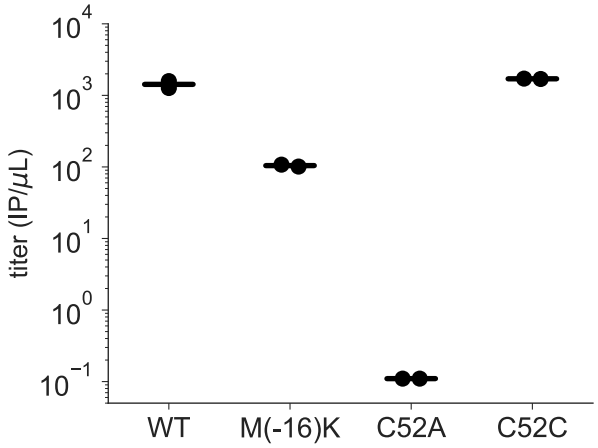

Figure A.4: **Validation that the Perth/2009 HA is somewhat tolerant to mutation of the canonical start codon.** We created variants of the Perth/2009 HA in which the canonical start codon was mutated (amino-acid mutation M(-16)K, codon mutation ATG→AAA), a conserved cysteine was mutated to alanine (C52A, codon mutation TGC→GCA), and the same cysteine was synonymously mutated (C52C, codon mutation TGC→TGT). We selected these mutations because our deep mutational scanning results in Figure 2.2 surprisingly suggest that the start codon (position -16) is fairly tolerant of mutations, but that site 52 is highly intolerant of mutation to anything other than cysteine. The synonymous C52C mutation is a negative control mutation that is not expected to have any effect. We then used reverse genetics to generate viruses carrying the wildtype HA or each point mutant, with GFP packaged in the PB1 segment to enable easy titering by flow cytometry [20, 100]. Each variant was generated in duplicate, and the plots show the viral titer in the supernatant at 53 hours post-transfection. As expected, the C52A virus is essentially non-viable, while the C52C mutation is roughly equivalent to wildtype. The M(-16)K mutation is only moderately attenuated, validating that the canonical start codon is not completely essential for viral growth.

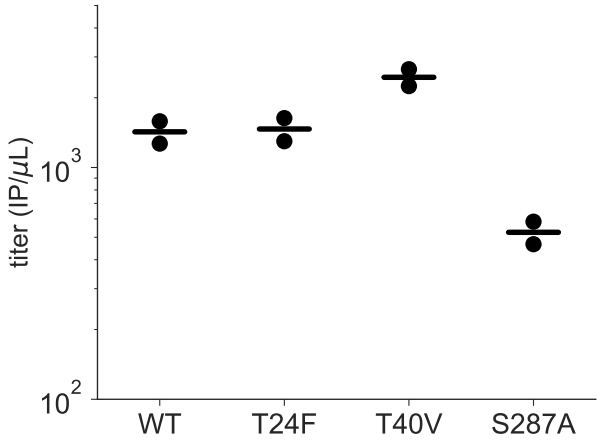

Figure A.5: **Validation of viral variants with mutations at N-linked glycosylation motifs.** We created variants of the Perth/2009 HA with mutations that eliminated N-linked glycosylation motifs (Asn-Xaa-Ser/Thr) at asparagine residues 22, 38, and 285 (these are mutations T24F, T40V, and S287A, respectively). The codon mutations were ACG→TTC, ACT→GTA, and AGC→GCG, respectively. We then used reverse genetics to generate viruses carrying the wildtype HA or each of these mutants. Each variant was generated in duplicate, and the plots show the viral titer in the supernatant at 53 hours post-transfection. The viruses with mutations at the motifs at residues 22 and 38 reached titers at least as high as wildtype, whereas the virus with a mutation to the motif at residue 285 was modestly attenuated.

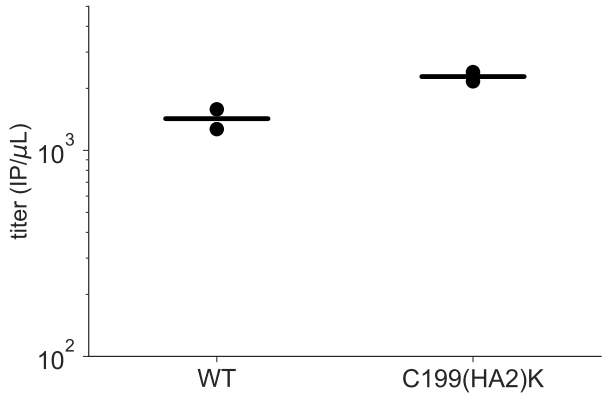

Figure A.6: **Validation of the mutational tolerance of a site in the transmembrane domain.** We created a variant of the Perth/2009 HA with a transmembrane domain mutation, C199(HA2)K (codon mutation TGT→AAG), at a site that our deep mutational scanning suggests should be highly mutationally tolerant (Figure 2.2). We then used reverse genetics to generate viruses carrying the wildtype HA or this mutant. Each variant was generated in duplicate, and the plots show the viral titer in the supernatant at 53 hours post-transfection. The virus with the mutation reached titers comparable to wildtype.

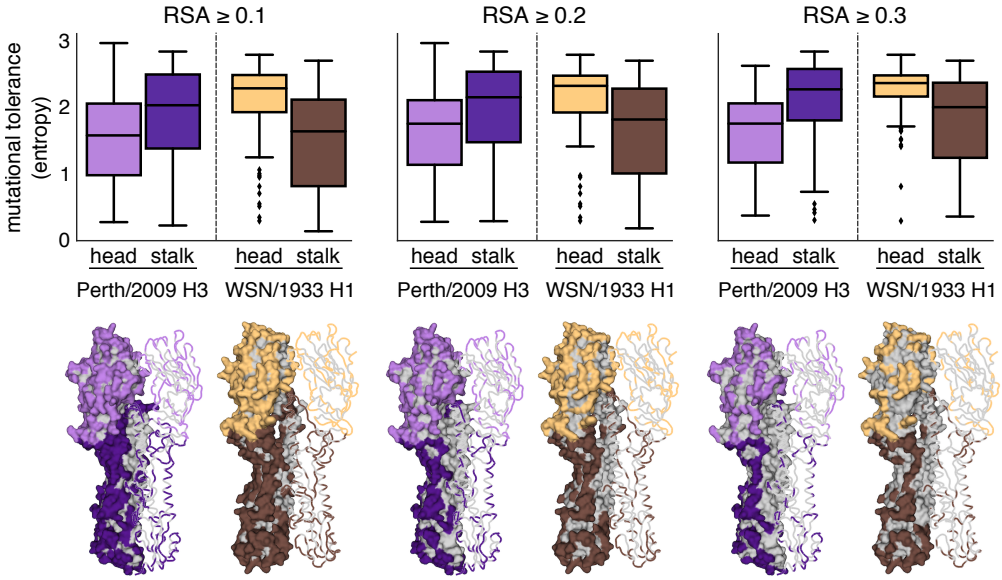

Figure A.7: **Mutational tolerances of the head and stalk domains at various relative solvent accessibility cutoffs.** The mutational tolerances of the head and stalk domains show less disparity for the Perth/2009 H3 HA compared to those for the WSN/1933 H1 HA. We used relative solvent accessibility (RSA) cutoffs of 0.1, 0.2, and 0.3 to define solvent-exposed residues and plotted the mutational tolerances (Shannon entropy of re-scaled preferences) of these residues in the head and stalk domains for the Perth/2009 H3 HA (purple) and the WSN/1933 H1 HA (brown). Residues falling in between the two cysteines at sites 52 and 277 were defined as belonging to the head domain, while all other residues were defined as the stalk domain. The HA structures color the residues that are defined as solvent exposed at a given RSA cutoff. One monomer is shown in surface representation and another monomer shown in ribbon representation. Residues in lighter shades of purple or brown are in the head domain, while residues in darker shades are in the stalk domain. Note that the mutational tolerance values are not comparable between the two HAs.

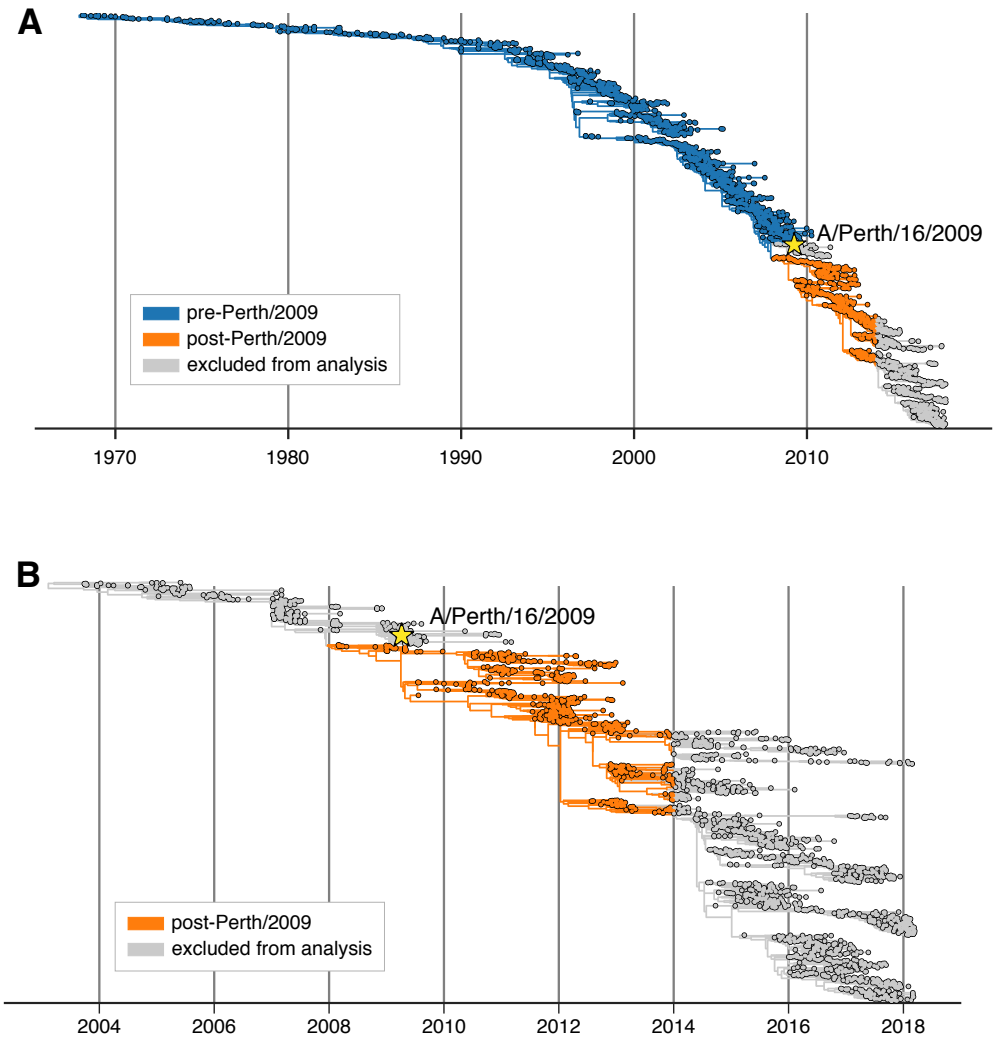

Figure A.8: **A phylogenetic tree of all HA sequences used in our analysis of mutation frequencies. (A)** HA sequences were sampled at a rate of six viruses per month from January 1, 1968 through February 1, 2018. The Perth/2009 strain used in our experiments is indicated. The rest of the tree is partitioned into nodes that preceded the split of the Perth/2009 strain from the trunk of the tree (blue) and nodes that branched off the trunk after the clade containing Perth/2009 (orange). In Figure 2.5, these two partitions of the tree are analyzed separately. Nodes in the clade containing the Perth/2009 strain and nodes sampled in 2014 or after were excluded from our analyses. The Perth/2009 strain was excluded to avoid artifacts related to mutations that occurred on the branches leading to the HA sequence used in the experiment. The post-2014 nodes were excluded because the evolutionary fates of many sequences after this date are not yet fully resolved. **(B)** The post-Perth/2009 partition of the tree containing only sequences from unpassaged isolates.

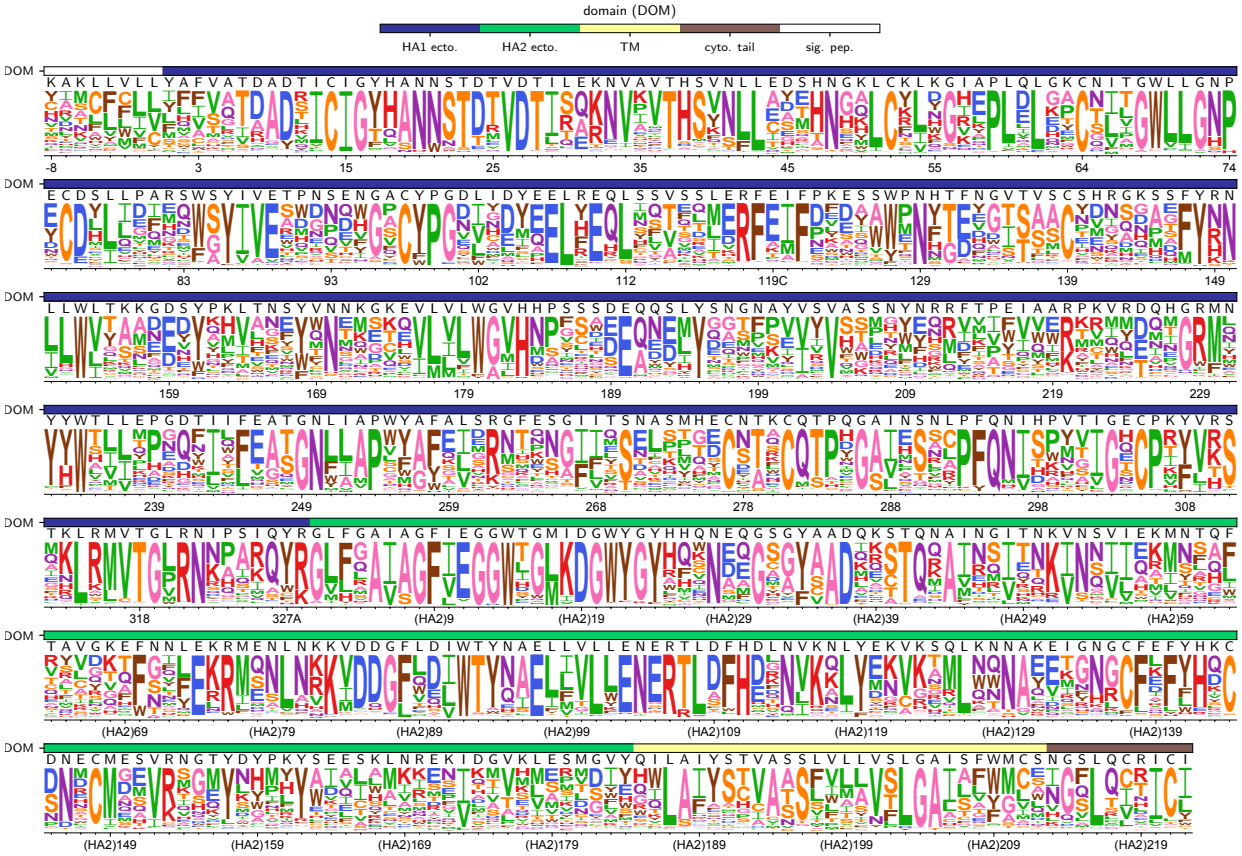

Figure A.9: **The site-specific amino-acid preferences of the WSN/1933 H1 HA.** The amino-acid preferences of the WSN/1933 H1 HA from [59] after taking the average of the experimental replicates and re-scaling [94] by a stringency parameter of 2.05 (see `https://github.com/jbloomlab/dms_tools2/blob/master/examples/Doud2016/analysis_notebook.ipynb`). The overlays show the same information as in Figure 2.2 (domain and wildtype amino acid). Note that [59] used libraries in which all codons were mutagenized *except* for the one encoding N-terminal methionine. Therefore, no data is shown for the first codon in the gene. The sites are in H3 numbering.

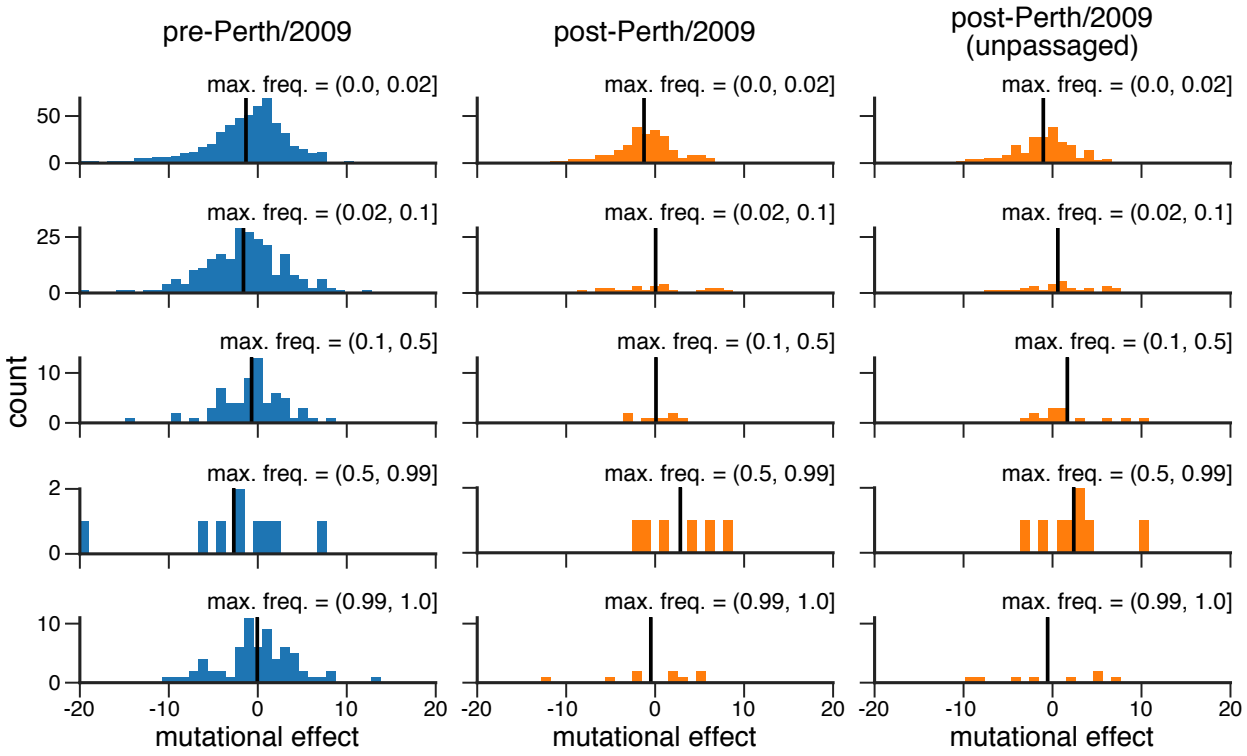

Figure A.10: **The distribution of mutational effects measured in H1 HA among H3N2 mutations binned by the maximum frequency that they reach.** This figure repeats the analysis of the H3N2 mutation frequencies in Figure 2.5B, but uses the deep mutational scanning data for an H1 HA as measured in [59].

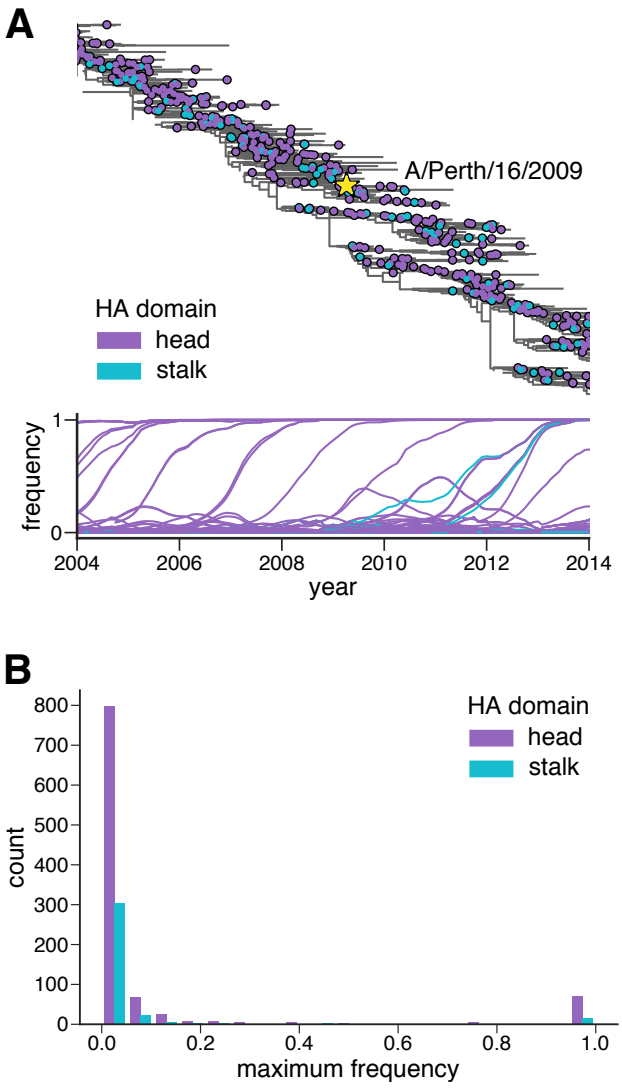

Figure A.11: **Frequency trajectories of head and stalk domain mutations. (A)** This figure repeats the analysis of the H3N2 mutation frequencies in Figure 2.4, but colors amino-acid mutations by whether they occur in the head (purple) or the stalk (blue) domain. **(B)** Histogram of mutation maximum frequencies by the number of mutations in the head and stalk domains. It is clear that mutations in the head domain are more numerous than those in the stalk, particularly among mutations that reach high frequencies.

Supplemental Files

Descriptions of each file are shown below. Please refer to the publication for the actual files [128].

File S1. (**pHW_Perth09-HA-G78D-T212I.txt**) Genbank file giving the full sequence of the bidirectional reverse-genetics plasmid pHW-Perth09-HA-G78D-T212I, which encodes the wildtype HA sequence used in this study.

File S2. (**Perth2009_subamplicon_primers.xlsx**) Excel file providing the primers used to generate the barcoded subamplicons for Perth/2009 HA deep sequencing.

File S3. Excel file giving the amino-acid preferences in sequential 1, 2, ... numbering of the Perth/2009 HA. The unscaled preferences for replicates 1, 2, 3-1, and 3-2 are each in a separate tab of the file. Additional tabs give the across-replicate averaged and re-scaled amino-acid preferences in sequential numbering and in H3 numbering as shown in Figure 2.2. There are also tabs that give the conversion from sequential to H3 numbering, and a list of the mutations in the 31 clones we Sanger sequenced to evaluate the mutation rate of the mutant plasmid libraries. Each tab can simply be exported to CSV for computational analyses.

File S4. (**gisaid_acknowledgment_table.xls**) Excel file providing acknowledgments and accessions for sequences downloaded from GISAID.

Appendix B

SUPPLEMENTARY MATERIAL FOR CHAPTER 3

antibody	concentration (μg/ml)	replicate	fraction surviving
FI6v3	0.1	1a	0.01662
FI6v3	0.1	1b	0.01390
FI6v3	0.2	1a	0.00465
FI6v3	0.2	1b	0.00345
FI6v3	0.1	2	0.02322
FI6v3	0.2	2	0.00278
FI6v3	0.1	3	0.00903
FI6v3	0.2	3	0.00144
S139/1	100.0	1	0.02490
S139/1	200.0	1	0.01470
S139/1	300.0	1	0.01270
S139/1	100.0	2	0.02190
S139/1	200.0	2	0.01720
S139/1	300.0	2	0.00854
S139/1	100.0	3	0.05180
S139/1	200.0	3	0.04060
S139/1	300.0	3	0.03750
C179	1.0	1a	0.00941
C179	1.0	1b	0.00890
C179	1.0	1c	0.00960
C179	2.5	1	0.00450
C179	1.0	2	0.00554
C179	2.5	2	0.00198
C179	1.0	3	0.00256
C179	2.5	3	0.00100

Table B.1: **The total fraction of virions surviving each antibody treatment at each concentration as estimated by qPCR.** These are the quantities referred to as γ. This table shows the values for the broad antibodies; values for the narrow H17-L17, H17-L10, and H17-L7 antibodies have been reported previously [60].

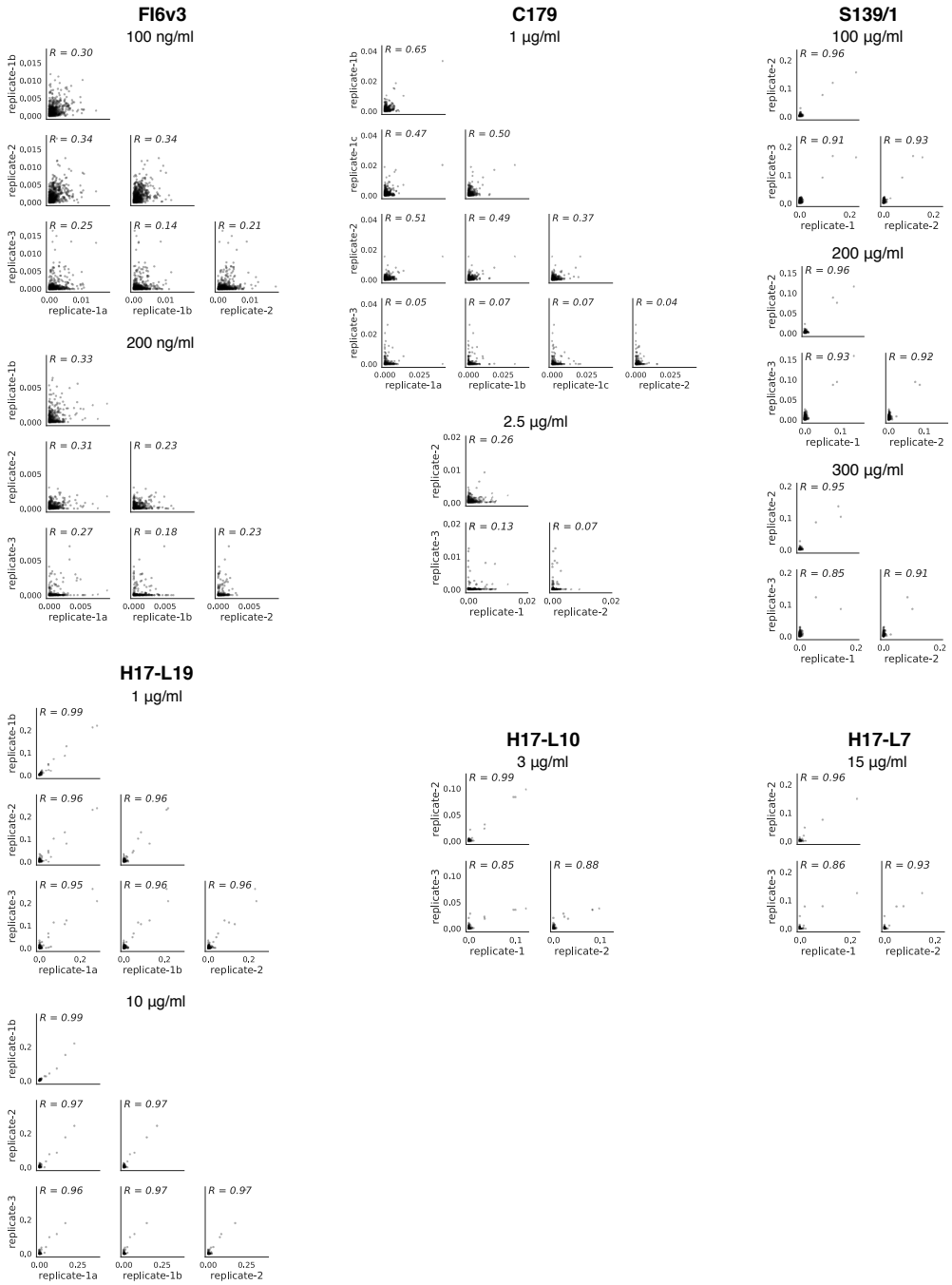

Figure B.1: **Correlations across experimental replicates.** Each point represents one site in HA, and gives the fraction surviving above average across all amino-acid mutations at that site, as calculated using Equation 3.10. The replicates are highly correlated for antibodies with strong escape mutations (S139/1, H17-L19, H17-L10, and H17-L7), and reasonably correlated for antibodies with only weak escape mutations (FI6v3 and C179).

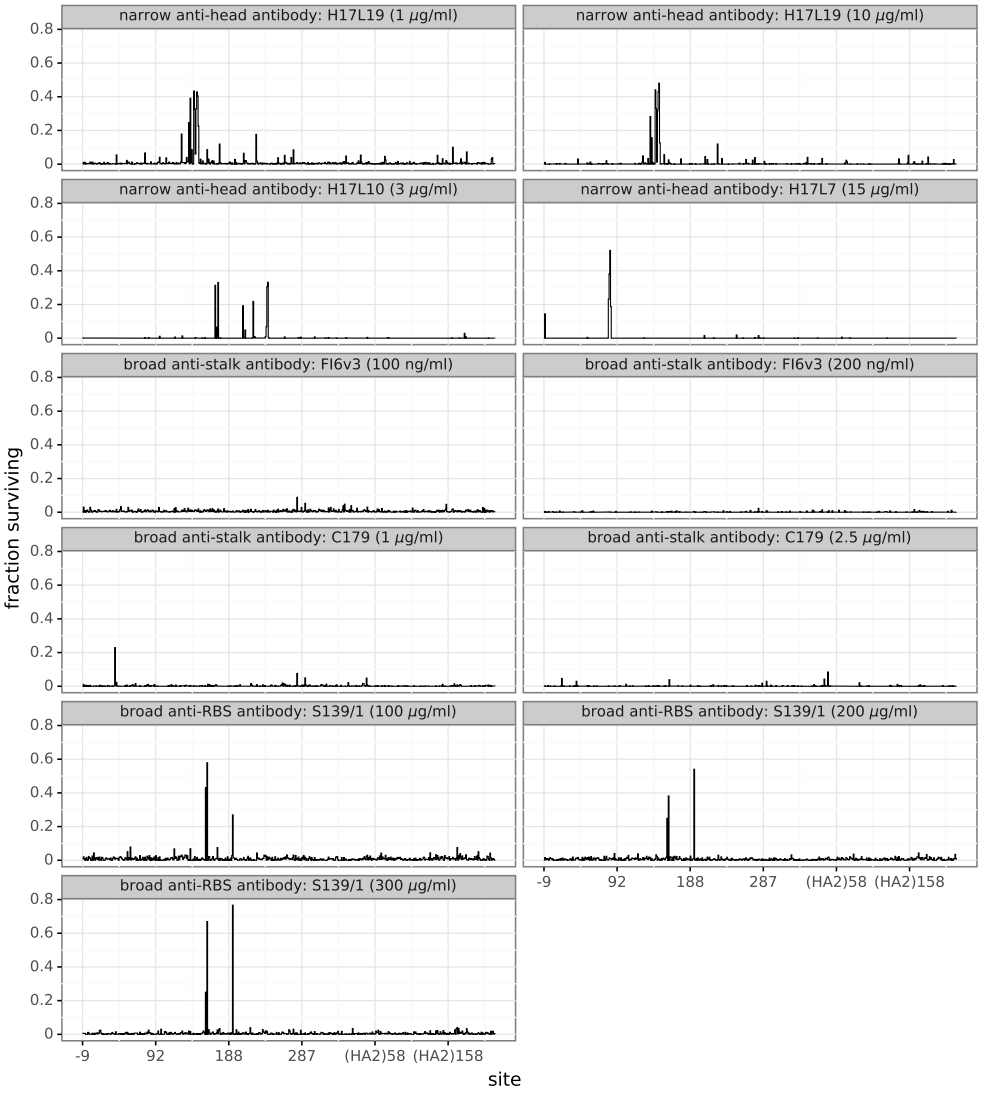

Figure B.2: **The excess fraction surviving for the single strongest escape mutation at each site.** This plot differs from Figure 3.4 in that the height of the line indicates the excess fraction of virions that survive the antibody selection for the single strongest escape mutation at that site, rather than the average across all amino-acid mutations at that site.

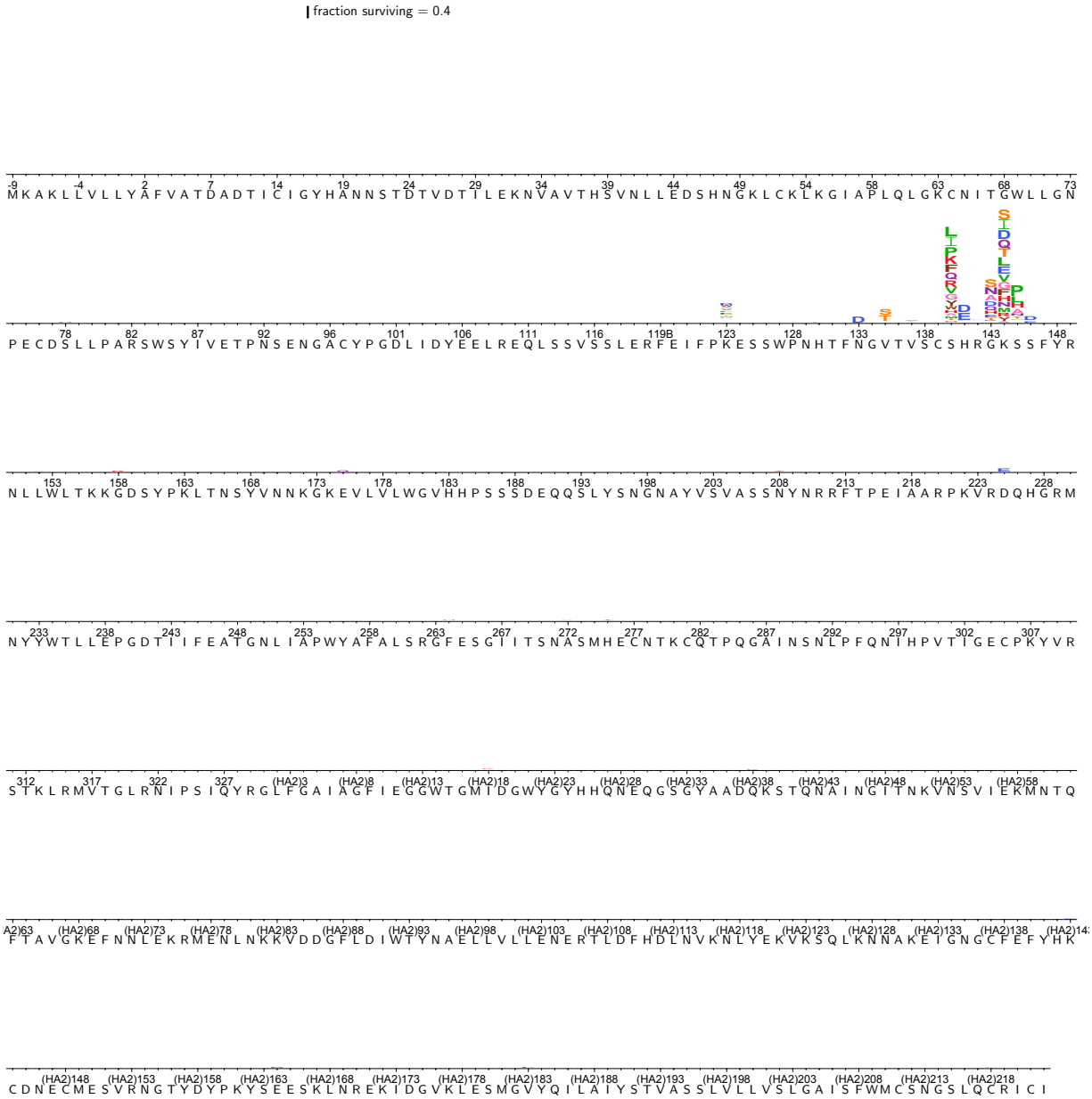

Figure B.3: **The excess fraction surviving selection with antibody H17L19 for all amino-acid mutations.** The excess fraction surviving for each replicate was computed using Equation 3.2, then we took the median across all technical and biological replicates for each antibody concentration, and then took the medians of those values across concentrations. The height of each letter is proportional to the excess fraction surviving of virions with that mutation. The scale bar at the top of the plot relates the letter heights to the actual fractions. The sites are labeled using H3 numbering.

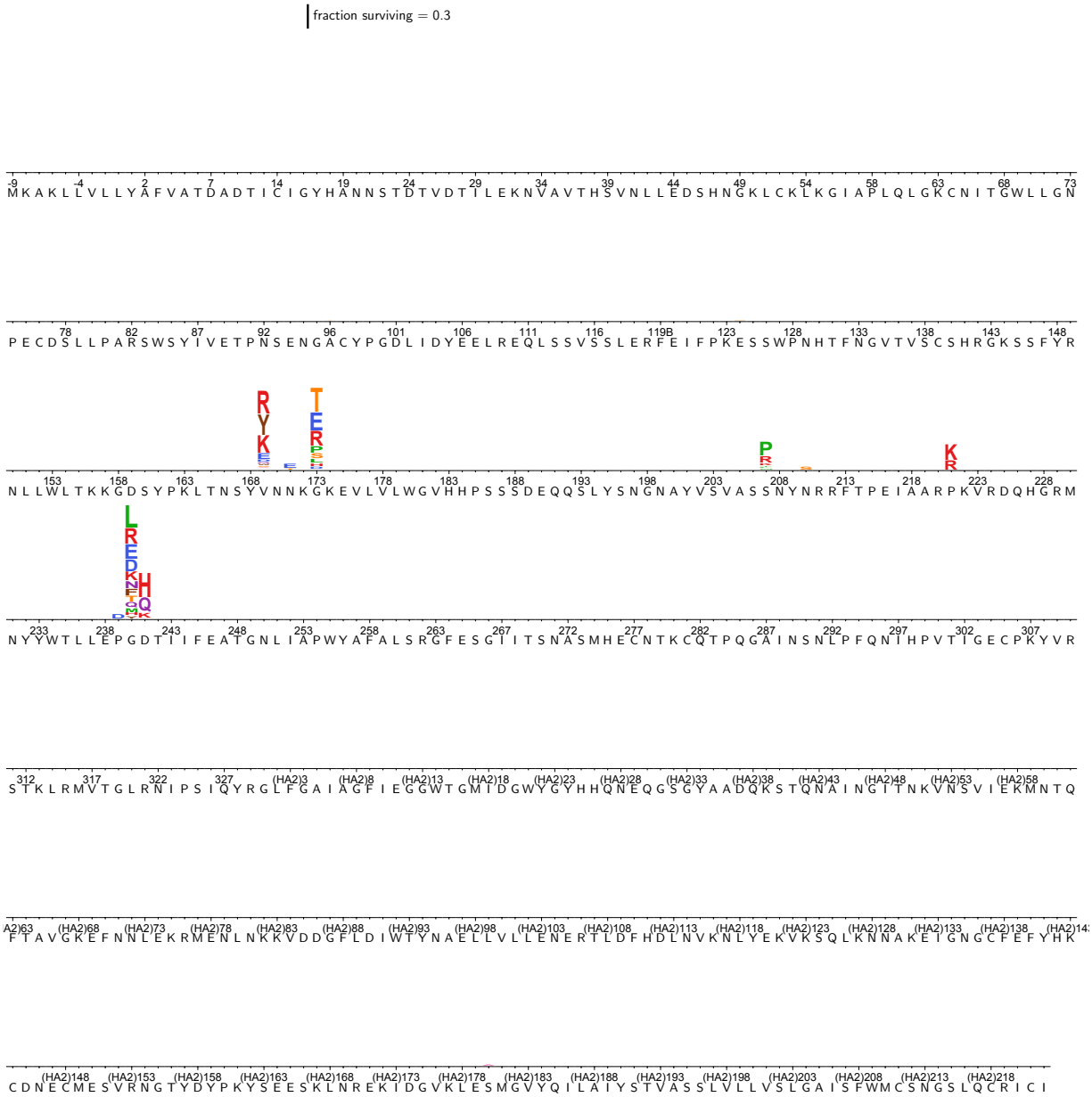

Figure B.4: **The excess fraction surviving selection with antibody H17L10 for all amino-acid mutations.** The excess fraction surviving for each replicate was computed using Equation 3.2, then we took the median across all technical and biological replicates for each antibody concentration, and then took the medians of those values across concentrations. The height of each letter is proportional to the excess fraction surviving of virions with that mutation. The scale bar at the top of the plot relates the letter heights to the actual fractions. The sites are labeled using H3 numbering.

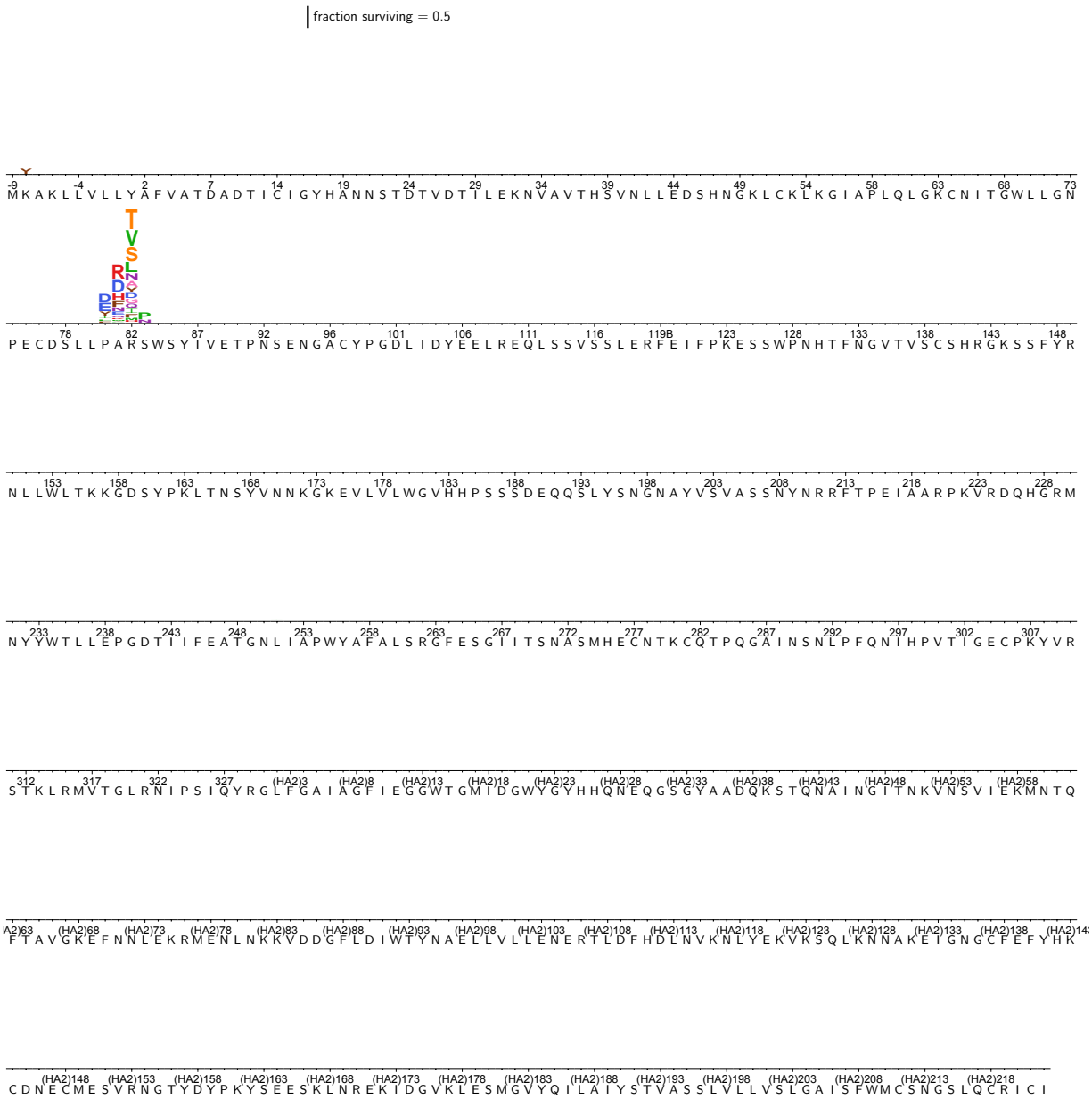

Figure B.5: **The excess fraction surviving selection with antibody H17L7 for all amino-acid mutations.** The excess fraction surviving for each replicate was computed using Equation 3.2, then we took the median across all technical and biological replicates for each antibody concentration, and then took the medians of those values across concentrations. The height of each letter is proportional to the excess fraction surviving of virions with that mutation. The scale bar at the top of the plot relates the letter heights to the actual fractions. The sites are labeled using H3 numbering.

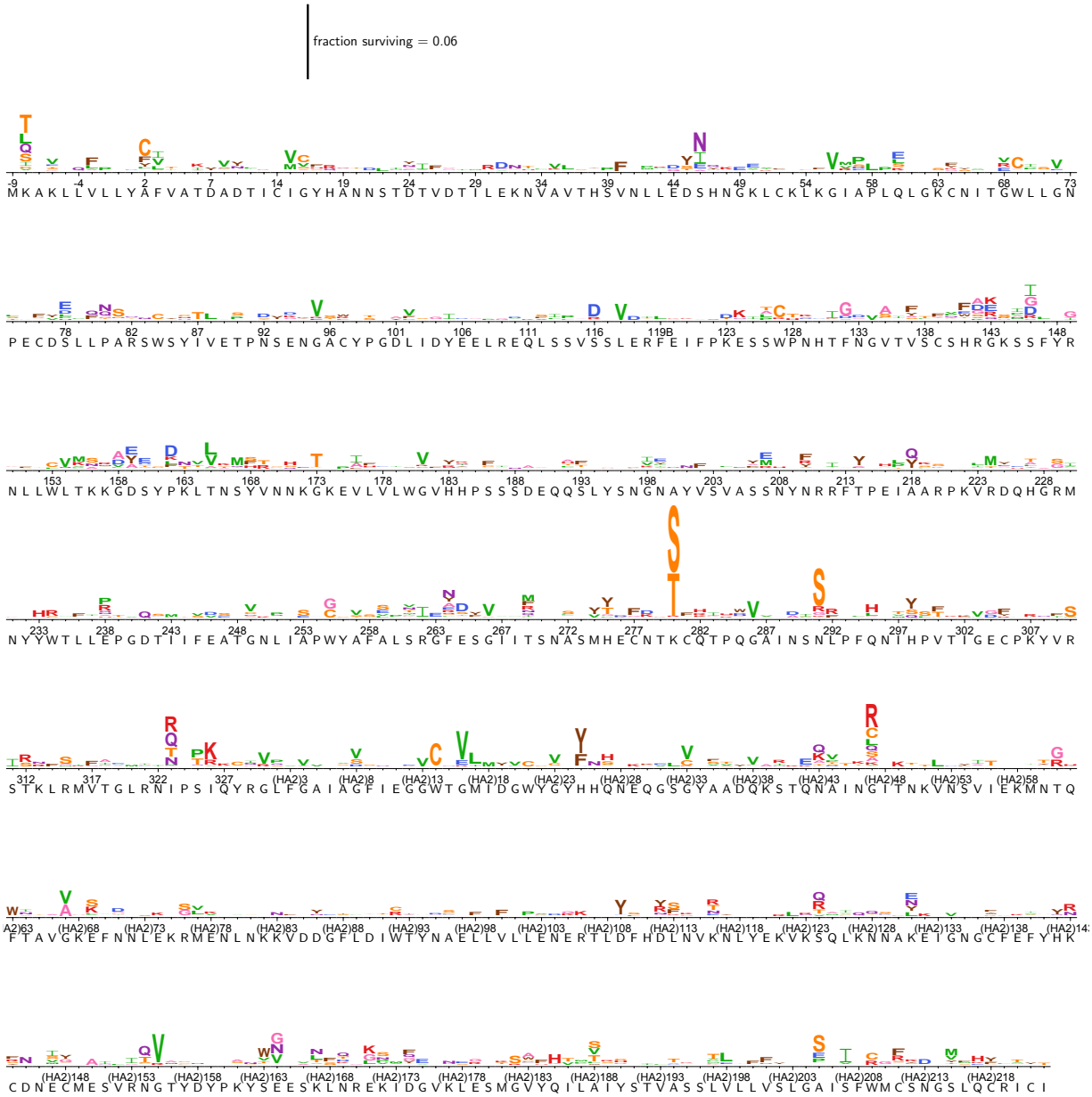

Figure B.6: **The excess fraction surviving selection with antibody FI6v3 for all amino-acid mutations.** The excess fraction surviving for each replicate was computed using Equation 3.2, then we took the median across all technical and biological replicates for each antibody concentration, and then took the medians of those values across concentrations. The height of each letter is proportional to the excess fraction surviving of virions with that mutation. The scale bar at the top of the plot relates the letter heights to the actual fractions. The sites are labeled using H3 numbering.

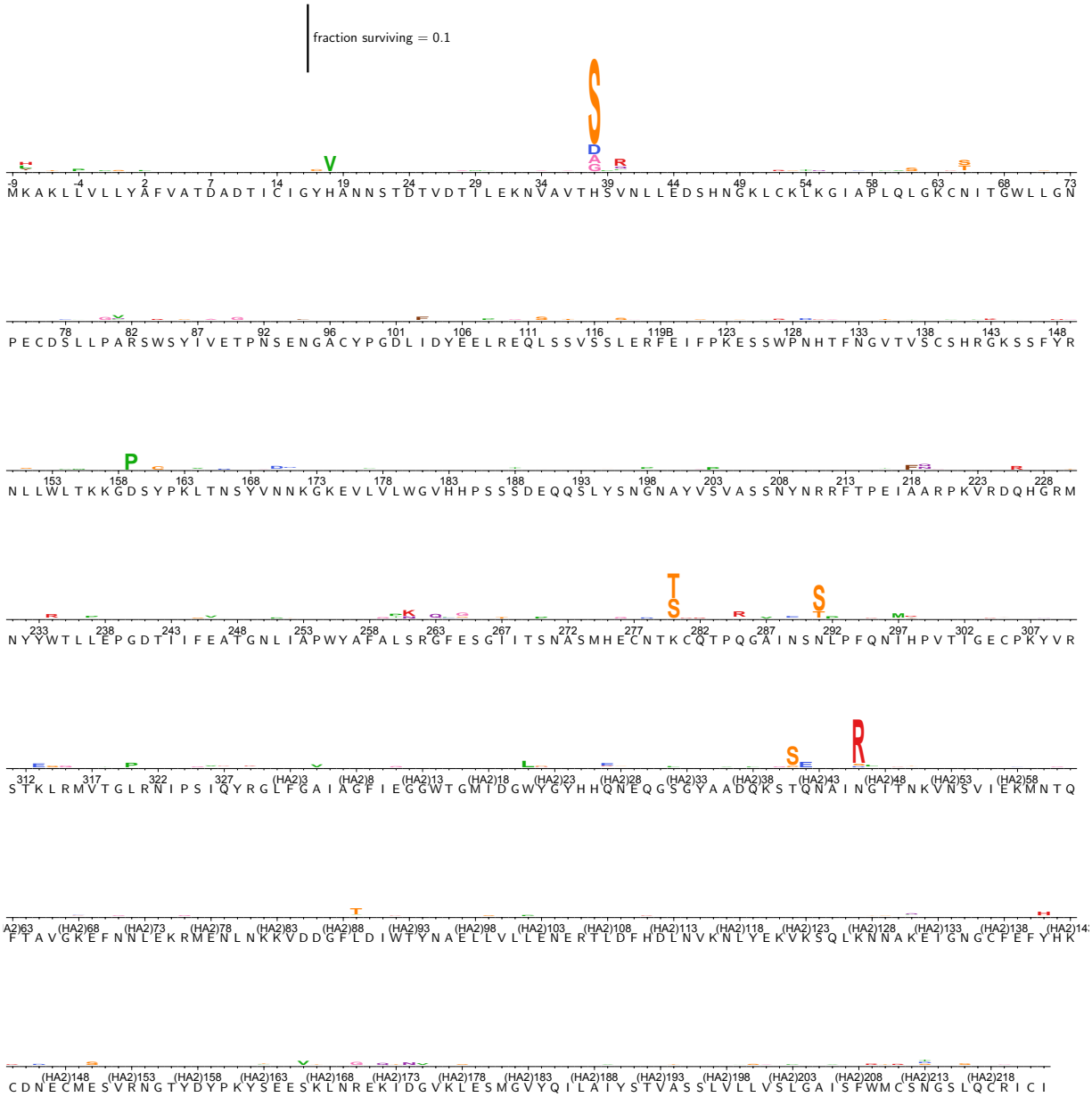

Figure B.7: **The excess fraction surviving selection with antibody C179 for all amino-acid mutations.** The excess fraction surviving for each replicate was computed using Equation 3.2, then we took the median across all technical and biological replicates for each antibody concentration, and then took the medians of those values across concentrations. The height of each letter is proportional to the excess fraction surviving of virions with that mutation. The scale bar at the top of the plot relates the letter heights to the actual fractions. The sites are labeled using H3 numbering.

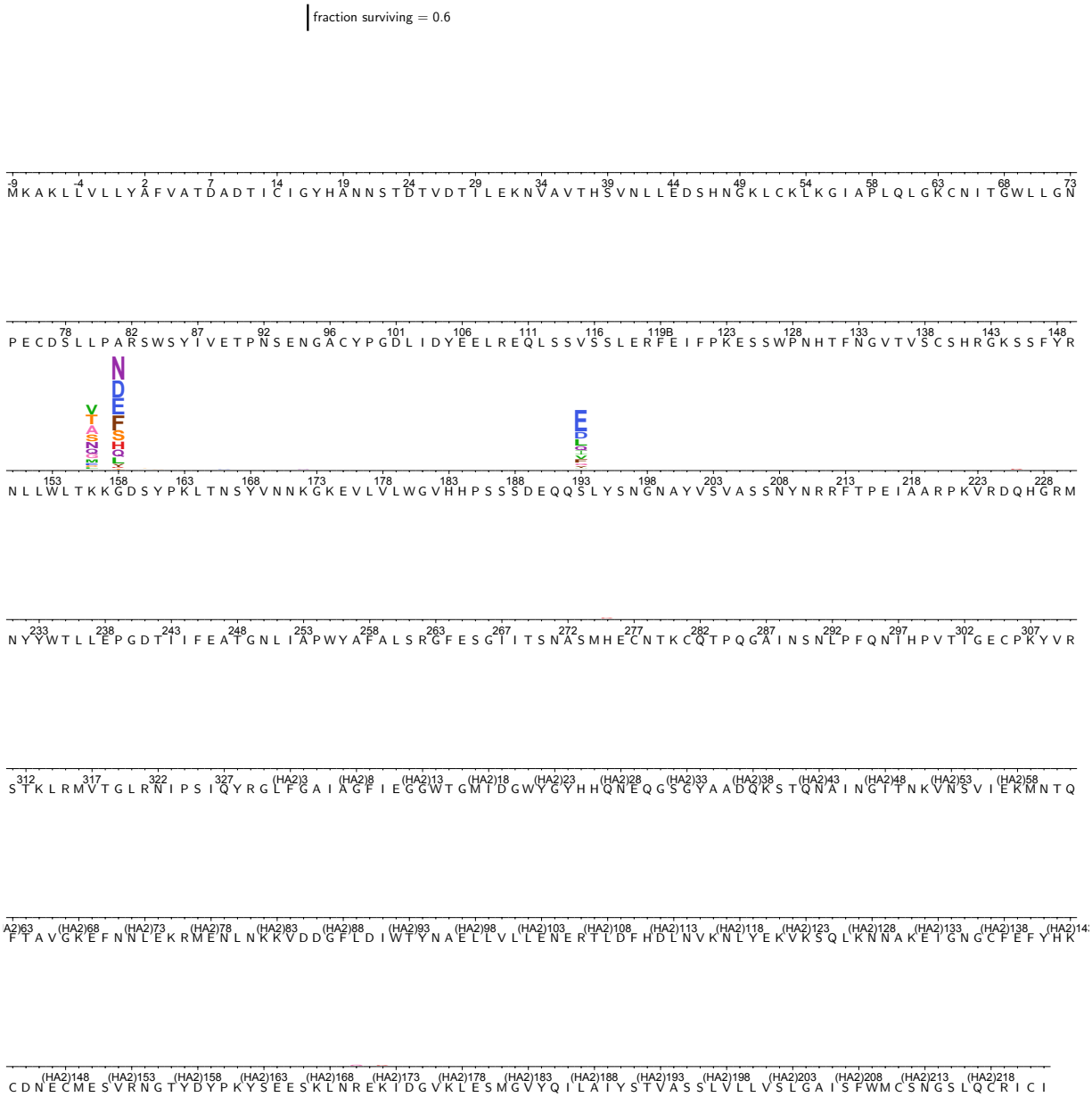

Figure B.8: **The excess fraction surviving selection with antibody S139/1 for all amino-acid mutations.** The excess fraction surviving for each replicate was computed using Equation 3.2, then we took the median across all technical and biological replicates for each antibody concentration, and then took the medians of those values across concentrations. The height of each letter is proportional to the excess fraction surviving of virions with that mutation. The scale bar at the top of the plot relates the letter heights to the actual fractions. The sites are labeled using H3 numbering.

A

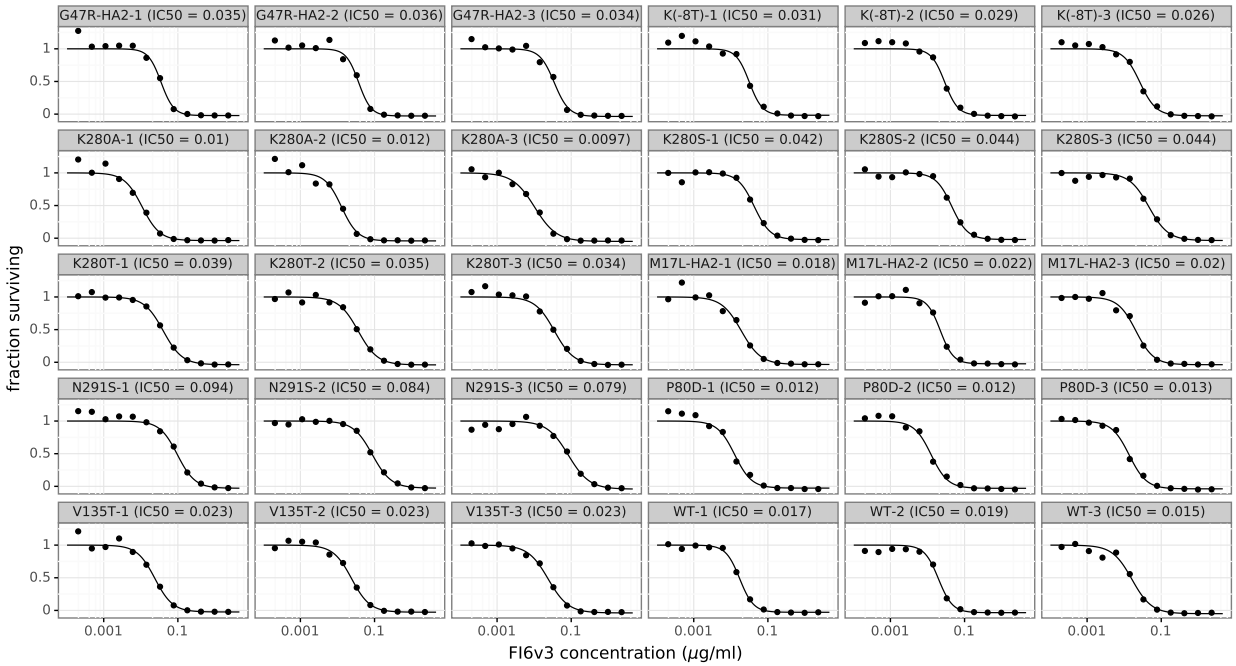

B

variant	replicate-1	replicate-2	replicate-3	mean	Pcorr
K280S	0.042	0.044	0.044	0.043	0.00072
G47R-HA2	0.035	0.036	0.034	0.035	0.0037
K280T	0.039	0.035	0.034	0.036	0.0087
N291S	0.094	0.084	0.079	0.086	0.023
K(-8T)	0.031	0.029	0.026	0.029	0.04
K280A	0.01	0.012	0.0097	0.011	0.12
V135T	0.023	0.023	0.023	0.023	0.27
P80D	0.012	0.012	0.013	0.013	0.42
M17L-HA2	0.018	0.022	0.02	0.02	1
WT	0.017	0.019	0.015	0.017	NaN

Figure B.9: **Replicates of the FI6v3 neutralization curves in Figure 3.6A.** The neutralization assays were performed in triplicate for all nine mutants and wildtype. Figure 3.6A shows the *average* of those replicates. (A) The neutralization data for each replicate shown individually, with IC50 values fit using a four-parameter logistic curve with the top value constrained to one (see `https://jbloomlab.github.io/dms_tools2/dms_tools2.neutcurve.html` for the code used for the fitting.) (B) Table of the IC50 values for each replicate. We used an unpaired Student's t-test with unequal variances to test the null hypothesis that each mutant had an IC50 indistinguishable from wildtype. We then used Bonferroni's method to correct the P-values for multiple testing, and report these corrected values.

Supplemental Files

Descriptions of each file are shown below. Please refer to the publication for the actual files [61].

File S5. (**Conversion from sequential numbering of the A/WSN/1933 HA to H3 numbering.**) In this CSV file, the *original* column gives the residue number in sequential (1, 2, ...) numbering of the A/WSN/1933 HA, and the *new* column gives the residue number in H3 numbering.

File S6. (**Sequences used to infer the tree for all HA subtypes.**) This FASTA file gives the HA sequences used to infer the tree of subtypes in Figure 3.2.

File S7. (**Computer code and data for the analysis of the mutational antigenic profiling data.**) The code in this ZIP file performs the entire computational analysis beginning with downloading the FASTQ files from the Sequence Read Archive. The ZIP file contains a `README` file that explains the contents in detail. The actual analysis is performed by the Jupyter notebook `analysis_notebook.ipynb`, which includes embedded plots summarizing key statistics and results. An HTML version of this notebook is also included as Supplementary Data 8.

File S8. (**HTML version of the analysis notebook.**) This file is an HTML rendering of the Jupyter notebook in Supplementary Data 7. It contains detailed plots for all aspects of the deep sequencing data and its analysis.

File S9. (**The excess fraction surviving for each mutation for each antibody.**) This file is a ZIP of CSV files giving the numerical values plotted in the logo plots. These are median excess fraction surviving taken first across replicates and then across antibody concentrations. See Equation 3.2.

File S10. (**The fraction surviving for each mutation for each antibody.**) This file differs from Supplementary Data 9 only in that the values are *not* adjusted to be in excess of the library average (e.g., they are from Equation 3.1 rather than Equation 3.2).

Appendix C

SUPPLEMENTARY MATERIAL FOR CHAPTER 4

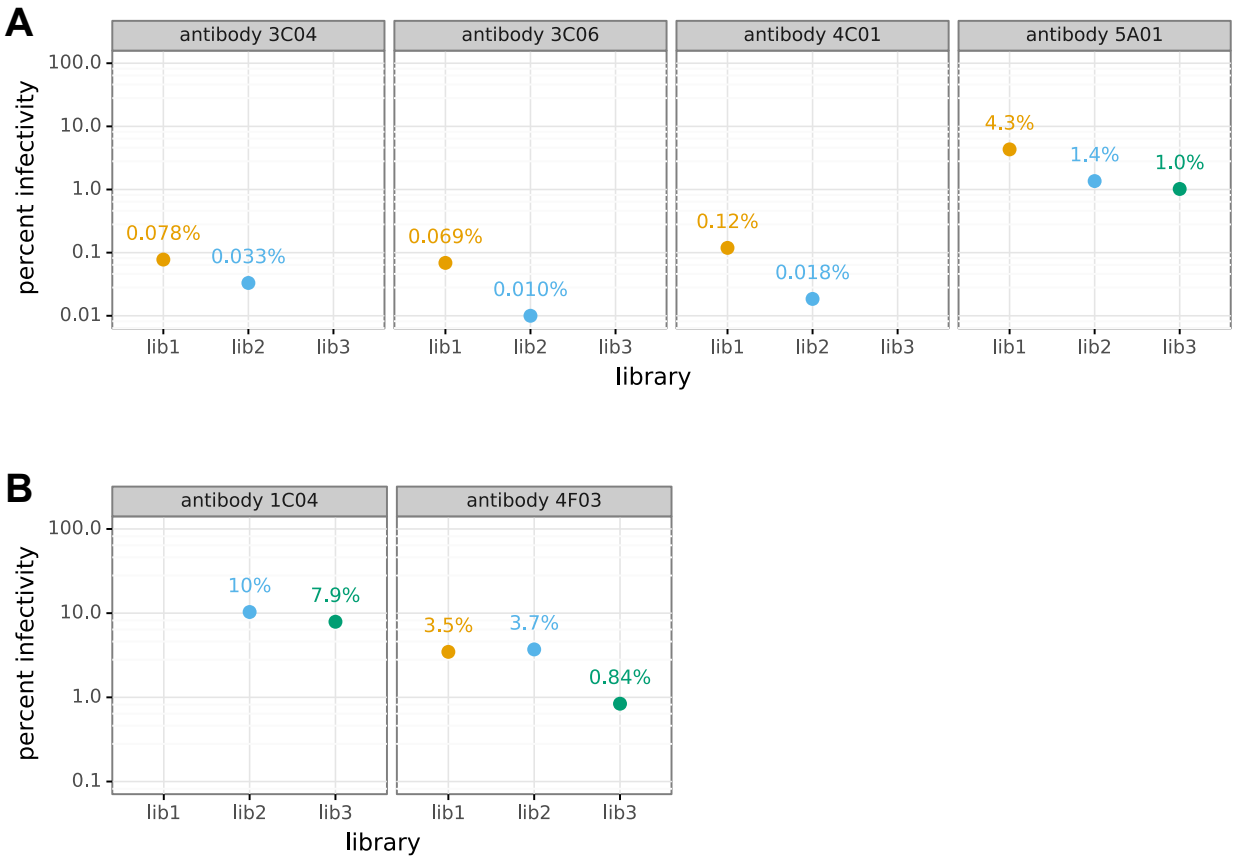

Figure C.1: **Percent of viral library retaining infectivity after antibody treatment during mutational antigenic profiling.** The percent of the mutant virus library that remained infectious after incubation with antibody was determined using qPCR for each replicate of the mutational antigenic profiling. Higher antibody concentrations generally lead to larger values of the immune selection measured in the mutational antigenic profiling.

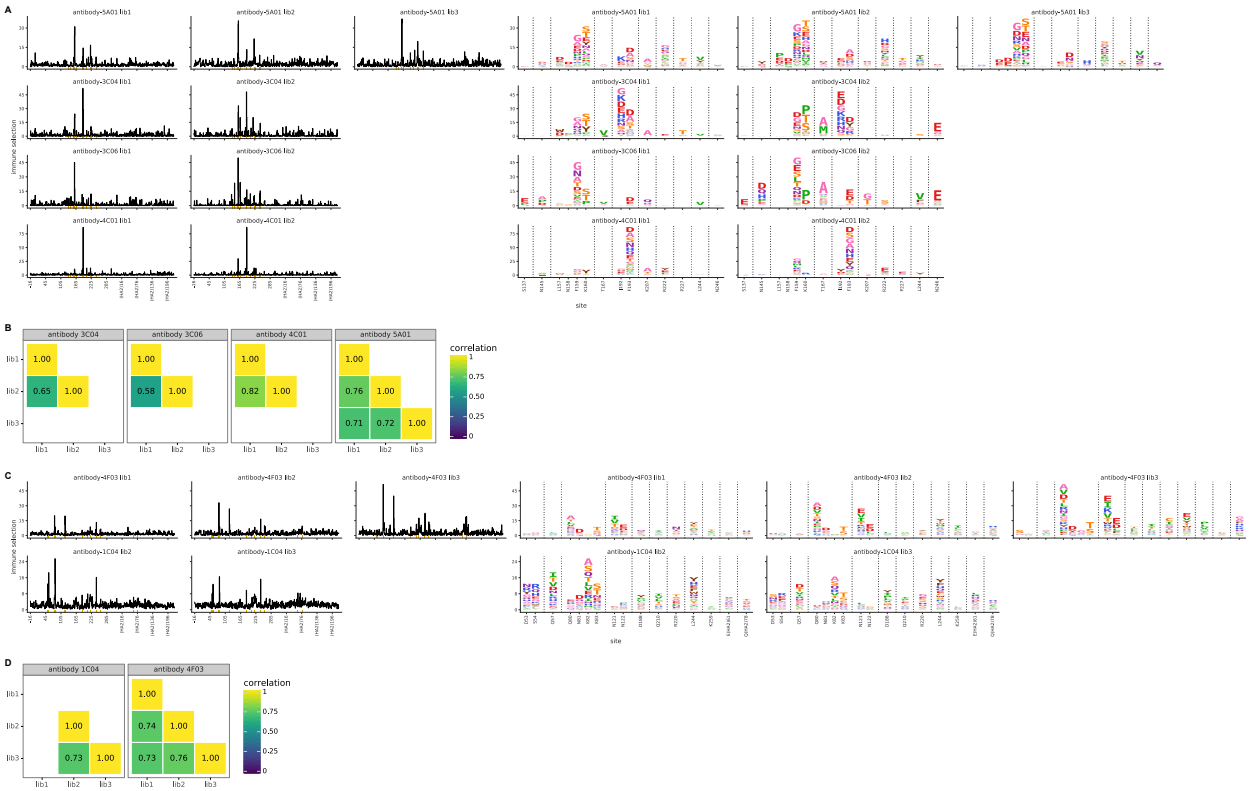

Figure C.2: **Biological replicates of the mutational antigenic profiling are well correlated.** For each antibody, we performed two or three biological replicates of the mutational antigenic profiling. Each replicate used a fully independently generated mutant library. **(A)** Maps of mutations selected by each antibody with each replicate viral mutant library ("lib1", "lib2", or "lib3"). These plots are replicate-to-replicate breakdowns of those in Figure 4.2A,C except that the logo plots are colored by the physicochemical properties of amino acids rather than using the color scheme in the main figure. Note that Figure 4.2A,C displays the median of the replicates shown here. **(B)** The Pearson correlation coefficients of the total immune selection at each site (height of the letter stack) computed over all sites for each pair of replicates. **(C)**, **(D)** are like (A) and (B) but for the antibodies targeting lower on the HA head.

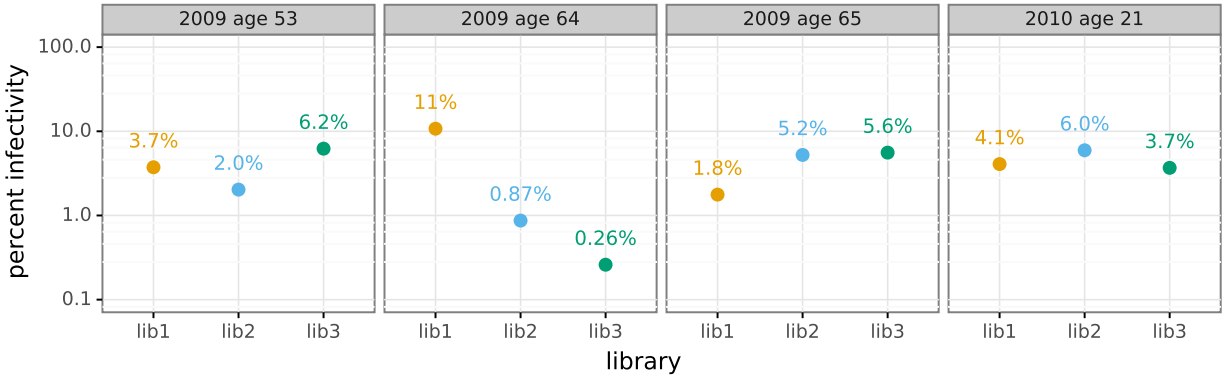

Figure C.3: **Percent of viral library retaining infectivity after serum treatment during mutational antigenic profiling.** The percent of the mutant virus library that remained infectious after incubation with serum was determined using qPCR for each replicate of the mutational antigenic profiling. Higher serum concentrations generally lead to larger values of the immune selection measured in the mutational antigenic profiling.

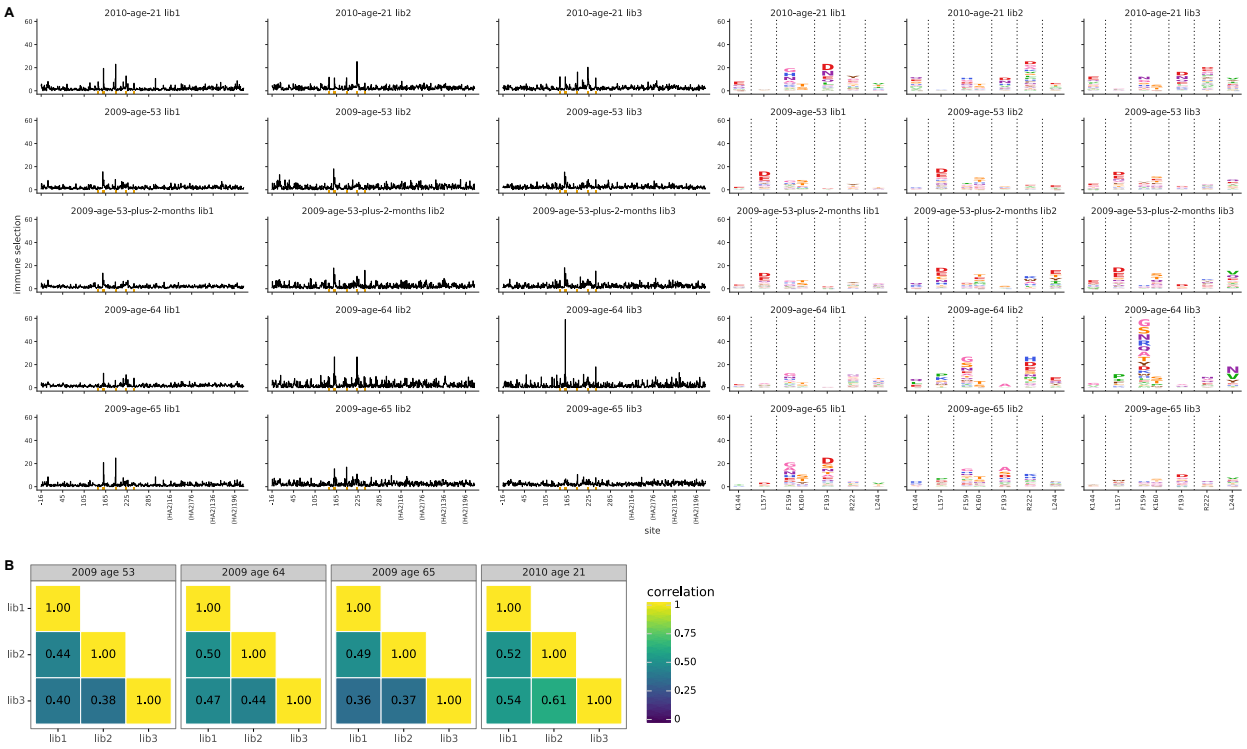

Figure C.4: **Biological replicates of the mutational antigenic profiling are well correlated.** For each serum, we performed three biological replicates of the mutational antigenic profiling. Each replicate used a fully independently generated mutant library. **(A)** Maps of mutations selected by each serum with each replicate viral mutant library ("lib1", "lib2", or "lib3"). These plots are replicate-to-replicate breakdowns of those in Figure 4.3A,B except that the logo plots are colored by the physicochemical properties of amino acids rather than using the color scheme in the main figure. Note that Figure 4.3A displays the median of the replicates shown here. Site 189 is not shown in the logo plots here since it is not a strongly selected mutation for any of the human serum samples in this figure, and is shown in the main Figure 4.3B simply for comparative purposes with the ferret sera. The serum sample labeled "2009 age 53 plus 2 months" is that described in Figure 4.4. **(B)** The Pearson correlation coefficients of the total immune selection at each site (height of the letter stack) computed over all sites for each pair of replicates.

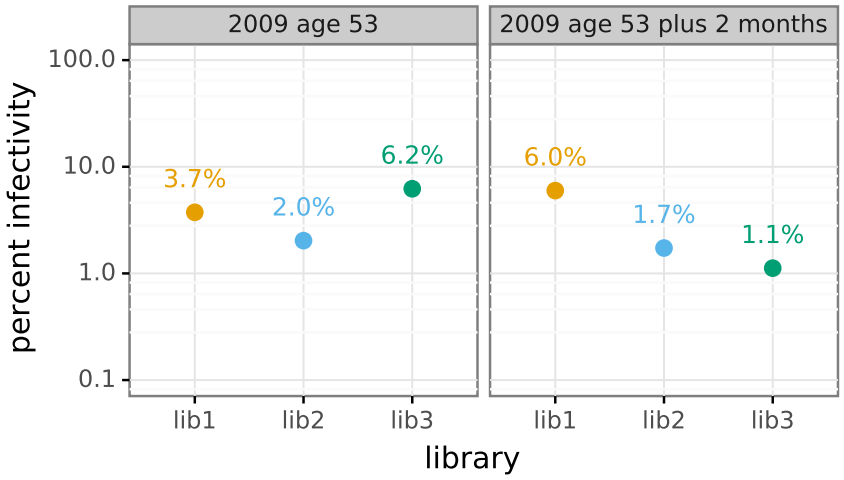

Figure C.5: **Percent of viral library retaining infectivity after serum treatment during mutational antigenic profiling.** The percent of the mutant virus library that remained infectious after incubation with serum was determined using qPCR for each replicate of the mutational antigenic profiling. Higher serum concentrations generally lead to larger values of the immune selection measured in the mutational antigenic profiling.

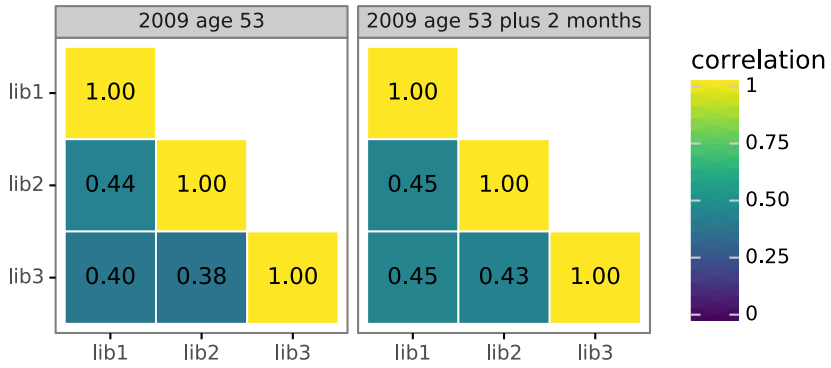

Figure C.6: **Biological replicates of the mutational antigenic profiling are well correlated.** For each serum, we performed three biological replicates of the mutational antigenic profiling. Each replicate used a fully independently generated mutant library. Shown are the Pearson correlation coefficients of the total immune selection at each site (positive site differential selection) computed over all sites for each pair of replicates. The full replicate-by-replicate maps are in Figure C.4A.

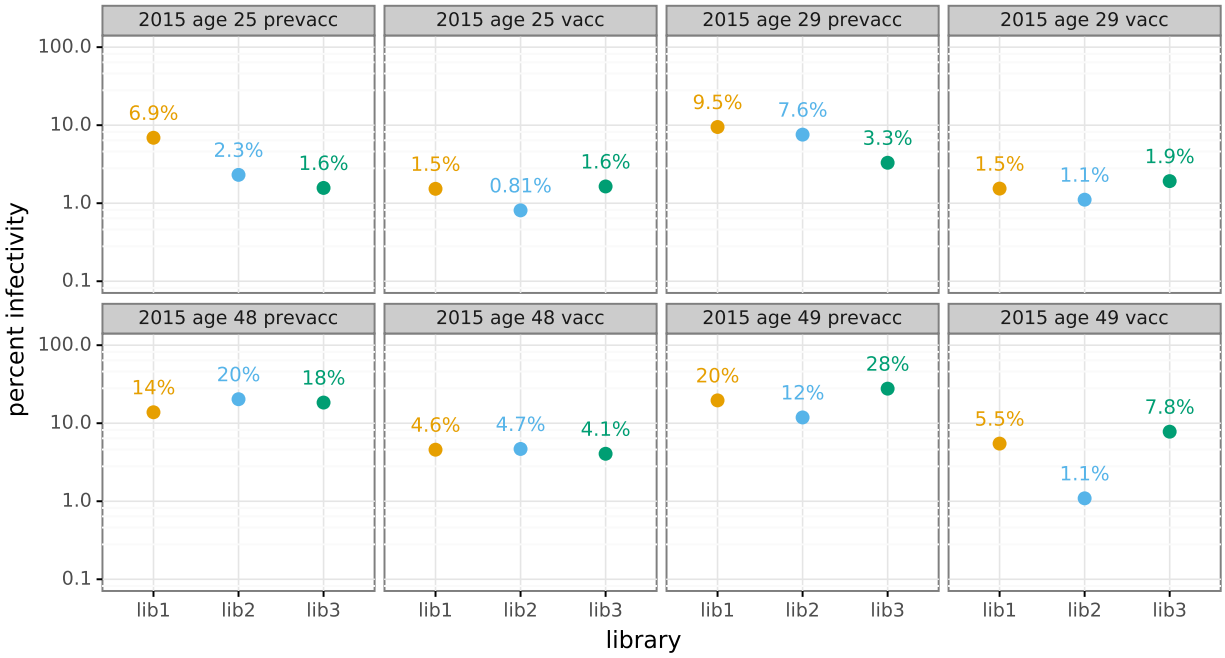

Figure C.7: **Percent of viral library retaining infectivity after serum treatment during mutational antigenic profiling.** The percent of the mutant virus library that remained infectious after incubation with serum was determined using qPCR for each replicate of the mutational antigenic profiling. Higher serum concentrations generally lead to larger values of the immune selection measured in the mutational antigenic profiling. For the pre-vaccination samples from the 48- and 49-year old individuals, we were unable to achieve a concentration that reduced the infectivity of the viral libraries to $<$10% because these sera were not very potent (Figure 4.5B).

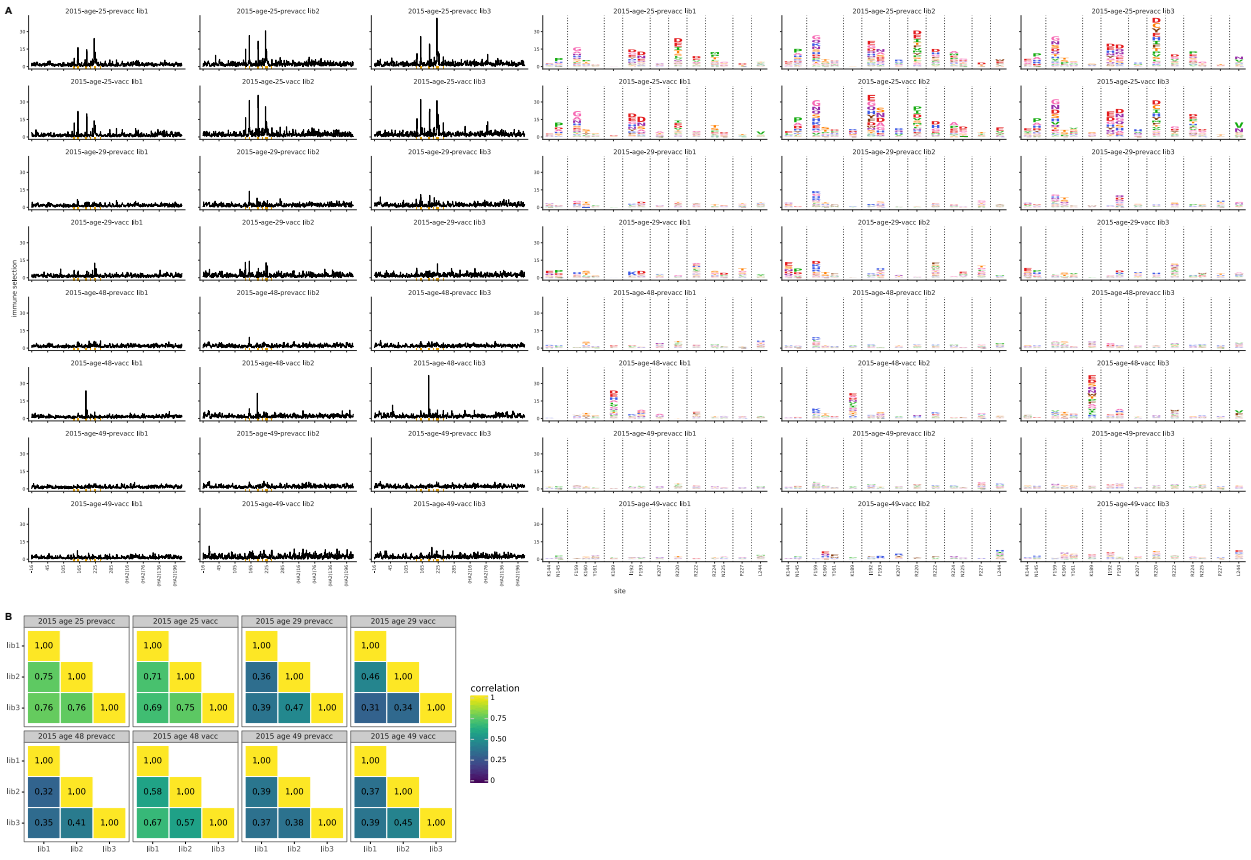

Figure C.8: **Biological replicates of the mutational antigenic profiling are well correlated.** For each serum, we performed three biological replicates of the mutational antigenic profiling. Each replicate used a fully independently generated mutant library. **(A)** Maps of mutations selected by each serum with each replicate viral mutant library ("lib1", "lib2", or "lib3"). These plots are replicate-to-replicate breakdowns of those in Figure 4.5A except that the logo plots are colored by the physicochemical properties of amino acids rather than using the color scheme in the main figure. Note that Figure 4.5A displays the median of the replicates shown here. **(B)** The Pearson correlation coefficients of the total immune selection at each site (height of the letter stack) computed over all sites for each pair of replicates.

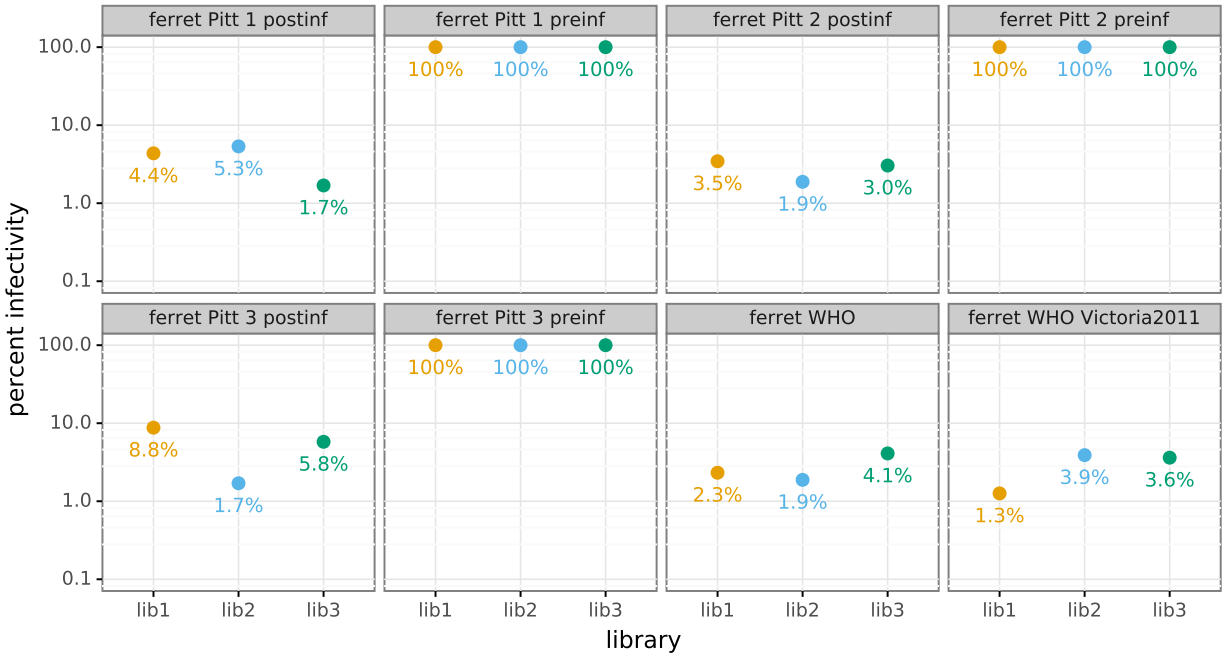

Figure C.9: **Percent of viral library retaining infectivity after serum treatment during mutational antigenic profiling.** The percent of the mutant virus library that remained infectious after incubation with serum was determined using qPCR for each replicate of the mutational antigenic profiling. Higher serum concentrations generally lead to larger values of the immune selection measured in the mutational antigenic profiling. For the pre-infection samples, we were unable to achieve a concentration that reduced the infectivity of the viral libraries to $<$10% because these sera do not neutralize the virus (Figure 4.6B).

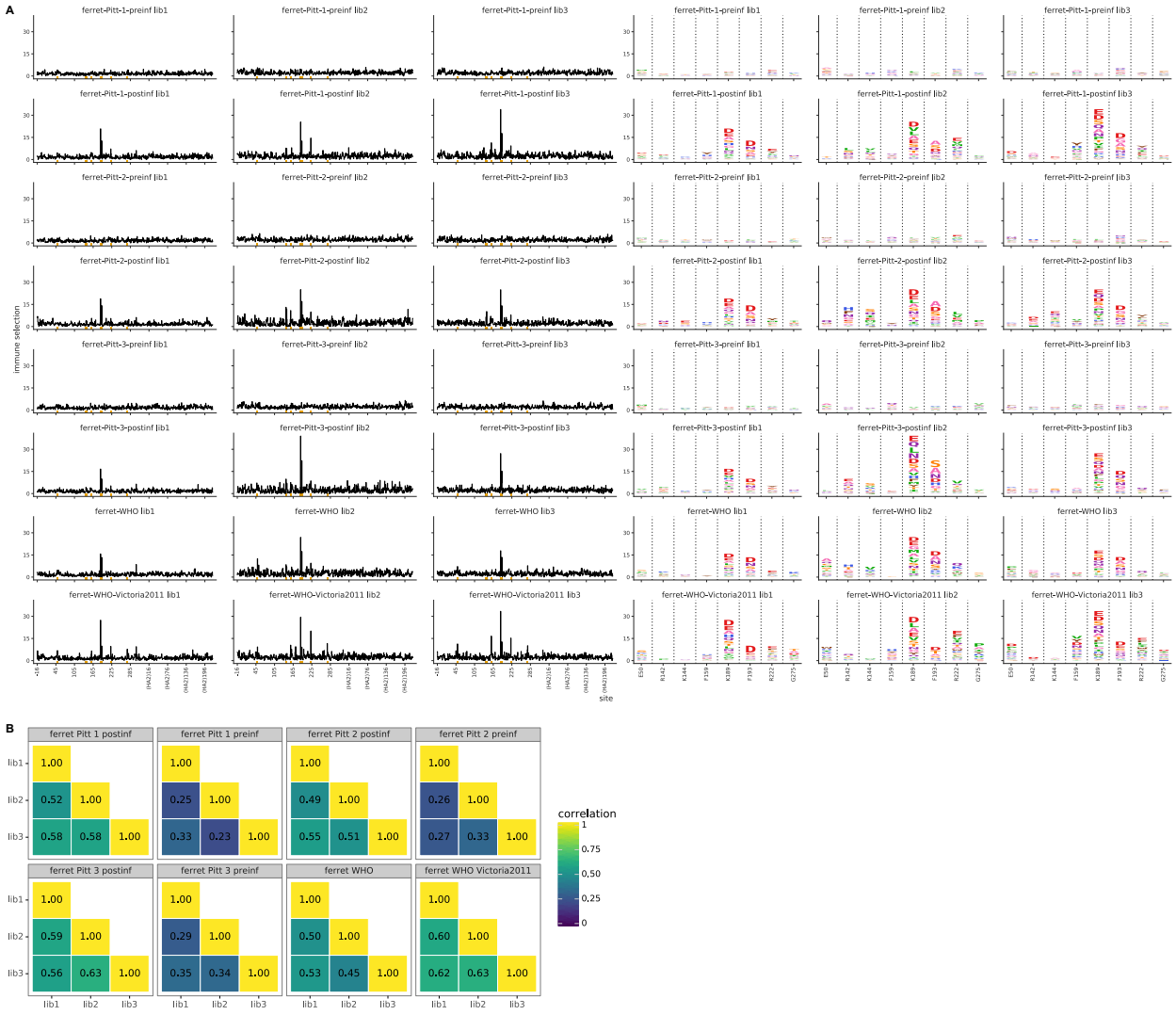

Figure C.10: **Biological replicates of the mutational antigenic profiling are well correlated.** For each serum, we performed three biological replicates of the mutational antigenic profiling. Each replicate used a fully independently generated mutant library. **(A)** Maps of mutations selected by each serum with each replicate viral mutant library ("lib1", "lib2", or "lib3"). These plots are replicate-to-replicate breakdowns of those in Figure 4.6A except that the logo plots are colored by the physicochemical properties of amino acids rather than using the color scheme in the main figure. Note that Figure 4.6A displays the median of the replicates shown here. **(B)** The Pearson correlation coefficients of the total immune selection at each site (height of the letter stack) computed over all sites for each pair of replicates. Note that the correlations are low for the pre-infection sera as these sera do not neutralize the virus and so do not consistently select any antigenic mutations.

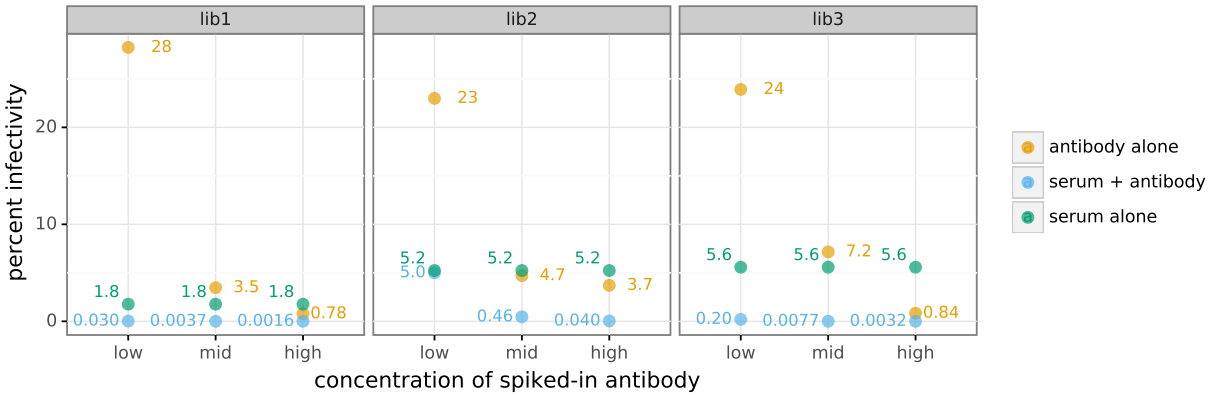

Figure C.11: **Percent of viral library retaining infectivity after treatment with each serum+antibody mix.** The percent of the mutant virus library that remained infectious after incubation with serum and/or antibody was determined using qPCR for each replicate of the mutational antigenic profiling. The blue points show the actual percent infectivity for each experiment in Figure 4.7A that used a mix of serum and antibody. The green points show the actual percent infectivity for the serum-alone selection in Figure 4.7A; in the serum-antibody mix selections the serum was at the same concentrations that gave these percent infectivities. The orange points show the percent infectivity measured at each antibody concentration used in the serum-antibody mix selections; the antibody concentrations used to generate the antibody-alone selection in Figure 4.7A are those shown in Figure C.1.

Supplemental Files

Descriptions of each file are shown below. Files will be made available upon publication.

File S11. The curve fit parameters for all neutralization curves shown in the figures. The IC50 values are *not* extrapolated, and so are shown as upper or lower bounds if they fall outside the range of the measurements. For sera, the IC50s are the serum dilution; for antibodies they are the antibody concentration in μg/ml. This CSV file is also available at `https://github.com/jbloomlab/map_flu_serum_Perth2009_H3_HA/blob/master/results/neutralization_assays/neut_assay_figs_fit_params.csv`.

File S12. The serum dilution or antibody concentration used for each replicate of the mutational antigenic profiling. For sera, the values indicate the dilution of serum. For antibodies, they are the concentration in μg/ml. For serum / antibody mixes, they are the dilution of serum followed by the antibody concentration in μg/ml. These dilutions / concentrations were chosen to give the desired percent of viral infectivity remaining for the libraries after treatment (see Dataset S 13). This CSV file is also available at `https://github.com/jbloomlab/map_flu_serum_Perth2009_H3_HA/blob/master/results/selection_tables/serum_dilution_table.csv`.

File S13. The percent of the overall viral library that retained infectivity after incubation with serum or antibody. This CSV file is also at `https://github.com/jbloomlab/map_flu_serum_Perth2009_H3_HA/blob/master/results/selection_tables/percent_infectivity_table.csv`.

File S14. HTML rendering of Jupyter notebook that analyzes the mutant virus libraries generated by reverse genetics. The Jupyter notebook is also available on GitHub at `https://github.com/jbloomlab/Perth2009-reversegen-DMS`.

File S15. A GenBank file providing the full sequence of the protein expression plasmid pHAGE2-EF1aInt-TCmut-P09-HA, which encodes for the wildtype Perth/2009 HA sequence.

File S16. Numerical values of the differential selection (immune selection) values for each amino-acid at each site after taking the median across replicates. These are the values plotted in the line and logo plots in the main figures. This tidy-format CSV file is also available at `https://github.com/jbloomlab/map_flu_serum_Perth2009_H3_HA/blob/master/results/avgdiffsel/avg_sel_tidy.csv`.

File S17. Logo plots of the positive differential selection for all sites in HA for each serum and antibody selection. The main figures in this paper just zoom in on the key sites of selection. These PDFs are also available at `https://github.com/jbloomlab/map_flu_serum_Perth2009_H3_HA/tree/master/results/avgdiffsel/full_logo_plots`.

BIBLIOGRAPHY

[1] Meghan O. Altman, Matthew Angel, Ivan Košík, Nídia S. Trovão, Seth J. Zost, James S. Gibbs, Lorenzo Casalino, Rommie E. Amaro, Scott E. Hensley, Martha I. Nelson, and Jonathan W. Yewdell. Human influenza A virus hemagglutinin glycan evolution follows a temporal pattern to a glycan limit. *mBio*, 10(2), 2019.

[2] Meghan O Altman, Jack R Bennink, Jonathan W Yewdell, and Brantley R Herrin. Lamprey VLRB response to influenza virus supports universal rules of immunogenicity and antigenicity. *eLife*, 4:e07467, 2015.

[3] Irina V Alymova, Ian A York, Gillian M Air, John F Cipollo, Shelly Gulati, Tatiana Baranovich, Amrita Kumar, Hui Zeng, Shane Gansebom, and Jonathan A McCullers. Glycosylation changes in the globular head of H3N2 influenza hemagglutinin modulate receptor binding without affecting virus virulence. *Scientific Reports*, 6:36216, 2016.

[4] Christopher S Anderson, Sandra Ortega, Francisco A Chaves, Amelia M Clark, Hongmei Yang, David J Topham, and Marta L DeDiego. Natural and directed antigenic drift of the H1 influenza virus hemagglutinin stalk domain. *Scientific Reports*, 7(1):14614, 2017.

[5] Sarah F Andrews, Kaval Kaur, Noel T Pauli, Min Huang, Yunping Huang, and Patrick C Wilson. High preexisting serological antibody levels correlate with diversification of the influenza vaccine response. *Journal of Virology*, 89(6):3308–3317, 2015.

[6] SF Andrews, Y Huang, K Kaur, LI Popova, IY Ho, NT Pauli, WM Taylor, S Lim,

M Huang, X Qu, et al. Immune history profoundly affects broadly protective B cell responses to influenza. *Science Translational Medicine*, 7(316):316ra192, 2015.

[7] Orr Ashenberg, Jai Padmakumar, Michael B Doud, and Jesse D Bloom. Deep mutational scanning identifies sites in influenza nucleoprotein that affect viral inhibition by MxA. *PLoS Pathogens*, 13(3):e1006288, 2017.

[8] Alejandro B Balazs, Jesse D Bloom, Christin M Hong, Dinesh S Rao, and David Baltimore. Broad protection against influenza infection by vectored immunoprophylaxis in mice. *Nature Biotechnology*, 31(7):647–652, 2013.

[9] Yiming Bao, Pavel Bolotov, Dmitry Dernovoy, Boris Kiryutin, Leonid Zaslavsky, Tatiana Tatusova, Jim Ostell, and David Lipman. The influenza virus resource at the national center for biotechnology information. *Journal of Virology*, 82(2):596–601, 2008.

[10] Trevor Bedford, Sarah Cobey, and Mercedes Pascual. Strength and tempo of selection revealed in viral gene genealogies. *BMC Evolutionary Biology*, 11(1):220, 2011.

[11] Trevor Bedford and Richard A Neher. Seasonal influenza circulation patterns and projections for 2017-2018. *bioRxiv*, DOI 10.1101/113035, 2017.

[12] Trevor Bedford, Steven Riley, Ian G Barr, Shobha Broor, Mandeep Chadha, Nancy J Cox, Rodney S Daniels, C Palani Gunasekaran, Aeron C Hurt, Anne Kelso, et al. Global circulation patterns of seasonal influenza viruses vary with antigenic drift. *Nature*, 523(7559):217–220, 2015.

[13] Trevor Bedford, Marc A Suchard, Philippe Lemey, Gytis Dudas, Victoria Gregory, Alan J Hay, John W McCauley, Colin A Russell, Derek J Smith, and Andrew Rambaut. Integrating influenza antigenic dynamics with molecular evolution. *eLife*, 3:e01914, 2014.

[14] Samir Bhatt, Edward C Holmes, and Oliver G Pybus. The genomic rate of molecular adaptation of the human influenza A virus. *Molecular Biology and Evolution*, 28(9):2443, 2011.

[15] Michael J Birrer, Stephen Udem, Stanley Nathenson, and Barry R Bloom. Antigenic variants of measles virus. *Nature*, 293(5827):67–69, 1981.

[16] Thierry Bizebard, Pascal Rigolet, Bjarne Rasmussen, Olivier Diat, BÃ Peter, Steve A Wharton, John J Skehel, Marcel Knossow, et al. Structure of influenza virus haemagglutinin complexed with a neutralizing antibody. *Nature*, 376(6535):92, 1995.

[17] Jesse D Bloom. An experimentally determined evolutionary model dramatically improves phylogenetic fit. *Molecular Biology and Evolution*, 31:1956–1978, 2014.

[18] Jesse D Bloom. Software for the analysis and visualization of deep mutational scanning data. *BMC Bioinformatics*, 16(1):1, 2015.

[19] Jesse D Bloom. Identification of positive selection in genes is greatly improved by using experimentally informed site-specific models. *Biology Direct*, 12(1):1, 2017.

[20] Jesse D Bloom, Lizhi I Gong, and David Baltimore. Permissive secondary mutations enable the evolution of influenza oseltamivir resistance. *Science*, 328:1272–1275, 2010.

[21] Maciej F Boni, Yang Zhou, Jeffery K Taubenberger, and Edward C Holmes. Homologous recombination is very rare or absent in human influenza A virus. *Journal of Virology*, 82(10):4807–4811, 2008.

[22] Eva Böttcher, Tatyana Matrosovich, Michaela Beyerle, Hans-Dieter Klenk, Wolfgang Garten, and Mikhail Matrosovich. Proteolytic activation of influenza viruses by serine proteases TMPRSS2 and HAT from human airway epithelium. *Journal of Virology*, 80:9896–9898, 2006.

[23] E Böttcher-Friebertshäuser, C Freuer, F Sielaff, S Schmidt, M Eickmann, J Uhlendorff, T Steinmetzer, H Klenk, and W Garten. Cleavage of influenza virus hemagglutinin by airway proteases TMPRSS2 and HAT differs in subcellular localization and susceptibility to protease inhibitors. *Journal of Virology*, 11:5605–5614, 2010.

[24] British Medical Journal. Influenza in a boarding school. *British Medical Journal*, 1(6112):587, 1978.

[25] Felix Broecker, Sean TH Liu, Weina Sun, Florian Krammer, Viviana Simon, and Peter Palese. Immunodominance of antigenic site B in the hemagglutinin of the current H3N2 influenza virus in humans and mice. *Journal of Virology*, 92(20):e01100–18, 2018.

[26] Christopher B Brooke, William L Ince, Jens Wrammert, Rafi Ahmed, Patrick C Wilson, Jack R Bennink, and Jonathan W Yewdell. Most influenza A virions fail to express at least one essential viral protein. *Journal of Virology*, 87(6):3155–3162, 2013.

[27] David F Burke and Derek J Smith. A recommended numbering scheme for influenza A HA subtypes. *PloS One*, 9(11):e112302, 2014.

[28] Robin M Bush, Walter M Fitch, Catherine A Bender, and Nancy J Cox. Positive selection on the H3 hemagglutinin gene of human influenza virus A. *Molecular Biology and Evolution*, 16(11):1457–1465, 1999.

[29] Andrew J Caton, George G Brownlee, Jonathan W Yewdell, and Walter Gerhard. The antigenic structure of the influenza virus A/PR/8/34 hemagglutinin (H1 subtype). *Cell*, 31(2):417–427, 1982.

[30] Giovanni Cattoli, Adelaide Milani, Nigel Temperton, Bianca Zecchin, Alessandra Buratin, Eleonora Molesti, Mona Meherez Aly, Abdel Arafa, Ilaria Capua, et al. Antigenic drift in H5N1 avian influenza virus in poultry is driven by mutations in major

antigenic sites of the hemagglutinin molecule analogous to those for human influenza virus. *Journal of Virology*, 85(17):8718–8724, 2011.

[31] Ning Chai, Lee R Swem, Mike Reichelt, Haiyin Chen-Harris, Elizabeth Luis, Summer Park, Ashley Fouts, Patrick Lupardus, Thomas D Wu, Olga Li, et al. Two escape mechanisms of influenza A virus to a broadly neutralizing stalk-binding antibody. *PLoS Pathogens*, 12(6):e1005702, 2016.

[32] Benjamin S Chambers, Kaela Parkhouse, Ted M Ross, Kevin Alby, and Scott E Hensley. Identification of hemagglutinin residues responsible for H3N2 antigenic drift during the 2014–2015 influenza season. *Cell Reports*, 12(1):1–6, 2015.

[33] Zhongying Chen, Helen Zhou, and Hong Jin. The impact of key amino acid substitutions in the hemagglutinin of influenza A (H3N2) viruses on vaccine production and antibody response. *Vaccine*, 28(24):4079–4085, 2010.

[34] Joshua L Cherry, David J Lipman, Anastasia Nikolskaya, and Yuri I Wolf. Evolutionary dynamics of N-glycosylation sites of influenza virus hemagglutinin. *PLoS Currents*, 1, 2009.

[35] Sarah Cobey. Pathogen evolution and the immunological niche. *Annals of the New York Academy of Sciences*, 1320(1):1–15, 2014.

[36] Sarah Cobey and Scott E Hensley. Immune history and influenza virus susceptibility. *Current Opinion in Virology*, 22:105–111, 2017.

[37] Constance S Copeland, Klaus-Peter Zimmer, Krystn R Wagner, Glenn A Healey, Ira Mellman, and Ari Helenius. Folding, trimerization, and transport are sequential events in the biogenesis of influenza virus hemagglutinin. *Cell*, 53(2):197–209, 1988.

[38] Davide Corti, Elisabetta Cameroni, Barbara Guarino, Nicole L Kallewaard, Qing Zhu, and Antonio Lanzavecchia. Tackling influenza with broadly neutralizing antibodies. *Current Opinion in Virology*, 24:60–69, 2017.

[39] Davide Corti, Jarrod Voss, Steven J Gamblin, Giosiana Codoni, Annalisa Macagno, David Jarrossay, Sebastien G Vachieri, Debora Pinna, Andrea Minola, Fabrizia Vanzetta, et al. A neutralizing antibody selected from plasma cells that binds to group 1 and group 2 influenza A hemagglutinins. *Science*, 333(6044):850–856, 2011.

[40] RB Couch. Assessment of immunity to influenza using artificial challenge of normal volunteers with influenza virus. *Developments in Biological Standardization*, 28:295–306, 1975.

[41] Robert B Couch and Julius A Kasel. Immunity to influenza in man. *Annual Reviews in Microbiology*, 37(1):529–549, 1983.

[42] R Crainic, P Couillin, B Blondel, N Cabau, A Boue, and F Horodniceanu. Natural variation of poliovirus neutralization epitopes. *Infection and Immunity*, 41(3):1217–1225, 1983.

[43] Brian C Cunningham and James A Wells. Comparison of a structural and a functional epitope. *Journal of Molecular Biology*, 234(3):554–563, 1993.

[44] William Dall'Acqua, Ellen R Goldman, Wenhong Lin, Connie Teng, Daisuke Tsuchiya, Hongmin Li, Xavier Ysern, Bradford C Braden, Yili Li, Sandra J Smith-Gill, et al. A mutational analysis of binding interactions in an antigen-antibody protein-protein complex. *Biochemistry*, 37(22):7981–7991, 1998.

[45] Robert Daniels, Brad Kurowski, Arthur E Johnson, and Daniel N Hebert. N-linked glycans direct the cotranslational folding pathway of influenza hemagglutinin. *Molecular Cell*, 11(1):79–90, 2003.

[46] RS Daniels, JC Downie, AJ Hay, M Knossow, JJ Skehel, ML Wang, and DC Wiley. Fusion mutants of the influenza virus hemagglutinin glycoprotein. *Cell*, 40(2):431–439, 1985.

[47] Suman R Das, Scott E Hensley, William L Ince, Christopher B Brooke, Anju Subba, Mark G Delboy, Gustav Russ, James S Gibbs, Jack R Bennink, and Jonathan W Yewdell. Defining influenza A virus hemagglutinin antigenic drift by sequential monoclonal antibody selection. *Cell Host & Microbe*, 13(3):314–323, 2013.

[48] JR Davies, AJ Smith, EA Grilli, and TW Hoskins. Christ's Hospital 1978–79: An account of two outbreaks of influenza A H1N1. *Journal of Infection*, 5(2):151–156, 1982.

[49] Amy KF Davis, Kevin McCormick, Megan E Gumina, Joshua G Petrie, Emily T Martin, Katherine S Xue, Jesse D Bloom, Arnold S Monto, Frederic D Bushman, and Scott E Hensley. Sera from individuals with narrowly focused influenza virus antibodies rapidly select viral escape mutations in ovo. *Journal of Virology*, 19(19):e00859–18, 2018.

[50] Kari Debbink, John T. McCrone, Joshua G. Petrie, Rachel Truscon, Emileigh Johnson, Emily K. Mantlo, Arnold S. Monto, and Adam S. Lauring. Vaccination has minimal impact on the intrahost diversity of H3N2 influenza viruses. *PLoS Pathogens*, 13(1):1–18, 2017.

[51] Marta L DeDiego, Christopher S Anderson, Hongmei Yang, Jeanne Holden-Wiltse, Theresa Fitzgerald, John J Treanor, and David J Topham. Directed selection of influenza virus produces antigenic variants that match circulating human virus isolates and escape from vaccine-mediated immune protection. *Immunology*, 148(2):160–173, 2016.

[52] David Charles Diamond, Bradford A Jameson, Jutta Bonin, Michinori Kohara, Shi-

nobu Abe, Heihachi Itoh, Toshihiko Komatsu, Mineo Arita, Shusuke Kuge, Akio Nomoto, et al. Antigenic variation and resistance to neutralization in poliovirus type 1. *Science*, 229(4718):1090–1093, 1985.

[53] David J. DiLillo, Peter Palese, Patrick C. Wilson, and Jeffrey V. Ravetch. Broadly neutralizing anti-influenza antibodies require Fc receptor engagement for in vivo protection. *The Journal of Clinical Investigation*, 126(2):605–610, 2016.

[54] David J. DiLillo, Gene S. Tan, Peter Palese, and Jeffrey V. Ravetch. Broadly neutralizing hemagglutinin stalk-specific antibodies require FcγR interactions for protection against influenza virus in vivo. *Nature Medicine*, 20:143–151, 2014.

[55] Adam S Dingens, Dana Arenz, Haidyn Weight, Julie Overbaugh, and Jesse D Bloom. An antigenic atlas of HIV-1 escape from broadly neutralizing antibodies distinguishes functional and structural epitopes. *Immunity*, 50(2):520–532, 2019.

[56] Adam S Dingens, Hugh K Haddox, Julie Overbaugh, and Jesse D Bloom. Comprehensive mapping of HIV-1 escape from a broadly neutralizing antibody. *Cell Host & Microbe*, 21:777–787, 2017.

[57] Jorge M Dinis, Nicholas W Florek, Omolayo O Fatola, Louise H Moncla, James P Mutschler, Olivia K Charlier, Jennifer K Meece, Edward A Belongia, and Thomas C Friedrich. Deep sequencing reveals potential antigenic variants at low frequencies in influenza A virus-infected humans. *Journal of Virology*, 90(7):3355–3365, 2016.

[58] Michael B Doud, Orr Ashenberg, and Jesse D Bloom. Site-specific amino acid preferences are mostly conserved in two closely related protein homologs. *Molecular Biology and Evolution*, 32:2944–2960, 2015.

[59] Michael B Doud and Jesse D Bloom. Accurate measurement of the effects of all amino-acid mutations to influenza hemagglutinin. *Viruses*, 8:155, 2016.

[60] Michael B Doud, Scott E Hensley, and Jesse D Bloom. Complete mapping of viral escape from neutralizing antibodies. *PLoS Pathogens*, 13(3):e1006271, 2017.

[61] Michael B Doud, Juhye M Lee, and Jesse D Bloom. How single mutations affect viral escape from broad and narrow antibodies to H1 influenza hemagglutinin. *Nature Communications*, 9(1):1386, 2018.

[62] Jan Felix Drexler, Gilda Grard, Alexander N Lukashev, Liubov I Kozlovskaya, Sindy Böttcher, Gökhan Uslu, Johan Reimerink, Anatoly P Gmyl, Raphaël Taty-Taty, Sonia Etenna Lekana-Douki, et al. Robustness against serum neutralization of a poliovirus type 1 from a lethal epidemic of poliomyelitis in the Republic of Congo in 2010. *Proceedings of the National Academy of Sciences*, 111(35):12889–12894, 2014.

[63] Cyrille Dreyfus, Damian C Ekiert, and Ian A Wilson. Structure of a classical broadly neutralizing stem antibody in complex with a pandemic H2 influenza virus hemagglutinin. *Journal of Virology*, 87(12):7149–7154, 2013.

[64] Cyrille Dreyfus, Nick S. Laursen, Ted Kwaks, David Zuijdgeest, Reza Khayat, Damian C. Ekiert, Jeong Hyun Lee, Zoltan Metlagel, Miriam V. Bujny, Mandy Jongeneelen, et al. Highly conserved protective epitopes on influenza B viruses. *Science*, 337(6100):1343–1348, 2012.

[65] Carole J Henry Dunand, Paul E Leon, Kaval Kaur, Gene S Tan, Nai-Ying Zheng, Sarah Andrews, Min Huang, Xinyan Qu, Yunping Huang, Marlene Salgado-Ferrer, et al. Preexisting human antibodies neutralize recently emerged H7N9 influenza strains. *The Journal of Clinical Investigation*, 125(3):1255–1268, 2015.

[66] ECDC. Influenza virus characterisation: summary Europe. *https://ecdc.europa.eu/sites/portal/files/media/en/publications/*

Publications/influenza-virus-characterisation-september-2015.pdf, 2015.

[67] Damian C Ekiert, Gira Bhabha, Marc-André Elsliger, Robert HE Friesen, Mandy Jongeneelen, Mark Throsby, Jaap Goudsmit, and Ian A Wilson. Antibody recognition of a highly conserved influenza virus epitope. *Science*, 324(5924):246–251, 2009.

[68] Damian C Ekiert, Robert HE Friesen, Gira Bhabha, Ted Kwaks, Mandy Jongeneelen, Wenli Yu, Carla Ophorst, Freek Cox, Hans Korse, and Boerries Brandenburg. A highly conserved neutralizing epitope on group 2 influenza A viruses. *Science*, 333(6044):843–850, 2011.

[69] Damian C. Ekiert, Arun K. Kashyap, John Steel, Adam Rubrum, Gira Bhabha, Reza Khayat, Jeong Hyun Lee, Michael A. Dillon, Ryann E. O'Neil, Aleksandr M. Faynboym, et al. Cross-neutralization of influenza A viruses mediated by a single antibody loop. *Nature*, 489(7417):526–532, 2012.

[70] Ali H Ellebedy, Florian Krammer, Gui-Mei Li, Matthew S Miller, Christopher Chiu, Jens Wrammert, Cathy Y Chang, Carl W Davis, Megan McCausland, Rivka Elbein, et al. Induction of broadly cross-reactive antibody responses to the influenza HA stem region following H5N1 vaccination in humans. *Proceedings of the National Academy of Sciences*, 111(36):13133–13138, 2014.

[71] Warren J Ewens. *Mathematical population genetics 1: theoretical introduction*. Springer Science & Business Media, 2012.

[72] Walter M Fitch, Robin M Bush, Catherine A Bender, and Nancy J Cox. Long term trends in the evolution of H(3) HA1 human influenza type A. *Proceedings of the National Academy of Sciences*, 94(15):7712–7718, 1997.

[73] J. M. Fonville, S. H. Wilks, S. L. James, A. Fox, M. Ventresca, M. Aban, L. Xue, T. C. Jones, Le N. M. H., Pham Q. T., Tran N. D., Y. Wong, A. Mosterin, L. C. Katzelnick, et al. Antibody landscapes after influenza virus infection or vaccination. *Science*, 346(6212):996–1000, 2014.

[74] Douglas M Fowler, Carlos L Araya, Sarel J Fleishman, Elizabeth H Kellogg, Jason J Stephany, David Baker, and Stanley Fields. High-resolution mapping of protein sequence-function relationships. *Nature Methods*, 7(9):741–746, 2010.

[75] Douglas M Fowler and Stanley Fields. Deep mutational scanning: a new style of protein science. *Nature Methods*, 11(8):801–807, 2014.

[76] Thomas Francis Jr. On the doctrine of original antigenic sin. *Proceedings of the American Philosophical Society*, 104(6):572–578, 1960.

[77] Robert H. E. Friesen, Peter S. Lee, Esther J. M. Stoop, Ryan M. B. Hoffman, Damian C. Ekiert, Gira Bhabha, Wenli Yu, Jarek Juraszek, Wouter Koudstaal, et al. A common solution to group 2 influenza virus neutralization. *Proceedings of the National Academy of Sciences*, 111(1):445–450, 2014.

[78] Benjamin O Fulton, David Sachs, Shannon M Beaty, Sohui T Won, Benhur Lee, Peter Palese, and Nicholas S Heaton. Mutational analysis of measles virus suggests constraints on antigenic variation of the glycoproteins. *Cell Reports*, 11(9):1331–1338, 2015.

[79] SJ Gamblin, LF Haire, RJ Russell, DJ Stevens, B Xiao, Y Ha, N Vasisht, DA Steinhauer, RS Daniels, A Elliot, et al. The structure and receptor binding properties of the 1918 influenza hemagglutinin. *Science*, 303(5665):1838–1842, 2004.

[80] Walter Gerhard, Jonathan Yewdell, Mark E Frankel, and Robert Webster. Antigenic structure of influenza virus haemagglutinin defined by hybridoma antibodies. *Nature*, 290(5808):713–717, 1981.

[81] Mary-Jane Gething, Robert W Doms, Deborah York, and Judy White. Studies on the mechanism of membrane fusion: site-specific mutagenesis of the hemagglutinin of influenza virus. *The Journal of Cell Biology*, 102(1):11–23, 1986.

[82] Geneviève Girard, Alexander P. Gultyaev, and René C.L. Olsthoorn. Upstream start codon in segment 4 of north american H2 avian influenza A viruses. *Infection, Genetics and Evolution*, 11(2):489–495, 2011.

[83] Lizhi Ian Gong, Marc A Suchard, and Jesse D Bloom. Stability-mediated epistasis constrains the evolution of an influenza protein. *eLife*, 2:e00631, 2013.

[84] Katelyn M Gostic, Monique Ambrose, Michael Worobey, and James O Lloyd-Smith. Potent protection against H5N1 and H7N9 influenza via childhood hemagglutinin imprinting. *Science*, 354(6313):722–726, 2016.

[85] Ya Ha, David J Stevens, John J Skehel, and Don C Wiley. H5 avian and H9 swine influenza virus haemagglutinin structures: possible origin of influenza subtypes. *The EMBO Journal*, 21(5):865–875, 2002.

[86] Hugh K Haddox, Adam S Dingens, and Jesse D Bloom. Experimental estimation of the effects of all amino-acid mutations to HIV's envelope protein on viral replication in cell culture. *PLoS Pathogens*, 12(12):e1006114, 2016.

[87] Hugh K Haddox, Adam S Dingens, Sarah K Hilton, Julie Overbaugh, and Jesse D Bloom. Mapping mutational effects along the evolutionary landscape of HIV envelope. *eLife*, 7:e34420, 2018.

[88] James Hadfield, Colin Megill, Sidney M Bell, John Huddleston, Barney Potter, Charlton Callender, Pavel Sagulenko, Trevor Bedford, and Richard A Neher. Nextstrain: real-time tracking of pathogen evolution. *Bioinformatics*, 34(23):4121–4123, 2018.

[89] Michael J Harms and Joseph W Thornton. Historical contingency and its biophysical basis in glucocorticoid receptor evolution. *Nature*, 512(7513):203–207, 2014.

[90] William T Harvey, Donald J Benton, Victoria Gregory, James PJ Hall, Rodney S Daniels, Trevor Bedford, Daniel T Haydon, Alan J Hay, John W McCauley, and Richard Reeve. Identification of low-and high-impact hemagglutinin amino acid substitutions that drive antigenic drift of influenza A (H1N1) viruses. *PLoS Pathogens*, 12(4):e1005526, 2016.

[91] Nicholas S Heaton, David Sachs, Chi-Jene Chen, Rong Hai, and Peter Palese. Genome-wide mutagenesis of influenza virus reveals unique plasticity of the hemagglutinin and NS1 proteins. *Proceedings of the National Academy of Sciences*, 110(50):20248–20253, 2013.

[92] Carole Henry, Nai-Ying Zheng, Min Huang, Alexandra Cabanov, Karla Thatcher Rojas, Kaval Kaur, Sarah F Andrews, Anna-Karin E Palm, Yao-Qing Chen, Yang Li, et al. Influenza virus vaccination elicits poorly adapted B cell responses in elderly individuals. *Cell Host & Microbe*, 25(3):357–366, 2019.

[93] Scott E Hensley, Suman R Das, Adam L Bailey, Loren M Schmidt, Heather D Hickman, Akila Jayaraman, Karthik Viswanathan, Rahul Raman, Ram Sasisekharan, Jack R Bennink, et al. Hemagglutinin receptor binding avidity drives influenza A virus antigenic drift. *Science*, 326(5953):734–736, 2009.

[94] Sarah K Hilton, Michael B Doud, and Jesse D Bloom. phydms: Software for phylogenetic analyses informed by deep mutational scanning. *PeerJ*, 5:e3657, 2017.

[95] George K. Hirst. Studies of antigenic differences among strains of influenza A by means of red cell agglutination. *Journal of Experimental Medicine*, 78(5):407–423, 1943.

[96] D Hobson, RL Curry, AS Beare, and A Ward-Gardner. The role of serum haemagglutination-inhibiting antibody in protection against challenge infection with influenza A2 and B viruses. *Epidemiology & Infection*, 70(4):767–777, 1972.

[97] Karin Hoelzer, Pablo R. Murcia, Gregory J. Baillie, James L. N. Wood, Stephan M. Metzger, Nikolaus Osterrieder, Edward J. Dubovi, Edward C. Holmes, and Colin R. Parrish. Intrahost evolutionary dynamics of canine influenza virus in naïve and partially immune dogs. *Journal of Virology*, 84(10):5329–5335, 2010.

[98] Erich Hoffmann, Gabriele Neumann, Yoshihiro Kawaoka, Gerd Hobom, and Robert G. Webster. A DNA transfection system for generation of influenza A virus from eight plasmids. *Proceedings of the National Academy of Sciences*, 97(11):6108–6113, 2000.

[99] John Holland, Katherine Spindler, Frank Horodyski, Elizabeth Grabau, Stuart Nichol, and Scott VandePol. Rapid evolution of RNA genomes. *Science*, 215(4540):1577–1585, 1982.

[100] Kathryn A Hooper and Jesse D Bloom. A mutant influenza virus that uses an N1 neuraminidase as the receptor-binding protein. *Journal of Virology*, 87(23):12531–12540, 2013.

[101] Kuan-Ying A Huang, Pramila Rijal, Lisa Schimanski, Timothy J Powell, Tzou-Yien Lin, John W McCauley, Rodney S Daniels, and Alain R Townsend. Focused antibody response to influenza linked to antigenic drift. *The Journal of Clinical Investigation*, 125(7):2631–2645, 2015.

[102] Toshihiro Ito, Yasuo Suzuki, Ayato Takada, Ayumi Kawamoto, Koichi Otsuki, Hiroyuki Masuda, Mika Yamada, Takashi Suzuki, Hiroshi Kida, and Yoshihiro Kawaoka. Differences in sialic acid-galactose linkages in the chicken egg amnion

and allantois influence human influenza virus receptor specificity and variant selection. *Journal of Virology*, 71(4):3357–3362, 1997.

[103] Sinthujan Jegaskanda, Jason T. Weinfurter, Thomas C. Friedrich, and Stephen J. Kent. Antibody-dependent cellular cytotoxicity is associated with control of pandemic H1N1 influenza virus infection of macaques. *Journal of Virology*, 87(10):5512–5522, 2013.

[104] Lei Jin, Brian M Fendly, and James A Wells. High resolution functional analysis of antibody-antigen interactions. *Journal of Molecular Biology*, 226(3):851–865, 1992.

[105] Patricia A Jorquera, Vasiliy P Mishin, Anton Chesnokov, Ha T Nguyen, Brian Mann, Rebecca Garten, John Barnes, Erin Hodges, Juan De La Cruz, Xiyan Xu, et al. Insights into the antigenic advancement of influenza a (h3n2) viruses, 2011–2018. *Scientific Reports*, 9(1):2676, 2019.

[106] M Gordon Joyce, Adam K Wheatley, Paul V Thomas, Gwo-Yu Chuang, Cinque Soto, Robert T Bailer, Aliaksandr Druz, Ivelin S Georgiev, Rebecca A Gillespie, Masaru Kanekiyo, et al. Vaccine-induced antibodies that neutralize group 1 and group 2 influenza A viruses. *Cell*, 166(3):609–623, 2016.

[107] Wolfgang Kabsch and Christian Sander. Dictionary of protein secondary structure: pattern recognition of hydrogen-bonded and geometrical features. *Biopolymers*, 22(12):2577–2637, 1983.

[108] Nicole L. Kallewaard, Davide Corti, Patrick J. Collins, Ursula Neu, Josephine M. Mcauliffe, Ebony Benjamin, Leslie Wachter-Rosati, Frances J. Palmer-Hill, Andy Q. Yuan, Philip A. Walker, et al. Structure and function analysis of an antibody recognizing all influenza A subtypes. *Cell*, 166(3):596–608, 2016.

[109] Kazutaka Katoh and Daron M Standley. MAFFT multiple sequence alignment soft-

ware version 7: improvements in performance and usability. *Molecular Biology and Evolution*, 30(4):772–780, 2013.

[110] Greg A. Kirchenbaum, Donald M. Carter, and Ted M. Ross. Sequential infection in ferrets with antigenically distinct seasonal H1N1 influenza viruses boosts hemagglutinin stalk-specific antibodies. *Journal of Virology*, 90(2):1116–1128, 2016.

[111] Ericka Kirkpatrick, Xueting Qiu, Patrick C Wilson, Justin Bahl, and Florian Krammer. The influenza virus hemagglutinin head evolves faster than the stalk domain. *Scientific Reports*, 8(1):10432, 2018.

[112] Shantha Kodihalli, Dominic M Justewicz, Larisa V Gubareva, and Robert G Webster. Selection of a single amino acid substitution in the hemagglutinin molecule by chicken eggs can render influenza A virus (H3) candidate vaccine ineffective. *Journal of Virology*, 69(8):4888–4897, 1995.

[113] Björn F Koel, David F Burke, Theo M Bestebroer, Stefan van der Vliet, Gerben CM Zondag, Gaby Vervaet, Eugene Skepner, Nicola S Lewis, Monique IJ Spronken, Colin A Russell, et al. Substitutions near the receptor binding site determine major antigenic change during influenza virus evolution. *Science*, 342(6161):976–979, 2013.

[114] Katia Koelle and David A Rasmussen. The effects of a deleterious mutation load on patterns of influenza A/H3N2's antigenic evolution in humans. *eLife*, 4:e07361, 2015.

[115] Florian Krammer. The human antibody response to influenza A virus infection and vaccination. *Nature Reviews Immunology*, 19:383–397, 2019.

[116] Florian Krammer and Peter Palese. Advances in the development of influenza virus vaccines. *Nature Reviews Drug Discovery*, 14(3):167–182, 2015.

[117] Adam Kucharski and Julia R Gog. Influenza emergence in the face of evolutionary constraints. *Proceedings of the Royal Society of London B: Biological Sciences*, page rspb20111168, 2011.

[118] Adam J Kucharski, Justin Lessler, Jonathan M Read, Huachen Zhu, Chao Qiang Jiang, Yi Guan, Derek AT Cummings, and Steven Riley. Estimating the life course of influenza A (H3N2) antibody responses from cross-sectional data. *PLoS Biology*, 13(3):e1002082, 2015.

[119] Seema S Lakdawala, Akila Jayaraman, Rebecca A Halpin, Elaine W Lamirande, Angela R Shih, Timothy B Stockwell, Xudong Lin, Ari Simenauer, Christopher T Hanson, Leatrice Vogel, et al. The soft palate is an important site of adaptation for transmissible influenza viruses. *Nature*, 526(7571):122, 2015.

[120] Adam S Lauring and Raul Andino. Quasispecies theory and the behavior of RNA viruses. *PLoS Pathogens*, 6(7):e1001005, 2010.

[121] Nick S Laursen and Ian A Wilson. Broadly neutralizing antibodies against influenza viruses. *Antiviral Research*, 98(3):476–483, 2013.

[122] W Graeme Laver, Gillian M Air, and Robert G Webster. Mechanism of antigenic drift in influenza virus: amino acid sequence changes in an antigenically active region of Hong Kong (H3N2) influenza virus hemagglutinin. *Journal of Molecular Biology*, 145(2):339–361, 1980.

[123] WG Laver, GM Air, RG Webster, W Gerhard, CW Ward, and TAA Dopheide. Antigenic drift in type A influenza virus: sequence differences in the hemagglutinin of Hong Kong (H3N2) variants selected with monoclonal hybridoma antibodies. *Virology*, 98(1):226–237, 1979.

[124] Chang-Won Lee, Dennis A Senne, and David L Suarez. Effect of vaccine use in

the evolution of Mexican lineage H5N2 avian influenza virus. *Journal of Virology*, 78(15):8372–8381, 2004.

[125] Hong Kai Lee, Julian Wei-Tze Tang, Debra Han-Lin Kong, Tze Ping Loh, Donald Kok-Leong Chiang, Tommy Tsan-Yuk Lam, and Evelyn Siew-Chuan Koay. Comparison of mutation patterns in full-genome A/H3N2 influenza sequences obtained directly from clinical samples and the same samples after a single MDCK passage. *PLoS One*, 8(11):e79252, 2013.

[126] J Lee, DR Boutz, V Chromikova, MG Joyce, C Vollmers, K Leung, AP Horton, BJ DeKosky, CH Lee, JJ Lavinder, EM Murrin, C Chrysostomou, KH Hoi, et al. Molecular-level analysis of the serum antibody repertoire in young adults before and after seasonal influenza vaccination. *Nature Medicine*, 22(12):1456–1464, 2016.

[127] Jiwon Lee, Philipp Paparoditis, Andrew P Horton, Alexander Frühwirth, Jonathan R McDaniel, Jiwon Jung, Daniel R Boutz, Dania A Hussein, Yuri Tanno, Leontios Pappas, et al. Persistent antibody clonotypes dominate the serum response to influenza over multiple years and repeated vaccinations. *Cell Host & Microbe*, 25(3):367–376, 2019.

[128] Juhye M Lee, John Huddleston, Michael B Doud, Kathryn A Hooper, Nicholas C Wu, Trevor Bedford, and Jesse D Bloom. Deep mutational scanning of hemagglutinin helps predict evolutionary fates of human H3N2 influenza variants. *Proceedings of the National Academy of Sciences*, 115(35):E8276–E8285, 2018.

[129] P. S. Lee, N. Ohshima, R. L. Stanfield, W. Yu, Y. Iba, Y. Okuno, Y. Kurosawa, and I. A. Wilson. Receptor mimicry by antibody F045-092 facilitates universal binding to the H3 subtype of influenza virus. *Nature Communications*, 5:3614, 2014.

[130] Peter S Lee, Reiko Yoshida, Damian C Ekiert, Naoki Sakai, Yasuhiko Suzuki, Ayato Takada, and Ian A Wilson. Heterosubtypic antibody recognition of the influenza

virus hemagglutinin receptor binding site enhanced by avidity. *Proceedings of the National Academy of Sciences*, 109(42):17040–17045, 2012.

[131] Justin Lessler, Steven Riley, Jonathan M. Read, Shuying Wang, Huachen Zhu, Gavin J. D. Smith, Yi Guan, Chao Qiang Jiang, and Derek A. T. Cummings. Evidence for antigenic seniority in influenza A (H3N2) antibody responses in southern china. *PLoS Pathogens*, 8(7):1–11, 2012.

[132] Min Z Levine, Emily T Martin, Joshua G Petrie, Adam S Lauring, Crystal Holiday, Stacie Jefferson, William J Fitzsimmons, Emileigh Johnson, Jill M Ferdinands, and Arnold S Monto. Antibodies against egg-and cell-grown influenza A (H3N2) viruses in adults hospitalized during the 2017–2018 influenza season. *The Journal of Infectious Diseases*, 219(12):1904–1912, 2019.

[133] Chengjun Li, Masato Hatta, David F Burke, Jihui Ping, Ying Zhang, Makoto Ozawa, Andrew S Taft, Subash C Das, Anthony P Hanson, Jiasheng Song, et al. Selection of antigenically advanced variants of seasonal influenza viruses. *Nature Microbiology*, 1:16058, 2016.

[134] Yang Li, Jaclyn L. Myers, David L. Bostick, Colleen B. Sullivan, Jonathan Madara, Susanne L. Linderman, Qin Liu, Donald M. Carter, Jens Wrammert, Susanna Esposito, et al. Immune history shapes specificity of pandemic H1N1 influenza antibody responses. *Journal of Experimental Medicine*, 210(8):1493–1500, 2013.

[135] Susanne L. Linderman, Benjamin S. Chambers, Seth J. Zost, Kaela Parkhouse, Yang Li, Christin Herrmann, Ali H. Ellebedy, Donald M. Carter, Sarah F. Andrews, et al. Potential antigenic explanation for atypical H1N1 infections among middle-aged adults during the 2013–2014 influenza season. *Proceedings of the National Academy of Sciences*, 111(44):15798–15803, 2014.

[136] Marc Lipsitch and Justin J O'Hagan. Patterns of antigenic diversity and the mech-

anisms that maintain them. *Journal of the Royal Society Interface*, 4(16):787–802, 2007.

[137] Michael Lubeck and Walter Gerhard. Conformational changes at topologically distinct antigenic sites on the influenza A/PR/8/34 virus HA molecule are induced by the binding of monoclonal antibodies. *Virology*, 118(1):1–7, 1982.

[138] Marta Łuksza and Michael Lässig. A predictive fitness model for influenza. *Nature*, 507(7490):57–61, 2014.

[139] SM Luoh, MW McGregor, and VS Hinshaw. Hemagglutinin mutations related to antigenic variation in H1 swine influenza viruses. *Journal of Virology*, 66(2):1066, 1992.

[140] Vamsee VA Mallajosyula, Michael Citron, Francesca Ferrara, Xianghan Lu, Cheryl Callahan, Gwendolyn J Heidecker, Siddhartha P Sarma, Jessica A Flynn, Nigel J Temperton, Xiaoping Liang, et al. Influenza hemagglutinin stem-fragment immunogen elicits broadly neutralizing antibodies and confers heterologous protection. *Proceedings of the National Academy of Sciences*, 111(25):E2514–E2523, 2014.

[141] Nicolle Marshall, Lalita Priyamvada, Zachary Ende, John Steel, and Anice C Lowen. Influenza virus reassortment occurs with high frequency in the absence of segment mismatch. *PLoS Pathogens*, 9(6):e1003421, 2013.

[142] Javier Martin, Stephen A Wharton, Yi Pu Lin, Darin K Takemoto, John J Skehel, Don C Wiley, and David A Steinhauer. Studies of the binding properties of influenza hemagglutinin receptor-site mutants. *Virology*, 241(1):101–111, 1998.

[143] Mikhail Matrosovich, Tatyana Matrosovich, Jackie Carr, Noel A Roberts, and Hans-Dieter Klenk. Overexpression of the α-2, 6-sialyltransferase in MDCK cells increases influenza virus sensitivity to neuraminidase inhibitors. *Journal of Virology*, 77(15):8418–8425, 2003.

[144] Peter McMinn, Angela Carrello, Catherine Cole, David Baker, and Alan Hampson. Antigenic drift of influenza A (H3N2) virus in a persistently infected immunocompromised host is similar to that occurring in the community. *Clinical Infectious Diseases*, 29(2):456–458, 1999.

[145] CD McWhite, AG Meyer, and CO Wilke. Sequence amplification via cell passaging creates spurious signals of positive adaptation in influenza virus H3N2 hemagglutinin. *Virus Evolution*, 2:vew026, 2016.

[146] Matthew J Memoli, Brett W Jagger, Vivien G Dugan, Li Qi, Jadon P Jackson, and Jeffery K Taubenberger. Recent human influenza A/H3N2 virus evolution driven by novel selection factors in addition to antigenic drift. *Journal of Infectious Diseases*, 200(8):1232–1241, 2009.

[147] Matthew S. Miller, Thomas J. Gardner, Florian Krammer, Lauren C. Aguado, Domenico Tortorella, Christopher F. Basler, and Peter Palese. Neutralizing antibodies against previously encountered influenza virus strains increase over time: A longitudinal analysis. *Science Translational Medicine*, 5(198):198ra107, 2013.

[148] M. Anthony Moody, Ruijun Zhang, Emmanuel B. Walter, Christopher W. Woods, Geoffrey S. Ginsburg, Micah T. McClain, Thomas N. Denny, Xi Chen, et al. H3N2 influenza infection elicits more cross-reactive and less clonally expanded anti-hemagglutinin antibodies than influenza vaccination. *PLoS One*, 6(10):1–14, 2011.

[149] Pablo R. Murcia, Gregory J. Baillie, Janet Daly, Debra Elton, Carley Jervis, Jennifer A. Mumford, Richard Newton, Colin R. Parrish, Karin Hoelzer, Gordon Dougan, et al. Intra- and interhost evolutionary dynamics of equine influenza virus. *Journal of Virology*, 84(14):6943–6954, 2010.

[150] Brian R Murphy, Julius A Kasel, and Robert M Chanock. Association of serum anti-

neuraminidase antibody with resistance to influenza in man. *New England Journal of Medicine*, 286(25):1329–1332, 1972.

[151] Raffael Nachbagauer, Angela Choi, Ruvim Izikson, Manon M. Cox, Peter Palese, and Florian Krammer. Age dependence and isotype specificity of influenza virus hemagglutinin stalk-reactive antibodies in humans. *mBio*, 7(1), 2016.

[152] Raffael Nachbagauer, Teddy John Wohlbold, Ariana Hirsh, Rong Hai, Haakon Sjursen, Peter Palese, Rebecca J. Cox, and Florian Krammer. Induction of broadly reactive anti-hemagglutinin stalk antibodies by an H5N1 vaccine in humans. *Journal of Virology*, 88(22):13260–13268, 2014.

[153] Katsuhisa Nakajima, Eri Nobusawa, Ken Tonegawa, and Setsuko Nakajima. Restriction of amino acid change in influenza A virus H3HA: comparison of amino acid changes observed in nature and in vitro. *Journal of Virology*, 77(18):10088–10098, 2003.

[154] Gerald Nakamura, Ning Chai, Summer Park, Nancy Chiang, Zhonghua Lin, Henry Chiu, Rina Fong, Donghong Yan, Janice Kim, et al. An invivo human-plasmablast enrichment technique allows rapid identification of therapeutic influenza A antibodies. *Cell Host & Microbe*, 14(1):93–103, 2013.

[155] A. Natali, J. S. Oxford, and G. C. Schild. Frequency of naturally occurring antibody to influenza virus antigenic variants selected in vitro with monoclonal antibody. *Journal of Hygiene*, 87(2):185–190, 1981.

[156] Chandrasekhar Natarajan, Noriko Inoguchi, Roy E Weber, Angela Fago, Hideaki Moriyama, and Jay F Storz. Epistasis among adaptive mutations in deer mouse hemoglobin. *Science*, 340(6138):1324–1327, 2013.

[157] Richard A Neher and Trevor Bedford. nextflu: real-time tracking of seasonal influenza virus evolution in humans. *Bioinformatics*, 31(21):3546–3548, 2015.

[158] Richard A Neher, Trevor Bedford, Rodney S Daniels, Colin A Russell, and Boris I Shraiman. Prediction, dynamics, and visualization of antigenic phenotypes of seasonal influenza viruses. *Proceedings of the National Academy of Sciences*, 113(12):E1701–E1709, 2016.

[159] Richard A Neher, Colin A Russell, and Boris I Shraiman. Predicting evolution from the shape of genealogical trees. *eLife*, 3:e03568, 2014.

[160] Gabriele Neumann, Tokiko Watanabe, Hiroshi Ito, Shinji Watanabe, Hideo Goto, Peng Gao, Mark Hughes, Daniel R. Perez, Ruben Donis, Erich Hoffmann, Gerd Hobom, and Yoshihiro Kawaoka. Generation of influenza A viruses entirely from cloned cDNAs. *Proceedings of the National Academy of Sciences*, 96(16):9345–9350, 1999.

[161] Hai Nguyen, David A Case, and Alexander S Rose. NGLview–interactive molecular graphics for Jupyter notebooks. *Bioinformatics*, 34(7):1241–1242, 2017.

[162] E Nobusawa, T Aoyama, H Kato, Y Suzuki, Y Tateno, and K Nakajima. Comparison of complete amino acid sequences and receptor-binding properties among 13 serotypes of hemagglutinins of influenza A viruses. *Virology*, 182(2):475–485, 1991.

[163] E Nobusawa, H Ishihara, T Morishita, K Sato, and K Nakajima. Change in receptor-binding specificity of recent human influenza A viruses (H3N2): a single amino acid change in hemagglutinin altered its recognition of sialyloligosaccharides. *Virology*, 278(2):587–596, 2000.

[164] Johan Nordholm, Jeanne Petitou, Henrik Östbye, Diogo V da Silva, Dan Dou, Hao Wang, and Robert Daniels. Translational regulation of viral secretory proteins by the 5' coding regions and a viral RNA-binding protein. *J Cell Biol*, 216:2283–2293, 2017.

[165] Yoshinobu Okuno, Yuji Isegawa, Fuyoko Sasao, and Shigeharu Ueda. A common neutralizing epitope conserved between the hemagglutinins of influenza A virus H1 and H2 strains. *Journal of Virology*, 67(5):2552–2558, 1993.

[166] Peter Ludwig Panum. *Iagttagelser, anstillede under Maesllinge-Epidemien paa Faeroerne i Aaret 1846: (Observations made during the epidemic of measles on the Faroe Islands in the year 1846)*, volume 3. Bibliothek for Laeger, 1847.

[167] Lauren Parker, Stephen A. Wharton, Stephen R. Martin, Karen Cross, Yipu Lin, Yan Liu, Ten Feizi, Rodney S. Daniels, and John W. McCauley. Effects of egg-adaptation on receptor-binding and antigenic properties of recent influenza A (H3N2) vaccine viruses. *Journal of General Virology*, 97(6):1333–1344, 2016.

[168] Jeffrey D Parvin, Anne Moscona, Wayne T Pan, Jason M Leider, and Peter Palese. Measurement of the mutation rates of animal viruses: influenza A virus and poliovirus type 1. *Journal of Virology*, 59(2):377–383, 1986.

[169] Matthew D Pauly, Megan C Procario, and Adam S Lauring. A novel twelve class fluctuation test reveals higher than expected mutation rates for influenza A viruses. *eLife*, 6:e26437, 2017.

[170] Joshua G Petrie, Kaela Parkhouse, Suzanne E Ohmit, Ryan E Malosh, Arnold S Monto, and Scott E Hensley. Antibodies against the current influenza A (H1N1) vaccine strain do not protect some individuals from infection with contemporary circulating influenza A (H1N1) virus strains. *The Journal of Infectious Diseases*, 214(12):1947–1951, 2016.

[171] David D Pollock, Grant Thiltgen, and Richard A Goldstein. Amino acid coevolution induces an evolutionary Stokes shift. *Proceedings of the National Academy of Sciences*, 109(21):E1352–E1359, 2012.

[172] Lyubov Popova, Kenneth Smith, Ann H West, Patrick C Wilson, Judith A James, Linda F Thompson, and Gillian M Air. Immunodominance of antigenic site B over site A of hemagglutinin of recent H3N2 influenza viruses. *PLoS One*, 7(7):e41895, 2012.

[173] David Posada and Thomas R Buckley. Model selection and model averaging in phylogenetics: advantages of Akaike information criterion and Bayesian approaches over likelihood ratio tests. *Systematic Biology*, 53(5):793–808, 2004.

[174] Oliver G Pybus, Andrew Rambaut, Robert Belshaw, Robert P Freckleton, Alexei J Drummond, and Edward C Holmes. Phylogenetic evidence for deleterious mutation load in RNA viruses and its contribution to viral evolution. *Molecular Biology and Evolution*, 24(3):845–852, 2007.

[175] Hangfei Qi, Nicholas C Wu, Yushen Du, Ting-Ting Wu, and Ren Sun. High-resolution genetic profile of viral genomes: why it matters. *Current Opinion in Virology*, 14:62–70, 2015.

[176] Jayna Raghwani, Robin N Thompson, and Katia Koelle. Selection on non-antigenic gene segments of seasonal influenza A virus and its impact on adaptive evolution. *Virus Evolution*, 3(2), 2017.

[177] Sylvia Ranjeva, Rahul Subramanian, Vicky J. Fang, Gabriel M. Leung, Dennis K. M. Ip, Ranawaka A. P. M. Perera, J. S. Malik Peiris, Benjamin J. Cowling, and Sarah Cobey. Age-specific differences in the dynamics of protective immunity to influenza. *Nature Communications*, 10(1):1660, 2019.

[178] Donald D Raymond, Shaun M Stewart, Jiwon Lee, Jack Ferdman, Goran Bajic, Khoi T Do, Michael J Ernandes, Pirada Suphaphiphat, Ethan C Settembre, Philip R Dormitzer, et al. Influenza immunization elicits antibodies specific for an egg-adapted vaccine strain. *Nature Medicine*, 22(12):1465, 2016.

[179] Kathryn B. Renegar, Parker A. Small, Lou G. Boykins, and Peter F. Wright. Role of IgA versus IgG in the control of influenza viral infection in the murine respiratory tract. *The Journal of Immunology*, 173(3):1978–1986, 2004.

[180] James S Robertson, Janet S Bootman, Robert Newman, John S Oxford, Rod S Daniels, Robert G Webster, and Geoffrey C Schild. Structural changes in the haemagglutinin which accompany egg adaptation of an influenza A (H1N1) virus. *Virology*, 160(1):31–37, 1987.

[181] RJ Russell, SJ Gamblin, LF Haire, DJ Stevens, B Xiao, Y Ha, and JJ Skehel. H1 and H7 influenza haemagglutinin structures extend a structural classification of haemagglutinin subtypes. *Virology*, 325(2):287–296, 2004.

[182] Pavel Sagulenko, Vadim Puller, and Richard A Neher. TreeTime: Maximum-likelihood phylodynamic analysis. *Virus Evolution*, 4(1):vex042, 2018.

[183] Jonas Salk. One-dose immunization against paralytic poliomyelitis using a non-infectious vaccine. *Reviews of Infectious Diseases*, 6(Supplement_2):S444–S450, 1984.

[184] Matthew R Sandbulte, Kim B Westgeest, Jin Gao, Xiyan Xu, Alexander I Klimov, Colin A Russell, David F Burke, Derek J Smith, Ron AM Fouchier, and Maryna C Eichelberger. Discordant antigenic drift of neuraminidase and hemagglutinin in H1N1 and H3N2 influenza viruses. *Proceedings of the National Academy of Sciences*, 108(51):20748–20753, 2011.

[185] Aaron G Schmidt, Matthew D Therkelsen, Shaun Stewart, Thomas B Kepler, Hua-Xin Liao, M Anthony Moody, Barton F Haynes, and Stephen C Harrison. Viral receptor-binding site antibodies with diverse germline origins. *Cell*, 161(5):1026–1034, 2015.

[186] Premal Shah, David M McCandlish, and Joshua B Plotkin. Contingency and entrenchment in protein evolution under purifying selection. *Proceedings of the National Academy of Sciences*, 112(25):E3226–E3235, 2015.

[187] MG Sheerar, BC Easterday, and VS Hinshaw. Antigenic conservation of H1N1 swine influenza viruses. *Journal of General Virology*, 70(12):3297–3303, 1989.

[188] Yuelong Shu and John McCauley. GISAID: Global initiative on sharing all influenza data – from vision to reality. *Eurosurveillance*, 22(13), 2017.

[189] John J Skehel and Don C Wiley. Receptor binding and membrane fusion in virus entry: the influenza hemagglutinin. *Annual Review of Biochemistry*, 69(1):531–569, 2000.

[190] DM Skowronski, S Sabaiduc, C Chamber, A Eshagi, JB Gubbay, M Krajden, SJ Drews, C Martineau, G De Serres, JA Dickinson, AL Winter, N Bastien, and Y Li. Mutations acquired during cell culture isolation may affect antigenic characterisation of influenza A(H3N2) clade 3C.2a viruses. *Eurosurveillance*, 21:30112, 2016.

[191] Derek J Smith, Alan S Lapedes, Jan C de Jong, Theo M Bestebroer, Guus F Rimmelzwaan, Albert DME Osterhaus, and Ron AM Fouchier. Mapping the antigenic and genetic evolution of influenza virus. *Science*, 305(5682):371–376, 2004.

[192] Kenneth Smith, Lori Garman, Jens Wrammert, Nai-Ying Zheng, J Donald Capra, Rafi Ahmed, and Patrick C Wilson. Rapid generation of fully human monoclonal antibodies specific to a vaccinating antigen. *Nature Protocols*, 4(3):372, 2009.

[193] Ashley Sobel Leonard, Micah T. McClain, Gavin J. D. Smith, David E. Wentworth, Rebecca A. Halpin, Xudong Lin, Amy Ransier, Timothy B. Stockwell, Suman R. Das, Anthony S. Gilbert, et al. Deep sequencing of influenza A virus from a human

challenge study reveals a selective bottleneck and only limited intrahost genetic diversification. *Journal of Virology*, 90(24):11247–11258, 2016.

[194] YQ Shirleen Soh, Louise H Moncla, Rachel Eguia, Trevor Bedford, and Jesse D Bloom. Comprehensive mapping of avian influenza polymerase adaptation to the human host. *bioRxiv*, page 512525, 2019.

[195] Nongluk Sriwilaijaroen, Sachiko Kondo, Hirokazu Yagi, Prapon Wilairat, Hiroaki Hiramatsu, Morihiro Ito, Yasuhiko Ito, Koichi Kato, and Yasuo Suzuki. Analysis of N-glycans in embryonated chicken egg chorioallantoic and amniotic cells responsible for binding and adaptation of human and avian influenza viruses. *Glycoconjugate Journal*, 26(4):433–443, 2009.

[196] Alexandros Stamatakis. RAxML-VI-HPC: maximum likelihood-based phylogenetic analyses with thousands of taxa and mixed models. *Bioinformatics*, 22(21):2688–2690, 2006.

[197] Alexandros Stamatakis. RAxML version 8: a tool for phylogenetic analysis and post-analysis of large phylogenies. *Bioinformatics*, 30(9):1312–1313, 2014.

[198] Tyler N Starr, Lora K Picton, and Joseph W Thornton. Alternative evolutionary histories in the sequence space of an ancient protein. *Nature*, 549(7672):409–413, 2017.

[199] Tyler N Starr and Joseph W Thornton. Epistasis in protein evolution. *Protein Science*, 25(7):1204–1218, 2016.

[200] J Stech, H Garn, M Wegmann, R Wagner, and HD Klenk. A new approach to an influenza live vaccine: modification of the cleavage site of hemagglutinin. *Nature Medicine*, 11(6):683–689, 2005.

[201] DA Steinhauer and JJ Holland. Rapid evolution of RNA viruses. *Annual Reviews in Microbiology*, 41(1):409–431, 1987.

[202] Natalja Strelkowa and Michael Lässig. Clonal interference in the evolution of influenza. *Genetics*, 192(2):671–682, 2012.

[203] Jianhua Sui, William C Hwang, Sandra Perez, Ge Wei, Daniel Aird, Li-mei Chen, Eugenio Santelli, Boguslaw Stec, Greg Cadwell, Maryam Ali, et al. Structural and functional bases for broad-spectrum neutralization of avian and human influenza A viruses. *Nature Structural & Molecular Biology*, 16(3):265–273, 2009.

[204] Hailiang Sun, Jialiang Yang, Tong Zhang, Li-Ping Long, Kun Jia, Guohua Yang, Richard J Webby, and Xiu-Feng Wan. Using sequence data to infer the antigenicity of influenza virus. *MBio*, 4(4):e00230–13, 2013.

[205] Xiangjie Sun, V Tse Longping, A Damon Ferguson, and Gary R Whittaker. Modifications to the hemagglutinin cleavage site control the virulence of a neurotropic H1N1 influenza virus. *Journal of Virology*, 84(17):8683–8690, 2010.

[206] Volker Ter Meulen, Sieglinde Löffler, Michael J Carter, and John R Stephenson. Antigenic characterization of measles and SSPE virus haemagglutinin by monoclonal antibodies. *Journal of General Virology*, 57(2):357–364, 1981.

[207] Masanori Terajima, John Cruz, Mary Dawn T. Co, Jane-Hwei Lee, Kaval Kaur, Patrick C. Wilson, and Francis A. Ennis. Complement-dependent lysis of influenza A virus-infected cells by broadly cross-reactive human monoclonal antibodies. *Journal of Virology*, 85(24):13463–13467, 2011.

[208] Mark Throsby, Edward van den Brink, Mandy Jongeneelen, Leo L. M. Poon, Philippe Alard, Lisette Cornelissen, Arjen Bakker, Freek Cox, Els van Deventer, et al. Heterosubtypic neutralizing monoclonal antibodies cross-protective against H5N1 and H1N1 recovered from human IgM+ memory B cells. *PLoS One*, 3(12):1–15, 2008.

[209] Bargavi Thyagarajan and Jesse D Bloom. The inherent mutational tolerance and antigenic evolvability of influenza hemagglutinin. *eLife*, 3:e03300, 2014.

[210] Matthew Tien, Austin G Meyer, Stephanie J Spielman, and Claus O Wilke. Maximum allowed solvent accessibilites of residues in proteins. *PLoS One*, 8:e80635, 2013.

[211] PA Underwood. An antigenic map of the haemagglutinin of the influenza Hong Kong subtype (H3N2), constructed using mouse monoclonal antibodies. *Molecular Immunology*, 21(7):663 – 671, 1984.

[212] Jean-Louis Virelizier. Host defenses against influenza virus: The role of anti-hemagglutinin antibody. *The Journal of Immunology*, 115(2):434–439, 1975.

[213] M. Waterfield, G. Scrace, and J. Skehel. Disulphide bonds of haemagglutinin of Asian influenza virus. *Nature*, 289:422–424, 1981.

[214] RG Webster and WG Laver. Determination of the number of nonoverlapping antigenic areas on Hong Kong (H3N2) influenza virus hemagglutinin with monoclonal antibodies and the selection of variants with potential epidemiological significance. *Virology*, 104(1):139–148, 1980.

[215] Chih-Jen Wei, Jeffrey C. Boyington, Kaifan Dai, Katherine V. Houser, Melissa B. Pearce, Wing-Pui Kong, Zhi-yong Yang, Terrence M. Tumpey, and Gary J. Nabel. Cross-neutralization of 1918 and 2009 influenza viruses: Role of glycans in viral evolution and vaccine design. *Science Translational Medicine*, 2(24):24ra21, 2010.

[216] W Weis, JH Brown, S Cusack, JC Paulson, JJ Skehel, and DC Wiley. Structure of the influenza virus haemagglutinin complexed with its receptor, sialic acid. *Nature*, 333:426–431, 1988.

[217] Frank Wen, Trevor Bedford, and Sarah Cobey. Explaining the geographical origins of seasonal influenza A (H3N2). *Proceedings of the Royal Society B: Biological Sciences*, 283(1838):20161312, 2016.

[218] Kim B Westgeest, Miranda de Graaf, Mathieu Fourment, Theo M Bestebroer, Ruud van Beek, Monique IJ Spronken, Jan C de Jong, Guus F Rimmelzwaan, Colin A Russell, Albert DME Osterhaus, et al. Genetic evolution of the neuraminidase of influenza A (H3N2) viruses from 1968 to 2009 and its correspondence to haemagglutinin evolution. *The Journal of General Virology*, 93(Pt 9):1996, 2012.

[219] James RR Whittle, Ruijun Zhang, Surender Khurana, Lisa R King, Jody Manischewitz, Hana Golding, Philip R Dormitzer, Barton F Haynes, Emmanuel B Walter, M Anthony Moody, et al. Broadly neutralizing human antibody that recognizes the receptor-binding pocket of influenza virus hemagglutinin. *Proceedings of the National Academy of Sciences*, 108(34):14216–14221, 2011.

[220] WHO. Recommended viruses for influenza vaccines for use in the 2010-2011 northern hemisphere influenza season. *http://www.who.int/influenza/vaccines/virus/recommendations/201002_Recommendation.pdf?ua=1*, 2010.

[221] WHO. Recommended composition of influenza virus vaccines for use in the 2011-2012 northern hemisphere influenza season. *http://www.who.int/influenza/vaccines/2011_02_recommendation.pdf?ua=1*, 2011.

[222] WHO. Seasonal influenza fact sheet. *https://www.who.int/en/news-room/fact-sheets/detail/influenza-(seasonal)*, 2018.

[223] WHO. WHO recommendations on the composition of influenza virus vaccines. *https://www.who.int/influenza/vaccines/virus/recommendations/en/*, 2019.

[224] DC Wiley, IA Wilson, JJ Skehel, et al. Structural identification of the antibody-binding sites of Hong Kong influenza haemagglutinin and their involvement in antigenic variation. *Nature*, 289(5796):373–378, 1981.

[225] IA Wilson, JJ Skehel, and DC Wiley. Structure of the haemagglutinin membrane glycoprotein of influenza virus at 3 Å resolution. *Nature*, 289:366–373, 1981.

[226] YI Wolf, C Viboud, EC Holmes, EV Koonin, and DJ Lipman. Long intervals of stasis punctuated by bursts of positive selection in the seasonal evolution of influenza A virus. *Biology Direct*, 1:34, 2006.

[227] NC Wu, SJ Zost, AJ Thompson, D Oyen, CM Nycholat, R McBride, JC Paulson, SE Hensley, and IA Wilson. A structural explanation for the low effectiveness of the seasonal influenza H3N2 vaccine. *PLoS Pathogens*, 13(10):e1006682, 2017.

[228] Nicholas C Wu, Andrew J Thompson, Jia Xie, Chih-Wei Lin, Corwin M Nycholat, Xueyong Zhu, Richard A Lerner, James C Paulson, and Ian A Wilson. A complex epistatic network limits the mutational reversibility in the influenza hemagglutinin receptor-binding site. *Nature Communications*, 9(1):1264, 2018.

[229] Nicholas C Wu and Ian A Wilson. A perspective on the structural and functional constraints for immune evasion: insights from influenza virus. *Journal of Molecular Biology*, 429(17):2694–2709, 2017.

[230] Nicholas C Wu, Jia Xie, Tianqing Zheng, Corwin M Nycholat, Geramie Grande, James C Paulson, Richard A Lerner, and Ian A Wilson. Diversity of functionally permissive sequences in the receptor-binding site of influenza hemagglutinin. *Cell Host & Microbe*, 21(6):742–753, 2017.

[231] Nicholas C Wu, Arthur P Young, Laith Q Al-Mawsawi, C Anders Olson, Jun Feng, Hangfei Qi, Shu-Hwa Chen, I-Hsuan Lu, Chung-Yen Lin, Robert G Chin, et al. High-

throughput profiling of influenza A virus hemagglutinin gene at single-nucleotide resolution. *Scientific Reports*, 4:4942, 2014.

[232] Katherine S Xue, Terry Stevens-Ayers, Angela P Campbell, Janet A Englund, Steven A Pergam, Michael Boeckh, and Jesse D Bloom. Parallel evolution of influenza across multiple spatiotemporal scales. *eLife*, 6:e26875, 2017.

[233] Hua Yang, Paul J Carney, Jessie C Chang, Zhu Guo, Julie M Villanueva, and James Stevens. Structure and receptor binding preferences of recombinant human A (H3N2) virus hemagglutinins. *Virology*, 477:18–31, 2015.

[234] Ziheng Yang, Rasmus Nielsen, Nick Goldman, and Anne-Mette Krabbe Pedersen. Codon-substitution models for heterogeneous selection pressure at amino acid sites. *Genetics*, 155(1):431–449, 2000.

[235] Jonathan W Yewdell, Andrew J Caton, and Walter Gerhard. Selection of influenza A virus adsorptive mutants by growth in the presence of a mixture of monoclonal antihemagglutinin antibodies. *Journal of Virology*, 57(2):623–628, 1986.

[236] JW Yewdell, RG Webster, and WU Gerhard. Antigenic variation in three distinct determinants of an influenza type A haemagglutinin molecule. *Nature*, 279(5710):246–248, 1979.

[237] Reiko Yoshida, Manabu Igarashi, Hiroichi Ozaki, Noriko Kishida, Daisuke Tomabechi, Hiroshi Kida, Kimihito Ito, and Ayato Takada. Cross-protective potential of a novel monoclonal antibody directed against antigenic site B of the hemagglutinin of influenza A viruses. *PLoS Pathogens*, 5(3):e1000350, 2009.

[238] Xiaocong Yu, Tshidi Tsibane, Patricia A McGraw, Frances S House, Christopher J Keefer, Mark D Hicar, Terrence M Tumpey, Claudia Pappas, Lucy A Perrone, Osvaldo Martinez, et al. Neutralizing antibodies derived from the B cells of 1918 influenza pandemic survivors. *Nature*, 455(7212):532, 2008.

[239] Y Zhang, BD Aevermann, TK Anderson, DF Burke, G Dauphin, Z Gu, S He, S Kumar, CN Larsen, AJ Lee, et al. Influenza Research Database: An integrated bioinformatics resource for influenza virus research. *Nucleic Acids Research*, 45(D1):D466–D474, 2017.

[240] Seth J Zost, Kaela Parkhouse, Megan E Gumina, Kangchon Kim, Sebastian Diaz Perez, Patrick C Wilson, John J Treanor, Andrea J Sant, Sarah Cobey, and Scott E Hensley. Contemporary H3N2 influenza viruses have a glycosylation site that alters binding of antibodies elicited by egg-adapted vaccine strains. *Proceedings of the National Academy of Sciences*, 114(47):12578–12583, 2017.